

SCUOLA DI SCIENZE

Dipartimento di Chimica Industriale "Toso Montanari"

Corso di Laurea Magistrale in

Chimica Industriale

Classe LM-71 - Scienze e Tecnologie della Chimica Industriale

Selective photo-oxidation of glucose

Tesi di laurea sperimentale

CANDIDATO

Carlo Recchi

RELATORE

Prof. Fabrizio Cavani

CORRELATORI

Dott. José Antonio Lopez Sánchez

Dott. Luigi Da Vià

Dott. Thomas Davies

SessioneII

Anno Accademico 2013-2014

Keywords

Photocatalysis

Selective oxidation

Glucose

Titania

Gold and silver nanoparticles

Acronim list

ACN Acetonitrile

CB electronic conduction band of a semiconductor

DAD Diode Array Detector

ESI ElectroSpray Ionization

GA Glyceraldehyde

HPLC High Pressure Liquid Chromatography

NHE normal hydrogen electrode

OES Optical Emission Spectrometry

P25 Titania Degussa

Q-TOF Quadrupole Time Of Flight Mass Spectrometry

RID Refractive Index detector

RSD relative standard deviation

SPR Surface Plasmon Resonance

TEM Transmission Electron Microscopy

UV Ultra Violet wavelength (100-400nm)

UV-VIS Ultra Violet-Visible spectroscopy

VB electronic valence band of a semiconductor

VIS Visible wavelength (400-800nm)

WI wetness impregnation method

XRD X-Ray diffractometry

Abstract:

Biomass transformation into high-value chemicals has attracted attention according to the “green chemistry” principles. Low price and high availability make biomass one of the most interesting renewable resources as it provides the means to create sustainable alternatives to the oil-derived building blocks of the chemical industry. In recent years, the need for alternative environmentally friendly routes to drive chemical reactions has in photocatalytic processes an interesting way to obtain valuable chemicals from various sources using the solar light as energy source. The purpose of this work was to use supported noble metal nanoparticles in the selective photo-oxidation of glucose through using visible light. Glucose was chosen as model molecule because it is the cheapest and the most common monosaccharide. Few studies about glucose photo oxidation have been conducted so far, and reaction mechanism is still not totally explained .

The aim of this work was to systematically analyze and assess the impact of several parameters (*eg.* catalyst/substrate ratio, reaction time, effect of the solvent and of the light source) on the reaction pathway and to monitor the product distribution in order to draw a general reaction scheme for the photo oxidation of glucose under visible light.

This study regards, first of all, the reaction mechanism and the influence of several parameters, such as solvent, light power and composition and substrate concentration. Furthermore, the work focuses on the influence of different noble metal nanoparticles, in particular gold and silver, and on the influence of metal loading as well. The glucose oxidation was monitored through the mass balance and the products selectivity. Reactions were evaluated in terms of glucose conversion, mass balance and selectivities towards the main products, such as arabinose and gluconic acid are.

In conclusion, this study is able to demonstrate that the photo oxidation of glucose under visible light is feasible; the full identification of the main products allows, for the first time, a comprehensive reaction mechanism scheme.

Summary:

Keywords	1
Acronim list	2
Abstract:	4
Summary:	6
Objective:	9
1. Introduction:	12
1.1. Biomass:	12
1.1.1. Importance of biomass in industrial chemistry:.....	14
1.1.2. Biochemical and chemical oxidation of biomass:	14
1.2. Nanotechnologies and metal nanoparticles:	16
1.2.1. Metal nanoparticles: synthesis and immobilization methods	17
1.2.2. Wetness impregnation method:.....	17
1.3. Photochemistry and photocatalysis:	19
1.3.1. Semiconductors as photocatalysts:	19
1.3.2. Titanium (IV) dioxide:	21
1.3.3. Surface Plasmon Resonance band on metal nanoparticles:	24
1.3.3.1. Gold nanoparticles:	28
1.3.3.2. Silver nanoparticles:	28
1.4. Photocatalysis for the upgrade of bio-derived molecules:.....	30
2. Chemicals and Experimental part:	31
2.1. Chemicals:	31
2.2. Experimental part:	32
2.2.1. Synthesis of catalysts and calcination of titania:	32
2.2.2. Reactivity tests:	32
2.2.3. HPLC and Q-TOF analyses:	35
2.2.4. Catalysts characterization:	38

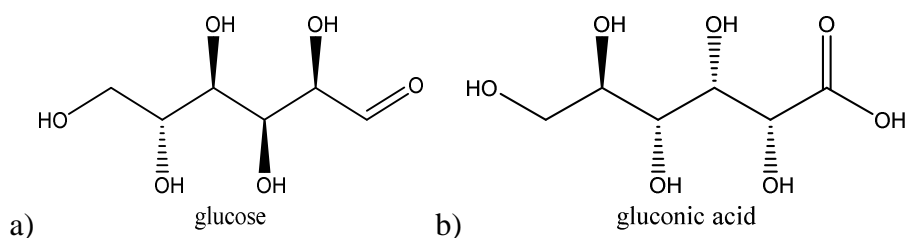
2.3.	Synthetic methods:.....	40
2.3.3.	Synthesis of gold catalyst:.....	40
2.3.4.	Synthesis of silver catalysts:.....	40
2.4.	Kinetic tests:.....	41
2.4.3.	Effect of a catalyst/substrate ratio:.....	41
2.4.4.	Effect of Solvent and lamp power:.....	41
2.4.5.	Adsorption of Glucose on catalyst:.....	41
2.5.	Photocatalytic tests:.....	43
2.5.3.	Reactions under visible and UV light:.....	43
2.5.4.	Long term reactions:.....	43
2.5.5.	Recycling tests:.....	43
3.	Results and discussion:	44
3.1.	Optimization of reactivity tests: catalyst to substrate ratio:.....	44
3.2.	Identification of the pathway and the products of reaction:.....	48
3.3.	Role of titania:.....	54
3.3.1.	Effect of structure:.....	54
3.3.2.	Effect of calcination temperature:.....	58
3.4.	Effect of the solvent and irradiation power:.....	64
3.5.	Effect of metal loading:.....	69
3.6.	Effect of different metal nanoparticles:.....	74
3.7.	24h reactions:.....	78
3.8.	Recyclability tests:.....	80
3.9.	Future Work:.....	81
4.	Conclusions:	82
5.	Appendix:	83
	Acknowledgements:	85
	Bibliography:	86

Objective:

Photocatalysis is one of the recently fields investigated for the exploitation of biomass. It has attracted great interest according to “green chemistry” principles, because it combines the use of renewable raw materials as biomass and the use of solar light. This new field of catalysis has been limited so far to the studies of few model molecules, such as cellulose cellobiose and glucose, in order achieve a greater understanding on the reaction mechanism and on the role of the catalyst in such reactions.

Titania P25 is one of the most used supports for this kind of catalyst, TiO_2 along with Al_2O_3 , are the most widely used supports in photocatalytic processes due to their activity under UV irradiation, their high efficiency and non-toxicity..^{1,2} Moreover, to improve the catalytic performances of the aforementioned supports, their surface can be decorated with supported metal nanoparticles, and experimental evidence of the increased activity can be found in the literature for alcohols oxidation reactions^{3,4}. This know-how was transferred to the biorefinery philosophy and for the upgrade of biomass into valuable chemicals.

In particular, the purpose of this project was to synthetize supported metal nanoparticles and use them in the selective photo-oxidation of glucose, and the main products expected from this oxidation were gluconic acid, derived from the oxidation of the aldehydic group of C_1 , and glucaric acid, derived from the further oxidation of the alcoholic group of C_6 . Arabinose was another product expected by degradation of glucose. These products were expected according to the experimental observations made by Colmenares *et al*⁵ and Chong *et al*.⁶, These work represents the state-of-the-art of photo-oxidation of glucose, the reaction mechanism and the influence of several parameters, such as solvent, pH, atmosphere, are not totally explained.



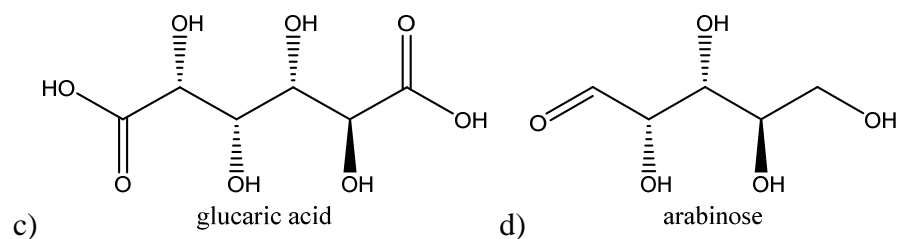


Figure 1: Structure of reactant (a) and main products expected (b, c, d).

Titania P25 was used as support for its catalytic activity under ultraviolet irradiations, but it can be doped with semiconductors to enhance its absorption under visible region of light spectrum. Doping Enhancement of photo efficiency of titania was done using noble metal nanoparticles for their capacity to act as electron acceptor through the characteristic phenomenon of Surface Plasmonic Resonance (SPR). In fact, they act as “antennas” through their SPR band,² and then they transfer electrons to the titania thus enhancing the activity of the support. The noble metal nanoparticles present good activity in few photocatalytic reactions as well.⁷

1. Introduction:

1.1. Biomass:

Biomass is defined as “any material, excluding fossil fuel, which was a living organism that can be used as a fuel either directly or after a conversion process”.⁸ Raw plant biomass consists of lignocellulosic material that is mainly made up of three primary fractions: cellulose, hemicellulose and lignin. The main constituent of that is cellulose ($C_6H_{10}O_5$)_x, a polysaccharide made up of a linear chain D-glucose linked by β -(1,4)-glycosidic bonds to each other, as shown in Figure 2.⁹ The degree of crystallinity and other peculiarities are influenced by inter and intramolecular hydrogen bonds and this peculiar framework make cellulose insoluble in most organic solvents and resilient to acid and alkali solutions under mild conditions.^{8,10}

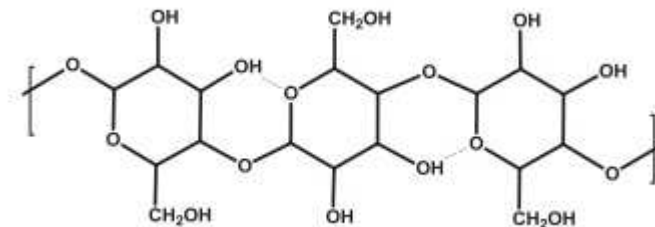


Figure 2: Structure of cellulose.¹¹

Hemicellulose ($C_5H_8O_4$)_m, reported in Figure 4, is the second most abundant polymer in biomass, and consists of heterogeneous branched biopolymers contains D-glucopyranose, D-galactopyranose, D-mannopyranose, L-arabinofuranose and D-xylopyranose monomers (Figure 3).¹¹ this polymer is relatively easy to hydrolyze because of the amorphous, and branched structure (with short lateral chain) which lowers the impermeability to the protons and hydroxyl anions.¹²

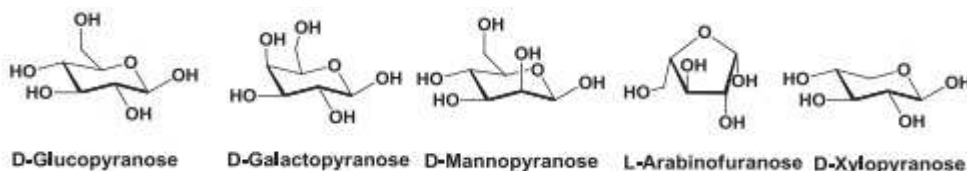


Figure 3: Main sugar monomers of hemicellulose.¹¹

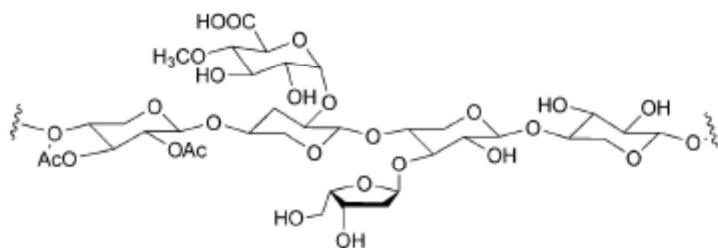


Figure 4: Structure of hemicellulose.

Finally, lignin (Figure 6) is an amorphous heteropolymer network built up of phenyl propane units reported in Figure 5. It is present in plant cell walls and it is responsible of some peculiar plant characteristics as rigidity, impermeability and resistance to microbial attack and oxidative stress.⁸



Figure 5: basic constituents of lignin.

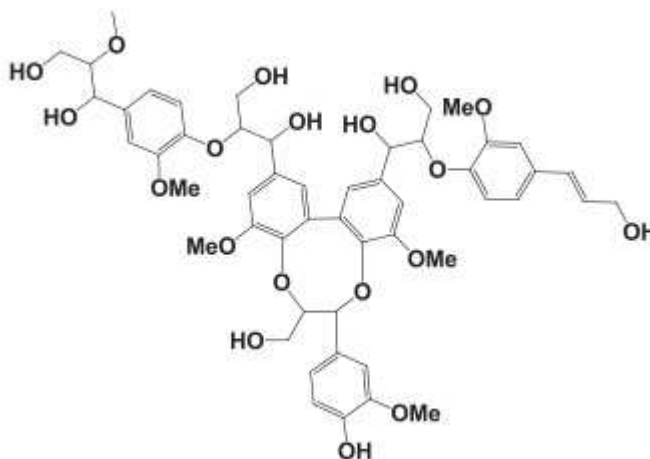


Figure 6: Example of lignin's structure.

The ratio between these three components varies according to the type of biomass, tissue type, growth stage and growing conditions of the plant.¹¹

This work is focused on glucose, indicated in Figure 3 as D-Glucopyranose, because it is the most common and cheapest carbohydrate available in nature. It is the main product of the photosynthetic processes and it is one of the biomass building blocks, as reported above. It can be obtained from the hydrolysis of cellulose and hemicellulose, and then it

can be easily convertible in valuable chemicals through chemical and biochemical transformations.

1.1.1. Importance of biomass in industrial chemistry:

The chemical industry of the last century was focused on crude oil exploitation, available in high amount and low prices. As fossil raw materials are decreasing, researchers worldwide had to focus their attention on the necessity to switch to renewable resources as feedstock. Because of the uncertain availability of fossil resources and the increasing concerns of the public opinion for the environment, alternative solutions able to mitigate environmental concerns, and the use of bio-compatible resources in the production of bio-fuels and specialty chemicals should be promoted.¹³ Different techniques have been developed to convert biomass into bio-fuels, mainly bio-ethanol that is derived from food crops. Nevertheless, one of the main problems with biofuels is the competition between their production and food demand.¹⁴ This issue was solved using second generation feedstock for fuel production. Biomass can be used for add-value chemicals using biorefinery processes.¹⁵

The biorefining concept is a way to join the use of bio-compatible resources as raw materials with the use of low environmental impact technologies, embodying the principles of the “green chemistry” and of the “green engineering”. Biorefining has increasingly drawn much attention, due the possibilities of provide a wide range of bio-based products, such as bio-fuels, bio-chemicals and bio-materials. Therefore, green chemistry and green engineering are integrated into the biorefining concept.¹³

1.1.2. Biochemical and chemical oxidation of biomass:

Biochemical oxidation of biomass and glucose was used since the ancient times. Biofermentation of glucose leads to several product such as succinic acid and gluconic acid, and bioethanol is obtained from batch fermentation of sugars derived from sugarcane and grain.⁸ Research on better processes was required because the fermentative ones had poor energy balance (energy output of the biofuel/energy inputs required during production), and grain-based fuel ethanol production also created a moral dilemma over the use of agricultural crops and/or land for fuel vs. food.⁸ Furthermore,

the biochemical methods still have various disadvantages such as slow reaction rate, low space-time and difficulty in the separation of enzyme from product.¹⁶

Several chemical processes have been investigated, especially the catalytic ones run through supported nanoparticles such as palladium, platinum and gold.

Biella *et al.*¹⁷ reported for the first time the oxidation of glucose on gold sols supported on carbon and found a total selectivity towards gluconic acid. Additionally, a recycling test of the gold catalyst was carried out, and after four runs a 50% decrease in activity was noted, mainly due to leaching.¹⁸ At the same time, the presence of fructose was observed during the oxidation of the glucose. The formation of fructose indicates the isomerization of glucose. It is known that by treating monosaccharides with concentrated alkaline solution, the sugars are destroyed, whereas alkaline media with lower pH induce an isomerization reaction of glucose to fructose resulting in an equilibrium mixture of the two sugars.

Temperature also influences reaction kinetic. Caramelisation is an effect observed when temperature reaches 353 K, but over 333 K a slight decrease in selectivity was observed.¹⁸

Nowadays, bio-products such as sorbitol, 5-hydroxy-methylfurfural (HMF),¹⁹ and levulinic acid²⁰ are produced in high yields and large scale production volumes through using supported metal nanoparticles catalysts. Nonetheless, the use of harsh reaction conditions and the high energy-demand make several processes uncompetitive, especially for new environment safeguard laws. In recent years industrial chemistry has changed its priority with the diffusion of “green chemistry” and “green technology” principles.²¹ These principles promote the reduction of impact of chemicals production on human health and environment performing chemical reactions under milder conditions and using greener solvents such as water.

1.2. Nanotechnologies and metal nanoparticles:

From 19th century, interest in the properties of materials in nanometric scale has been increasing.. In this scale, properties of materials are different from individual atoms or bulk materials, and the study of them allowed to create a new field in chemistry.²²

Those differences are mainly influenced by the shape and the surface to volume ratio of atoms, instead of the nature of material, and changes in the properties can be obtained from the same starting material.²²

Metals have been deeply studied because of their distinctly different physic-chemical properties at a nanometric scale, from the most hidden tiniest to the most evident properties such as the color. For example, thermal and electrical conductivities are two features influenced by size. Bulk systems possess high thermal and electrical conductivity because electrons can be delocalized on the surface, while in metal nanoparticles electrons cannot be delocalized and they move in confined spaces allowing different properties.²³

Among these features, nanoparticles typically provide highly active centers for superficial reactions but are very small and are not at a thermodynamic stable state. Structures at this size range regime are unstable due to high surface energy and the large surface. Several synthetic pathways have been developed to achieve the production of stable particles,²³ but nanoparticle research is still focused on that due to the difficulty in generating the desired shape, size and monodispersity of the nanoparticles.²²

Several features, such as size, shape, monodispersity, defects, plasmonic band and oxidation state of metal, can be used to classify the nanoparticles systems. Characterization of the nanoparticles systems permits the evaluation of those features, and it is done *via* several analytical instruments and techniques, typically X-Ray photoelectron spectroscopy (XPS), X-ray diffraction (XRD) and transmission electron microscopy (TEM).²³ According to catalyst characterization, not only the nanoparticles features have to be assessed, but also the support ones. Supports are described in terms of accessibility of the catalytic sites, textural properties (pore volumes, dimension and micro- or mesopore capacity), particle size, morphology, chemical nature, surface functionality (species, loading and acidity/basicity), and surface energy characteristics (hydrophobicity/hydrophilicity).²³

Recent studies on nanoparticles have been mainly focused on silver and gold nanoparticles due to their particular stability at a nanoscale level.²⁴ The increase of knowledge in synthesis and the development of new applications of nanoparticles have improved their exploitation in a lot of different sciences, such as medicine (as contrast agents and magnetic resonance imaging [MRI]), chemical sensors (as electrochemical sensors and biosensors) and heterogeneous catalysis (oxidations, hydrogenations and C-C coupling reactions).²³

1.2.1. Metal nanoparticles: synthesis and immobilization methods

Different methods for the synthesis of nanoparticles and their support have been developed in the last years. There are two general strategies to obtain materials on the nanoscale: top down method where material is removed from the bulk material, leaving only the desired nanostructures, or bottom up method where the atoms (produced from reduction of ions) are assembled to generate nanostructures.²² The first comprehends photo and electron beam lithography, but they require an expensive instrumentation and, for photolithography, size resolution is currently limited to 60 nm.²²

Bottom up methods can be divided in four main categories: reduction of transition metal salts precursors, electrochemical synthesis, reduction of organic ligands in organometallic precursors and metal vapor chemistry.²⁵ These methods are the most used but they suffer poor monodispersity because of the need to stop the growth of the nanoparticles at the same level.²² Other less common methods include thermal and photochemical decomposition of metal complex precursors, redox surface techniques and sonochemical synthesis.²⁵

Of the synthetic methods mentioned above, wetness impregnation was the one applied in this work due to its easy application to supporting nanoparticles.

1.2.2. Wetness impregnation method:

Wetness impregnation is one of the most used method to immobilize metal nanoparticles on supports such as metal oxides (Titanium, zinc, cerium, zirconium and aluminum oxides) and mesoporous materials.²⁶

It is widely used because it is the simplest immobilization method, temperatures needed for the synthesis are around 353-373 K²⁷ and nanoparticles are formed *in situ*.

Despite of the quantity of metal immobilized with this method, which is generally higher than other techniques such as deposition precipitation or CVD, the activity of the wetness impregnation catalysts sometimes is lower than other methods such as reduction deposition.²⁸

Wetness impregnation consists of a few steps; the first of them is the addition of the metal salt solution to the support. Then, the drying step allows the immobilization of nanoparticles on the surface, and finally the metal is reduced by calcination in air or heat treated under hydrogen atmosphere, according to the type of metal used.²⁷

Several parameters need to be monitored carefully during the nanoparticles formation, such as the control of thermal activation and reduction as they can have a huge effect on the final dispersion and on the dimension of the particles on the surface of the catalysts.²⁹

In addition to the mediocre dispersion of the nanoparticles,²⁸ as previously described, their size and shape are influenced by the different parts of support where they grow and the heating ramp used. The latter influences the growth and multinucleation of nanoparticles, because allows the switch among thermodynamic and kinetic controls. Growth and multinucleation, in fact, are influenced by those controls, and the heating ramp needs to be accurately programmed.

Wetness impregnation is also used with mesoporous supports due to their higher pore dimensions. Those pores are able to encapsulate big nanoparticles on themselves. Size and dispersion of nanoparticles are indeed influenced by pore dimensions.

The use of metal salt solution leads to the problem of counter ion, because it can affect and compromise the catalytic activity. Chlorine is widely used as counter ion, but it can poison the active sites and enhanced the nanoparticles sintering. Several solutions have been studied to avoid this problems, from the thorough washing of catalyst² to the double precipitation with a base. The second one allows the deposition of gold in the hydroxide form facilitating the removal of chlorine ion.³⁰

1.3.Photochemistry and photocatalysis:

IUPAC defines photochemistry as “a branch of chemistry concerned with the chemical effects of light (far UV to IR)”. Chemical reactions caused by absorption of UV, Vis or IR radiation are called photochemical reactions, or simply photoreactions, and involve photochemical counter parts of normal chemical reactions, such as photooxidations, photodegradations, photocycloadditions, etc. Therefore, photocatalysis can be defined as the acceleration of a photoreaction by the presence of a catalyst.³¹

When the light is absorbed by the catalyst, the system represents a sensitized photoreaction which may occur through energy transfer or electron transfer. The first involves the formation of activated state of the reactant of interest, which is more easily oxidized than their ground state. The latter allows catalyst to act as an electron donor or acceptor.

Until now the most analyzed applications for photocatalysis were only the destruction of pollutants in water³² and water splitting.³³

1.3.1. Semiconductors as photocatalysts:

Semiconductors are materials that exploit their optical features to convert light into chemical energy, behaving as photocatalysts. Their electronic structure, made up of a filled valence band (VB) and an empty conduction band (CB), has a characteristic gap among these bands that permits the excitation of electron through a specific electromagnetic radiation wavelength.

The semiconductors band gap influences their behavior as photocatalysts, because the redox potential for the generation of reactive oxygenated compounds from water (as oxygen radicals) has to lie within their band gap.³⁴

The activation of the semiconductor photocatalyst is achieved through the absorption of a photon of light corresponding to the bandgap energy which excite electrons from the valence band to the conduction band leaving holes in the valence band. A necessary condition for this phenomenon is that the appropriate wavelength of the incident radiation has to be equal to the energy of band gap. The electron/hole pair is the driving force of this kind of catalyst², and the redox potential of the e^-/h^+ couple must lie within the bandgap domain of the photocatalyst.³²

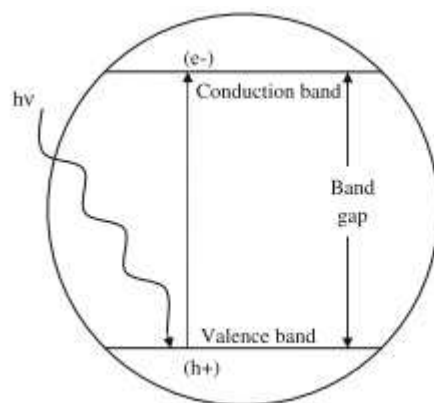


Figure 7: Photoactivation of a semiconductor and generation of electron⁻/hole⁺ pair.³⁵

Bandgap energies can be evaluated in electron volts using the Normal Hydrogen Electrode (NHE) as reference.³² Band gap energies of most common semiconductors are illustrated in . Redox potentials of electron/hole pair can be influenced by the material and the pH of the environment. According to their potential vs NHE, conduction band electrons can act as reductants (+0.5 to -1.5 V) and valence band holes can act as oxidants (+1 V to +3.5 V).³²

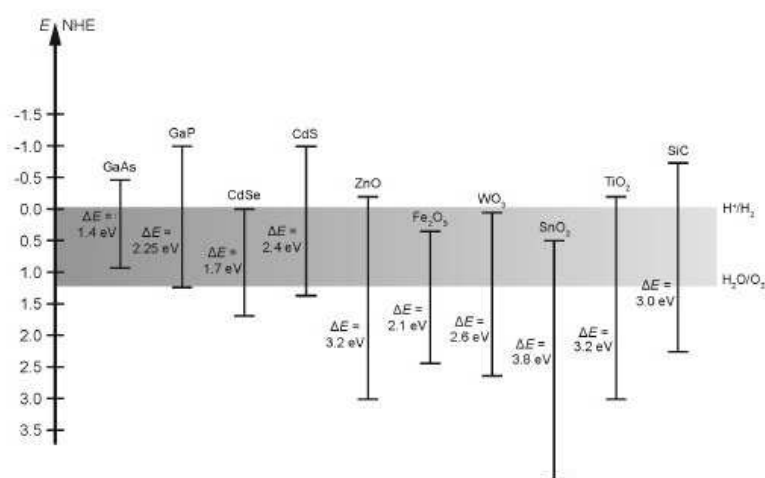


Figure 8: Bandgaps of semiconductors in aqueous electrolytic solution at pH 1.

The deactivation of photocatalysts can be due to the electron/hole pair recombination. The catalytic activity of a semiconductor that acts as photocatalyst can be evaluated through the ratio among the activation by light and the deactivation described above.

The surface area is an important feature for the valuation of photocatalytic activity. A high surface area of the material involves a high density of localized states, which have energy within the conduction and the valence band.³⁶ These localized states enhance the charge separation because they can act as trapping sites for electrons, and adsorbed

species density can promote the radical formation through the trapped charge carriers preventing the recombination.³⁵

Semiconductors are evaluated according to the green chemistry principles and economical sustainability of the process. Non toxicity, simple synthetic method, low production cost, catalytic effects, solar light activation³², stability and durability under irradiation or in water and air-saturated environment³⁴ are some catalyst's features appreciated. Several materials, generally metal sulfides and chalcogenides, despite of their photo activity cannot be used as photocatalysts because of their photocorrosion, especially in aqueous environments.²

1.3.2. Titanium (IV) dioxide:

The first studies about the effects of light on titanium dioxide was published on 1921 by Renz, who reported that titania was partially reduced under sunlight irradiation in presence of glycerol, turning its color from white to grey or blue.³⁷ Applications of titania in photocatalysis started 50 years later, when in 1972 Fujishima and Honda published a paper where explained that titania could photolyze water under UV light in presence of an appropriate electrochemical system.³⁸ Titania had started to be exploited in photocatalysis for its peculiar features, first of all its potential bandgap, that reflected the appreciated characteristics described in the paragraph 1.3.1.³⁴

Titania is present in nature in different allotropic structures: the most common are anatase, rutile and brookite. Rutile is the only stable structure while anatase and brookite are metastable, so they tend to transform in rutile under harsh conditions.³⁵ Brookite is photocatalytically inactive, so it is not studied in this field, while anatase and rutile show photocatalytic activity under UV light.^{2,39}

Anatase shows better photoactivity due to its higher density of localized states. The localized states, as previously described, act as trapping sites for electrons slowing their recombination and letting them reacting with other molecules in solution.³⁵ Rutile presents a worse photoactivity than anatase, because of a larger grain size that not allows a good surface absorption of species along with a higher charge carriers recombination.³⁵

Due to the phase composition, the presence of impurities, particle size, surface area and other physicochemical parameters that strongly affect charge recombination and electron/hole trapping, a large variation in the photocatalytic activity of the material depending on the origin can be observed. Commercial P25 TiO₂ from Degussa

(constituted by 80% anatase and 20% rutile) prepared by spray pyrolysis has become a standard material because it had exhibited good photocatalytic activity and reproducibility.² Although the use of standard material, huge number of factors present in the reaction systems or in the environment can affect the reproducibility of the results. Light intensity, spectra distribution of the emissions, geometry, impurities are common variables⁴⁰ of this kind of reactions and have to be considered during the design of the system.²

The excitation of electrons of anatase and rutile requires photons whose wavelength belongs of the UV region of spectrum due to their large band gap, which is $\sim 3.2\text{eV}$ for anatase³⁴ and $\sim 3.0\text{eV}$ for rutile.⁴¹

The electrons produced by UV radiation in the conduction band can present a mild reducing ability (E_{red} ca. -0.3V), on the other hand, holes in the valence band can act as strong oxidizers (E_{ox} ca. $+3.0\text{V}$)⁴² towards the molecules adsorbed on the surface, as O_2 or H_2O . The bandgap of titania is compared with several redox couples in . The first potential allows the reduction of the electron acceptors as oxygen with the formation of superoxide ($\bullet\text{O}_2^-$) and then hydroperoxide radicals ($\bullet\text{OOH}$) whilst, the latter, permits the oxidation of water generating hydroxyl ($\bullet\text{OH}$) radicals.² These radicals can subsequently interact with target molecules as occurring during the degradation of pollutants in wastewaters.^{2,43}

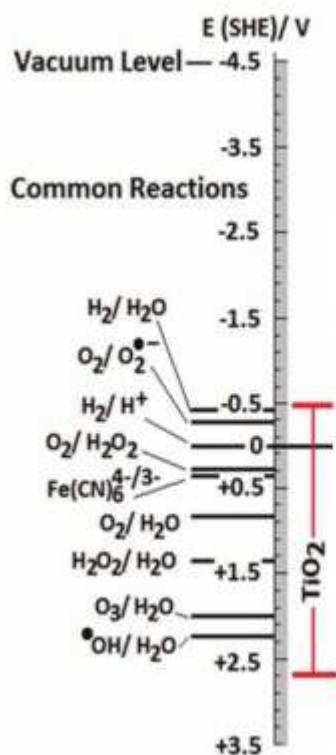


Figure 9: Titania bandgap compared to different redox couples.⁴⁴

The UV region, at ground level, is the most energetic part of light which compose the solar radiation, but it is present for ca. 5% of the total emission. On the other hand, visible and infrared compose the solar light for ca. 43% and ca. 52% but they cannot be utilized in the photo activation of titania due to their low energy content. Solar light is the most attractive energy for its renewability, and research is now focused on bandgap tuning of titania that allows the exploitation of the visible region of spectrum for the excitation of the electrons. This bandgap tuning expands the possible applications of titania as a photocatalyst.³⁴

Different techniques can be used to enhance the titania band gap that space from the coupling with other semiconductors to doping with ions and noble metal nanoparticles deposition. Noble metal nanoparticles deposition is one of the most common techniques because the metal modifies the electronic band structure leading to an opportune surface structure. This surface structure conducts to an higher quantum efficiency that is reflected, for example, in higher rates of organics degradation in water under solar irradiation.³⁴

1.3.3. Surface Plasmon Resonance band on metal nanoparticles:

Noble metal nanoparticles are one of the most utilized strategies of visible-enhancement of semiconductors bandgap, because they can capture the solar radiation and transfer the incoming energy through the charge carriers to the support (generally titanium, zirconium and silicon oxide).^{45,46}

Two different absorption bands are involved in the photo-excitation of nanoparticles, and the mechanism is well explained by gold example in . The first one, called Surface Plasmon Resonance band, originates from intraband excitation of 6sp electrons through visible irradiation. The latter results of the interband transition of electrons from 5d to 6sp orbitals through UV irradiation.

The electronic transitions caused by the visible irradiation are more frequent, and the excited electrons leave reactive holes on the nanoparticles. On the other hand, holes in the 5d band, caused by UV irradiation, are more powerful oxidant than the 6sp ones. That allows the exploitation of nanoparticles as photocatalysts under irradiation of light with wavelength from UV to visible region of spectrum.⁴⁵

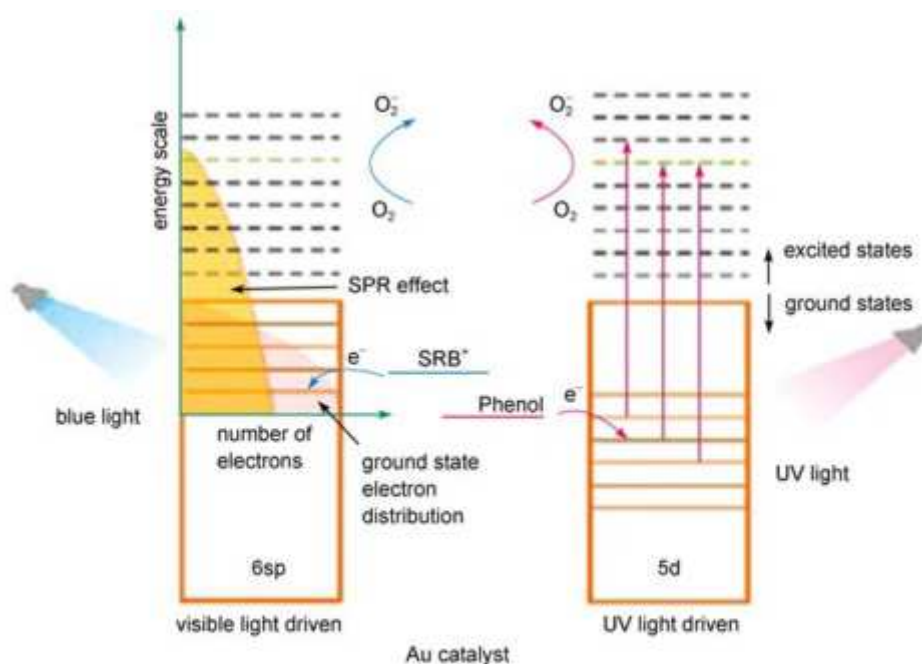


Figure 10: proposed mechanism for photocatalysis through gold nanoparticles for the degradation of organic molecules such as SRB⁺ and phenol.⁴⁷

Moreover, supported materials have to satisfy specific requisites to be used as catalysts, such as a suitable surface for thermodynamically favourable reactions and a high catalytic activity with low activation barriers for the selected reaction.³³

These features, along with the specific characteristics regarding photocatalysis and supported materials, such as solar photoactivation and interaction between nanoparticles and support, make complex the development and the large-scale applications of this kind of catalysts.⁴⁸

Plasmonic photocatalysis has recently come into focus as a very promising technology for high-performance. It involves dispersal of noble metal nanoparticles (Au and Ag are the most used, in the range size of nanometers) into semiconductor photocatalysts and obtains drastic enhancement of photoreactivity under the irradiation of UV and a broad range of visible light. Localized Surface Plasmon Resonance band (LSPR) and Schottky junction are the two peculiar features of plasmonic photocatalysis, and each influences photocatalysis differently.⁴⁸

Localized Surface Plasmon Resonance band is originated by the collective oscillation of the metal nanoparticle's free electrons in phase with the varying electric field of the incident light ($E_0 \cos(kz - \omega t)$), and it can be tailored to fall in the visible range or the near-UV range, depending on the size, the shape and the surrounding environment.

This phenomenon is strongly dependent on the particle's dimension, because surface plasmons decay in different ways if the particles are bigger than 50nm or smaller than 30nm. In the first case, radiative scattering of resonance photons occurs from the bulk, while in smaller particles there is a formation of charge carriers that they can be transferred to the support.³³ Therefore, all interactions are expected to be with the surface if particles are smaller than 30nm.²² This charge transfer creates "hot spots", high surface energy density regions around the nanoparticles.

When the wavelength of light is much larger than the nanoparticle size it can set up the resonance conditions as illustrated in . When the wave front of the light passes, the electron density in the particle is polarized to the opposite side and oscillates in resonance with the light's frequency causing a standing oscillation.

The resonance condition is determined by absorption and scattering spectroscopy and it is influenced by several features, not only of the nanoparticles but also of the environment. Nanoparticles can be tailored in the size and the shape to have a SPR band

that falls in different region of the spectrum. That is possible because surface geometry is modified and it leads to a change in the surface electrical density.

Dielectric constant of the media can influence the oscillation frequency of the electrons because it modify the interactions between nanoparticle's electrons present on the surface and other molecules present nearby. The influence of the chemical bonded molecules on the electron density of the surface induces a shift in the surface absorption maximum.²²

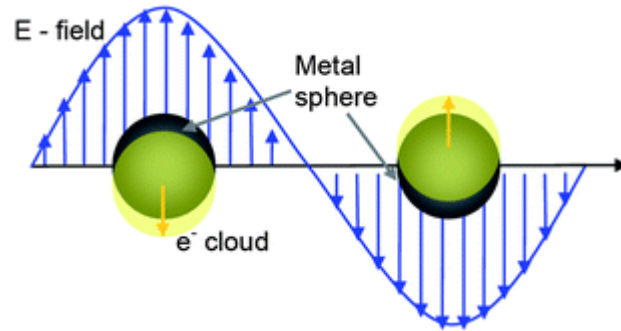


Figure 11: Interaction among electromagnetic radiation and nanoparticle electron cloud.⁴⁹

The interactions among the nanoparticle and the incident light are well described by solving the Maxwell's equation taking into account proper boundary conditions. Mie's theory⁵⁰ described rigorously these interactions for a single spherical nanoparticle.

He used the total extinction cross section (σ_{ext}), given by absorption and scattering, as the product over all electric and magnetic multipole oscillations. For particles that have size a much smaller than the light wavelength λ ($a \ll \lambda$), the *quasi-static approximation*⁵¹ can be applied and the equation 1 can be used. That approximation can be applied also for gold nanoparticles with size smaller than 25nm.⁵² That approximation considers the dipole absorption as the only that contributes to the extinction cross section of the nanoparticle.

$$\sigma_{ext} = \frac{9V\epsilon_m^{3/2}}{c} \cdot \frac{\omega\epsilon_2(\omega)}{[\epsilon_1(\omega) + 2\epsilon_m]^2 + \epsilon_2(\omega)^2}$$

Equation 1: Mie's equation with quasi-static approximation.⁵³

Where V is the volume of the spherical particles, ω is the angular frequency of the exciting radiation, c is the speed of light, and ϵ_m is the dielectric constant of the medium (assumed as frequency independent). $\epsilon_1(\omega)$ and $\epsilon_2(\omega)$ are respectively the real and

imaginary part of the dielectric function of the particle material, according to $[\varepsilon(\omega) = \varepsilon_1(\omega) + i\varepsilon_2(\omega)]$.⁵³ If ε_2 is small or weakly dependent on ω , resonance occurs when $\varepsilon_1(\omega) \approx -2\varepsilon_m$, while the width of band and the peak height are approximated by $\varepsilon_2(\omega)$.⁵² This theory presents some problems in predicting the results for small nanoparticles, due to its approximations.⁵³

The *quasi-static* approximation doesn't comprehend the variation of the individual radius, because it limits the dependence on the size to the variation of the total volume of particles. Instead, particle size affects plasmon bandwidth and the position of the adsorption maximum can suffer blue or red-shift with decreasing the particle size.⁵⁴

When nanoparticle diameter is below 20nm quadrupole and other high-order terms become significant.⁵¹ Subsequently, Mie's theory has to assume the dielectric function of the metal nanoparticle as size dependent $[\varepsilon(\omega) = \varepsilon(\omega, R)]$, and for small nanoparticles it has to be considered also the size in the total extinction cross section, due to the intrinsic size effects.⁵³

Mie's theory has been modified by Gans. Mie-Gans model expands the validity to the particles that have different structures or shapes, because it allows the correction of the overall extinction spectra of spheroids.⁵⁵ This model is corroborated by experimental UV-Vis spectra of spheroidal nanoparticles, because they present the characteristic plasmonic bands.⁵⁵ However, SPR band is not a common behavior for every metal presents in nanometer size, as demonstrated by Creighton *et al.*⁵¹

SPR band can improve the presence of the charge carriers in the support through some different ways, and direct contact is most used of them.

Noble metal particle and semiconductor contact causes an effect called Schottky junction. That effect consists of an bulk electric field close to the surface of contact between metal and support. When the electron/hole pair is created, Schottky junction forces the electrons and holes to move in different directions, avoiding the recombination.⁴⁸ Furthermore, the nanoparticles allow a fast-lane charge transfer and their surface acts as a charge-trap center to host more active sites for photoreactions.

Energy position of bands is important to value, because it influences the energy of the excited electrons produced. As reported in and described in paragraph 1.3.1, conduction band is around +0.5 and -1.5 V and valence band starts from +1 V to +3.5 V,⁷ while Surface Plasmon Resonance band energy is comprehended among 1.0 and 4.0 V.

Only the excited electrons can be transferred from the metal to the semiconductor, while the positive holes remaining on the metal are often energetically insufficient to run a reaction, especially in case of particles size greater than 50nm.³³

Several studies about the supported semiconductors, the plasmon photocatalysis and the possible application involved are been conducted recently.^{56,57}

1.3.3.1. Gold nanoparticles:

The most important feature of gold is its difference from massive dimension to nanometer size. The first is considered chemically inert, and the origin of the adjective “noble” is attributed to this feature. The latter has received more attention in the last decades, especially after the work conducted by Haruta *et al.* They demonstrated that nanoparticles of gold could be active on the oxidation of CO at low temperatures,⁵⁸ but this activity disappeared when particle size exceeded 20nm.⁵⁹ After that, supported gold nanoparticles has attracted the interest in heterogeneous catalysis,⁶⁰⁻⁶² above all for oxidation and hydrogenation reactions.^{2,17,63}

Gold nanoparticles present an absorption band around 560nm that causes the red color observed in gold colloidal solutions. The mechanism of electrons excitation in metal nanoparticles is already described, and electron/hole recombination can be avoided by other molecules that can trap them.

Low gold loading and small size of nanoparticles lead to a good activity as a photocatalyst² for gold supported on titania, due to the capability of producing charge separations under mild redox potentials. Titania is the most used as support for photocatalytic systems, but several metal oxides as CeO₂, ZrO₂, Fe₂O₃ are used due to their high surface area.^{3,4}

Nowadays different reactions are performed with Au/TiO₂ as catalyst, above all selective oxidations⁶⁴⁻⁶⁶ and hydrogenation² of organic compounds.

1.3.3.2. Silver nanoparticles:

Silver nanoparticles have shown good activity as catalysts, and their peculiar optical features have led to application in Raman scattering, fluorescence and plasmon photocatalysis fields.⁶⁷ Furthermore, Ag/TiO₂ have found applications as bactericide due to its enhanced activity under UV light.

Silver nanoparticles, through their LSPR band, can expand the absorption of titania into the visible part of the light spectrum. They can also slow the recombination of charge carriers.⁶⁸ The mechanism³² is similar to the one described for gold and follows the general rules explained in paragraph 1.3.3. The metal nanoparticle's free electrons are excited by Plasmon Resonance effect under visible light, generating electron/hole pairs. Excited electrons are then transferred to the semiconductor where they finally act as superfacial reactions with the adsorbed molecules.

Photochemical activity of silver nanoparticles can be modified by changing size, shape and geometry. These features can be tailored to obtain optimal performance for a particular photoreaction as described by Christopher *et al.*⁶⁹

Particularly interesting for the purposes of this work is the study conducted on silver nanoparticles supported on titania Degussa P25 by Grabowska *et al.*⁶⁷ They have demonstrated that metal loading and catalytic activity under visible light are not linearly correlated, mainly due to the increase of particle size and support coverage caused by the increasing of metal loading. In fact, under visible light, the catalyst with low content of silver (1% w/w) reached the best performances, while under UV light the best results are obtained by higher percentage of silver loading (2% w/w).

The optical characteristics of silver nanoparticles, in addition to the low cost of the raw material have improved the interests for potential applications in photocatalysis.

1.4. Photocatalysis for the upgrade of bio-derived molecules:

The “green chemistry” principles have encouraged the study of different ways to run chemical reactions by using bio-derived molecules and greener solvents under milder conditions. Photocatalysis is one of the most interesting routes for the upgrade of bio-molecules, as sugars, into add-value chemicals. Until now, photocatalysis is mainly used for the degradation of pollutant³² or organic compounds, but the aim is the production of “green” fuels and chemicals through using solar energy and renewable raw materials such as biomass.

Colmenares *et al.*⁵ have demonstrated that the selective oxidation of glucose occurs on titania-based photocatalysts, and some add-value chemicals, such as gluconic acid and glucaric acid, can be obtained. The oxidation reactions are not the only studied, but also hydrogen production⁷⁰ has attracted much attention.

Nowadays, water splitting is used to obtain H₂,³³ but yields remains quite low. Recent studies have obtained hydrogen from biomass, such as glucose, sucrose, and starch.^{70,71}

Titania and metal nanoparticles are the most studied in the field photocatalysis, but the studies can be expanded to Al₂O₃, ZrO₂ and every material that shows photochemical activity. In a study of Pei *et al.*, a degradation of an organic carboxylic acid (2,4-Dichlorophenoxyacetic acid) has been performed with bismuth tungstate (Bi₂WO₆) and hydrogen peroxide under UV irradiation.⁷²

2. Chemicals and Experimental part:

2.1. Chemicals:

All chemicals were used as purchased without further purification.

- *Metal salts:* Gold (III) chloride trihydrate 99.9% (Sigma-Aldrich), Silver nitrate >99.0% (Sigma-Aldrich).
- *Supports:* Titanium (IV) Oxide Aeroxide P25 (Acros Organics), Titanium (IV) oxide anatase (Sigma-Aldrich), Titanium (IV) oxide rutile 99.99% (Sigma-Aldrich).
- *HPLC calibration standards:* D-(-)-Arabinose $\geq 98\%$ (Sigma-Aldrich), D-(+)-Glyceraldehyde $\geq 98\%$ (Sigma-Aldrich), D-(-)-Erythrose $\geq 75\%$ (Sigma-Aldrich), Formic acid $\geq 95\%$ (Sigma-Aldrich), D-(+)-Glucose $\geq 99.5\%$ (Sigma-Aldrich), D-Glucaric acid potassium salt $\geq 98\%$ (Sigma-Aldrich), D-Gluconic acid sodium salt $\geq 99\%$ (Sigma-Aldrich).
- *Other chemicals:* NaOH.
- *Solvents:* Ultrapure water (purification system Millipore MILLI-DI resistivity $>1\text{M}\Omega\times\text{cm}$ at 25°C , UK), Acetonitrile $\geq 99\%$ (Fisher).

2.2.Experimental part:

2.2.1. Synthesis of catalysts and calcination of titania:

Catalysts synthesis were carried following the method used by Sugano *et al.*²⁷ The method is quite different from the common WI method, because hydrogen flow is used during the calcination to avoid the oxidation of the metal. The catalysts were filtrated in one all-glass filter holder (Millipore, UK) with 0.2µm nylon filters (Whatman). Subsequently, the catalysts were dried in a Vacuum oven (Mod. OV-11, Fischer Scientific, UK). Finally, calcination of catalysts were done in a 1100°C ashing furnace (Mod. AAF-1100, Carbolite, UK) equipped with a temperature control (Mod. 2416 Carbolite, UK) under hydrogen flow or static air. This furnace was also applied to calcine Degussa TiO₂ P25 powders used to study the effect of calcination temperature.

2.2.2. Reactivity tests:

Tests were carried out in 16 mL glass vials, at 303 K and under magnetic stirring. Glucose solutions were prepared solubilising the substrate in pure water or in a 50/50 v/v ACN/H₂O solution.⁵ Subsequently, 14 mg of catalyst were added to the solution. The reactions were performed for 2 or 4 hours and samples were taken every 30 minutes for the first 2 hours and then every hour until the end of the reaction. Long run tests were carried for 24 hours and samples were taken every 2 hours for the first 6 hours and then at 22 and 24 hours. The TiO₂ (Degussa, P25) was used without any further purification and it was used as blank.

Reactions were run in two different photoreactor systems, one for the UV tests and the other for the visible light tests. These two different systems are needed in order to evaluate correctly the impact of the visible and UV region of the spectrum in the reaction.

For UV tests, a Luzchem photoreactor was used (Mod. LZC-4, Luzchem Research Inc. ON, CAN) equipped with 14 UVA lamps (Mod. Hitachi FL8BL-B) arranged 6 at the top and 4 on each side. The temperature controller was set at 303 K for the whole reaction and the temperature was kept constant with a computer controlled fan. The emission spectra of the UV set of lamps is reported in Figure 12 for UVA lamps.

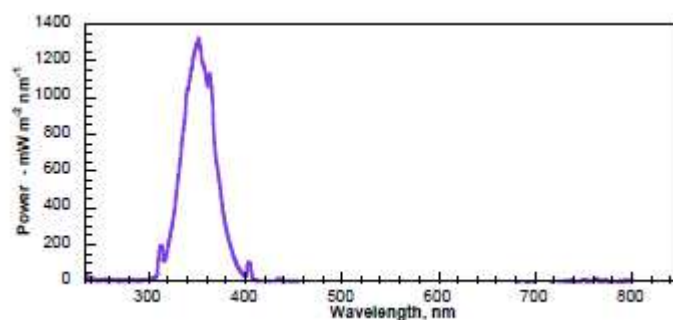


Figure 12: Emission spectrum of the UVA Luzchem lamps measured in the range 235-850nm. Data from www.luzchem.com.

Region	Range, nm	Dose mWm^{-2}	% energy
UVA	316-400	52670	95.51
UVB	281-315	1209	2.19
UVC	235-280	387.5	0.67
Visible	401-700	711.0	1.29
NIR	701-850	187.0	0.34

Table 1: Energy distribution at the target expressed as a percentage of the total energy in the monitored range. Data from www.luzchem.com.

For Visible tests, a Universal Arc Lamp Housing Family (Mod. 66902, Newport, UK) equipped with a Xenon lamp with nominal power 300W was used. Figure 13 is taken from the manual and reports the irradiance spectrum of the lamp. Several filters were used to select only the visible region of the spectrum. In order to remove the IR radiation, the lamp was provided with a distilled water liquid filter (Newport, UK) with circulating water moved by a peristaltic pump (speed 60rpm, Mod. 505S, Watson-Marlow, USA). The transmittance spectrum of the liquid filter is in Figure 14. Furthermore, a colored glass filter (Mod. FSQ-GG420, Newport, UK) with a cut-off value of 420nm was put to maintain only the visible part of the emission spectrum, and its transmittance is reported in Figure 15. The filters were positioned in the order in which they are reported here, in the direction of the beam.

The reaction vial was positioned at a distance of ca. 14cm from the filters on a stirring plate. The shade of the fumed cupboard was covered with tinfoil and kept closed during reaction, in order to avoid the influence from external light sources.

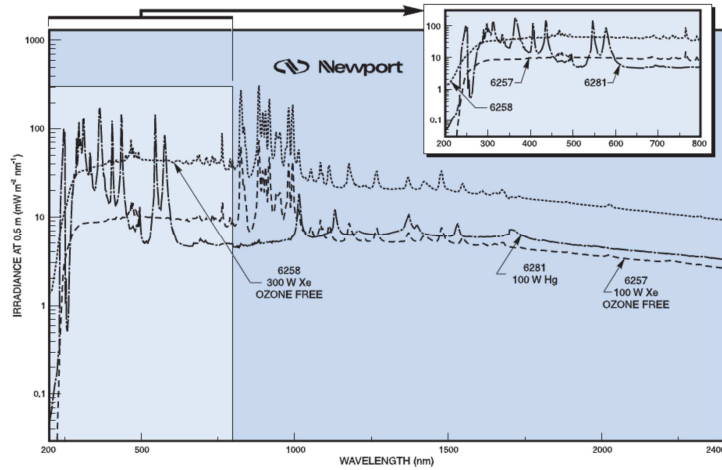


Figure 13: Irradiance spectrum of 300W Xe lamp (dotted line). Vertical axis is in logarithmic scale. Data from www.newport.com.

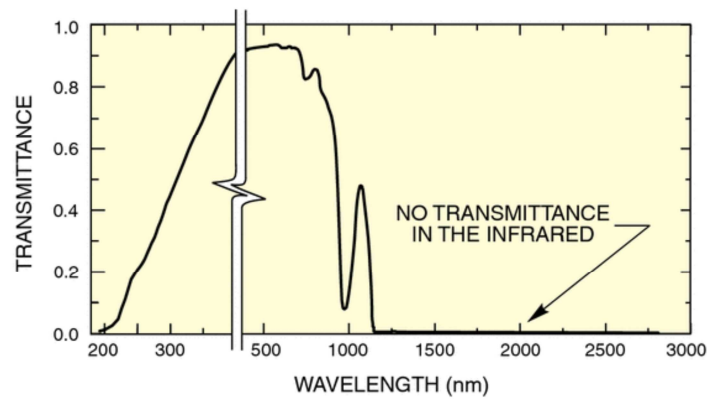


Figure 14: Transmittance spectrum of the distilled water liquid filter. Data from www.newport.com.

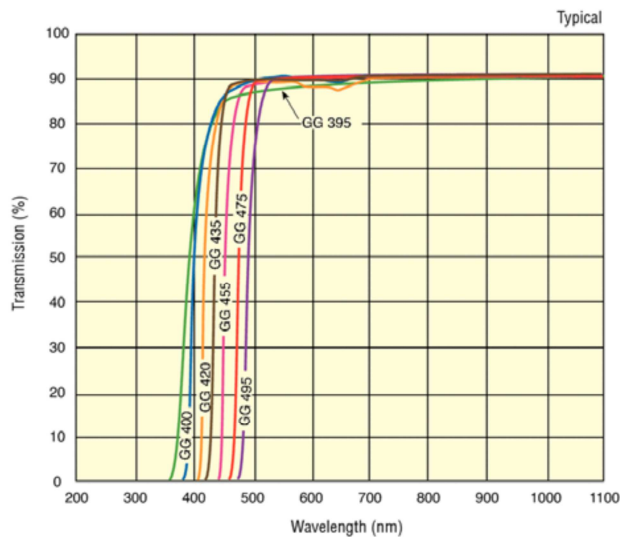


Figure 15: Transmittance spectrum of the colored glass filter Mod.GG420. Data from www.newport.com.

2.2.3. HPLC and Q-TOF analyses:

Reaction solutions consist of a mixture of glucose and several products that need to be identified and quantified. HPLC samples were made taking 0.5 mL of solution and centrifuging them for 60 seconds at 13400 rpm to remove any suspended catalyst particles from solution. Centrifuging time was increase to 3 minutes in case of pure water solvent due to the greater difficult to separate the powders from the solution. Samples were filtered with HPLC filters if the catalyst powders still suspended.

The utilized HPLC (Mod. 1200 Santa Clara, Agilent, USA) was equipped with an inline degasser, a quaternary pump, an autosampler and a column switch. The selected detectors were: Diode Array Detector (DAD) and a refractive index one (RID); the analytical column was an Aminex HPX-87H 300mm×7.8mm, 9 μm particle size (Bio-Rad CA, USA). The system was controlled by the Agilent Chemstation software running on a desktop computer. Sugar standard method was used for the analysis. It consist of 0.65mL/min flux of 25mM sulfuric acid in ultrapure water throughout Aminex HPX-87H column. Injection volume was 10μL, Column Temperature was 65°C and RID Temperature was 50°C.

RI detector was used to measure glucose and arabinose amount while Diode-Array (DA) detector was used to measure gluconic acid and glucaric acid amounts. In fact, RI is a system based on different refractive index between the mobile phase and the analyte, and it is characterized by high sensitivity. DA system adds a new dimension of analytical capability to liquid chromatography because it permits qualitative information to be obtained beyond simple identification by retention time. The major advantage is related to the problem of peak purity. Often, the peak shape in itself does not reveal that it actually corresponds to two (or even more) components. In this case, absorbance rationing at several wavelengths is particularly helpful in deciding whether the peak represents a single compound or is, in fact, a composite peak.⁷³

The injection of each standard solution was repeated 3 times and the values for the retention times (t_r) were obtained by averaging the 15 retention times collected for each sample. As it can be seen in Table 2, the instrument had a linear response in the concentration range considered, and the linearity between the concentration and the signal is confirmed by the linear regression coefficient R^2 which is greater than 0.99 for each of the molecules considered. For DA detection, wavelength of 210nm was used,

because absorbance of glucose is negligible at this wavelength compared to gluconic and glucaric acid absorbance, as recommended by Prati *et al.*¹⁷.

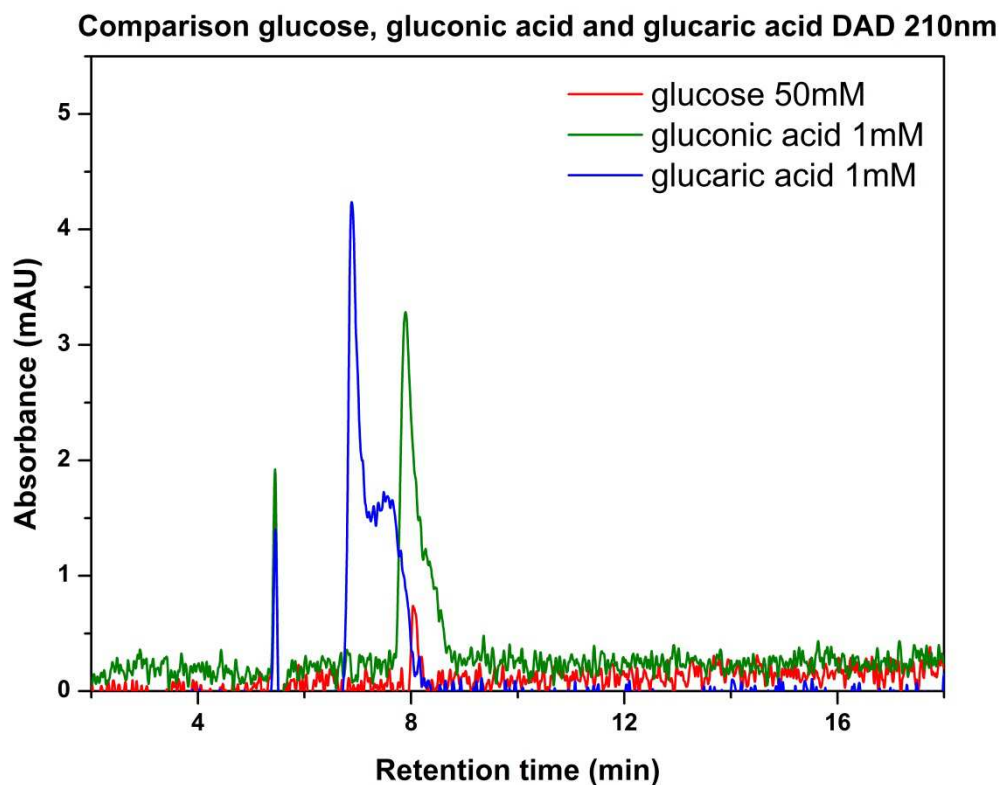


Figure 16: Comparison between Glucose 50mM, Gluconic acid 1mM and Glucaric acid 1mM absorbance at 210nm with DAD.

Difference in absorbance can be seen in Figure 16. Peak of most concentrated glucose solution (50mM) is comparable with most diluted gluconic and glucaric acid solutions (1mM) peaks. Retention times of these three compounds are different, and peaks of glucose and gluconic acid can be evaluated with different detectors (RID for glucose, DAD for gluconic acid). Calibration curves were made in the range of 1-50mM for glucose. Due to low concentrations of some products, calibrations in the range of 0.05-5mM were made for gluconic acid and arabinose.

Calibration curves were made in the range of 0.2-2mM for some by-products, such as formic acid, erythrose and glyceraldehyde. It was impossible to define precisely the amount of erythrose and glyceraldehyde because they coelut. Their peak was evaluated using the erythrose's calibration curve. The selectivity and the production of both were simply calculated as 50% of the total amount.

Stock solution of 50mM was prepared, and then 1-2-5-10-20-50mM solutions were used for calibration curve. Table 2 reported the calibration curve for each substance.

Table 2: Calibration curves of reactant and products recognized.

Analyte	Retention time (min)	Range (mmol l ⁻¹)	Detection	Equation	R ²
Glucose	8.665	1-50	RID	$y = 25537x - 58.818$	0.9999
Gluconic Acid	8.234	0.05-5	DAD 210	$y = 85.308x - 2.8859$	0.9908
Arabinose	10.02	0.05-5	RID	$y = 21878x + 232.63$	0.9996
Arabitol	10.381	0.05-5	RID	$y = 20344x + 183.23$	0.9998
Glyceraldehyde	10.718	0.1-2	RID	$y = 12320x + 698.47$	0.9977
Erythrose	10.871	0.1-2	RID	$y = 12771x - 73.12$	0.9999
Formic Acid	12.944	0.25-2	DAD 202	$y = 36.163 - 0.3251$	0.9988

The accurate mass of the oxidized products obtained from cellobiose were analysed with an Agilent 6510 Q-TOF LC/MS system and interpreted using Agilent MassHunter Workstation Software (Version B.06.00). The column used for the mass spectrometry analysis was a Varian MetaCarb 67H (300 mm x 6.5 mm) (Agilent, USA) kept at 65 °C using a 0.1 % w/w formic acid aqueous solution at a flow rate of 0.8 mL min⁻¹. The Q-TOF was operated in positive ESI mode.

Before the analysis the samples were centrifuged at 13400 rpm for 60 seconds to remove any suspended particles. The glucose and the reaction products were determined using the same commercial standards used for the HPLC analyses. The total ion chromatograms (TIC) for the samples obtained for the reaction with the 10mM glucose solution after 4 hours under visible and UV light are reported in Figure 17. In figure **Errore. L'origine riferimento non è stata trovata.** are also reported the TIC for the same reaction samples along with the TIC relative to the glucose, arabinose, and arabitol standards. It can be seen how the retention time of the arabinose matches the peak observed in the samples, presence confirmed with the presence of the [M-Na]⁺ adduct.

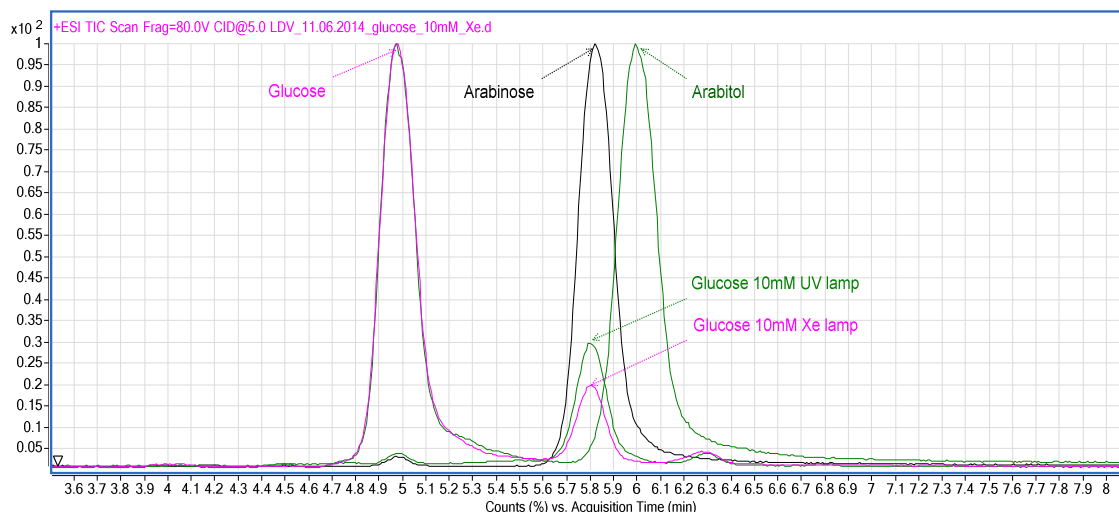


Figure 17: Total Ion Chromatogram for the reaction samples of the 10mM glucose solution with the UV lamp (green) and the Xe lamp (pink) after 4 hours of reaction, compared with arabinose (black) and arabitol (green) standards.

2.2.4. Catalysts characterization:

The solid UV-VIS reflectance spectra were done in the range 200-800nm (Instrument Mod. UV-2550, Shimadzu, USA). Instrument settings were: sampling interval 0.5nm, slit 5nm and BaSO₄ was used as reference. The catalyst powder was put in a quartz sample holder. The Kubelka-Munk function for scattered light was used to transform the reflectance data into absorbance data (Equation 1). The assumption of this theory is that the particle distribution is random and the dimension is much smaller than the thickness of the layer. Regular reflections of the light on the sample are not considered by this law. This function is related to the extinction factor (ϵ) in transmission spectroscopy and it is proportional to the concentration (as Lambert-Beer law) for dilute species. The function, as absorbance, depends on the wavelength (λ).

$$F(R_{\infty})_{\lambda} = \frac{(1 - R_{\infty})^2}{2R_{\infty}} = \frac{k}{s} \propto \frac{\epsilon * c}{s}$$

Equation 1: Kubelka-Munk function.

Where R_{∞} is the absolute Reflectance of the sample but it is typically substituted with the reflectance relative to a standard R'_{∞} (BaSO₄ is a usual standard for UV-VIS range); k is the absorption factor, s is the scattering factor and c is the concentration of the sample.

The relative LSPR band was recognized evaluating the indirect allowed transition. Kubelka-Munk function for the indirect allowed transition $(F(R_{\infty}) * h\nu)^2$ was plot in

function of the energy (eV) and the peak of characteristic LSPR value was observed. Energy bandgap (eV) and wavelength (nm) are mathematically correlated, and the equation is explained below.

XRD instrument (Mod. D8 Advance, Bruker, USA) was equipped with a Cu- $k\alpha$ = 1.54 Å source of radiation and a Ge monochromator in reflection mode. Scans were done for 2h in the range 2θ : 10-80. Catalyst powders were loaded on zero background silica wafers. Nanoparticle TEM images were obtained with JEOL 2100 operated at 200kV. Samples were prepared by dispersion in methanol with sonication and depositing on 300 mesh holey carbon film.

2.3.Synthetic methods:

2.3.3. Synthesis of gold catalyst:

The synthesis follows the method used by Sugano *et al.*²⁷. Concentrated aqueous solution of gold salt was prepared. P25 (1.0 g) was added to water (50 mL) containing H₂AuCl₄ · 4H₂O (45.8 mg). The pH of solution was adjusted to ca. 7 with 1mM NaOH, and the solution was stirred at 353 K for 3 h. The particles were recovered by centrifugation, washed thoroughly with water, and dried at 353 K for 12 h. The powders were calcined at 673 K for 2 hours under hydrogen flow, with the heating rate of 2 K min⁻¹. Metal loadings were calculated as weight percent of total metal on the support as in Equation 2.

$$\% \frac{w}{w} = \frac{m_{metal}(g)}{m_{support}(g)} \times 100$$

Equation 2: Calculation of metal loading of a supported catalyst.

2.3.4. Synthesis of silver catalysts:

This method was used to prepare silver catalysts with different amount of metal loaded. Different AgNO₃ solutions were prepared solubilizing the salt in H₂O. TiO₂ P25 has been suspended in 4ml of H₂O in a vial under magnetic stirring. Subsequently, the appropriate volume of the metal solution has been added and the solution was left to evaporate under magnetic stirring at 353 K. The paste obtained has been then dried overnight under vacuum at 383 K. Calcination has been conducted under static air at 673 K for 3 hours at 2 K min⁻¹.

2.4. Kinetic tests:

2.4.3. Effect of a catalyst/substrate ratio:

First of all, the optimum ratio between catalyst and substrate was investigated maintaining constant the catalyst concentration (1 g/L) as used in literature^{18,74}, while glucose concentration was varied from 2.8mM to 50mM. Different stock solution of glucose were prepared (2.8-5-10-20-50mM) using a mixture of water/acetonitrile 50/50 v/v.⁵ Tests were carried out for 4 hours as previously reported, in Luzchem photoreactor for the UV tests and Xenon lamp for Visible light tests. Analysis were made as reported, but for 50mM tests the samples were diluted 1:1 with a mixture of water/acetonitrile 50/50 v/v due to the calibration range.

2.4.4. Effect of Solvent and lamp power:

The solvent effect was studied using two different solutions and two different catalysts. Luzchem and Xenon lamp systems were respectively used to perform these tests under UV and visible light. Two different glucose stock solutions were made, using pure water and the mixture of water/acetonitrile 50/50 v/v. Concentration of glucose was fixed at 20mM, and 1% Ag/TiO₂ WI and TiO₂ P25 were used. Reaction time was fixed at 2 hours, and samples were taken every 30 minutes. HPLC analyses were carried out as previously reported, without any further dilutions or purifications.

The effect of solvent was crossed with the effect of lamp power. For the study of this effect, a Universal Arc Lamp Housing Family (Mod. 66902, Newport, UK) equipped with a Xenon lamp with nominal power 1000W was used. The reactions were carried out with 14mg of catalyst and 14mL of 20mM glucose solution. Reaction time was set at 2 hours, with the same procedure to take samples.

Furthermore, to compare effect of different light composition, 300W and 1000W Xenon systems were used with and without UV glass filter, in the same reaction conditions used above.

2.4.5. Adsorption of Glucose on catalyst:

Adsorption of glucose was investigated using the same system reported above. A 16mL vials were used at 303 K under magnetic stirring in Luzchem photoreactor. Glucose concentration of 20mM was used, and the stock solution was made of a mixture of

water/acetonitrile 50/50 v/v. The lamps were kept turned off, and tests were carried out in dark conditions for 120 minutes, with an intermediate sample after 30 minutes.

2.5. Photocatalytic tests:

2.5.3. Reactions under visible and UV light:

Visible and UV reactions were carried out using the same system described for the kinetic tests. These systems were used for the investigation several parameters such as the effect of the crystalline structure, the calcination, the metal loading and the different metal used. Reaction time was kept constant at 2 hours, and samples were taken every 30 minutes. Degussa TiO₂ P25 was used as a blank, and silver and gold supported catalysts were compared.

2.5.4. Long term reactions:

Long term reactions were conducted for 24 hours with the same reaction conditions used for the kinetic studies. Luzchem and 300W Xenon lamp systems was used to carry out these tests, and TiO₂ P25, 1% Au/TiO₂ and 1% Ag/TiO₂ were used as catalysts. Samples were taken at 2-4-6-22-24 hours and treated as previously described.

2.5.5. Recycling tests:

The recycling tests of the catalyst were done to see how much activity was lost if the catalyst was reuse several time. The tests were conducted using 1% Ag/TiO₂ as sample catalysts. The reaction conditions used were the same of the photocatalytic tests, with 20mM glucose solution in 50/50 Acetonitrile/water for 2 hours at 303 K under UV and visible light. These tests were divided in three runs. In the first one, 3 reactions were performed using 14mg of catalysts, and catalysts were recovered, centrifuged and washed with water. After an overnight drying, the powders were grinded and 28mg of catalyst was used for the second run, in 2 reaction with 14mg of catalyst each. After 2 hours, the catalyst was recovered and the same procedure was applied to recover 14 mg with which the third run was conducted. The final results obtained for the conversion and selectivity values are the average of the first 3 and 2 runs respectively.

3. Results and discussion:

3.1. Optimization of reactivity tests: catalyst to substrate ratio:

First of all, initial glucose photo oxidation testing focused on finding the optimum catalyst to substrate ratio for the standard Degussa P25. The selected range of glucose concentration varied from 2.8 to 50mM maintaining constant the quantity of the catalyst (1 g/L). The different catalyst to substrate ratios were tested in a water/acetonitrile 50/50 v/v mixture for 4 hours under visible light, using a 300W Xenon Lamp, and under UV irradiation, through Luzchem photoreactor. Selectivity values of the reaction products are comparable for all the catalyst to substrate ratios, but at the lowest glucose concentration the contribution of mineralization is significant. The total mass balances have been calculated, and for the lowest glucose concentration it was of 92% with a glucose conversion of 41% for the Xenon lamp and of 85% with a conversion of 33% for the Luzchem photoreactor.

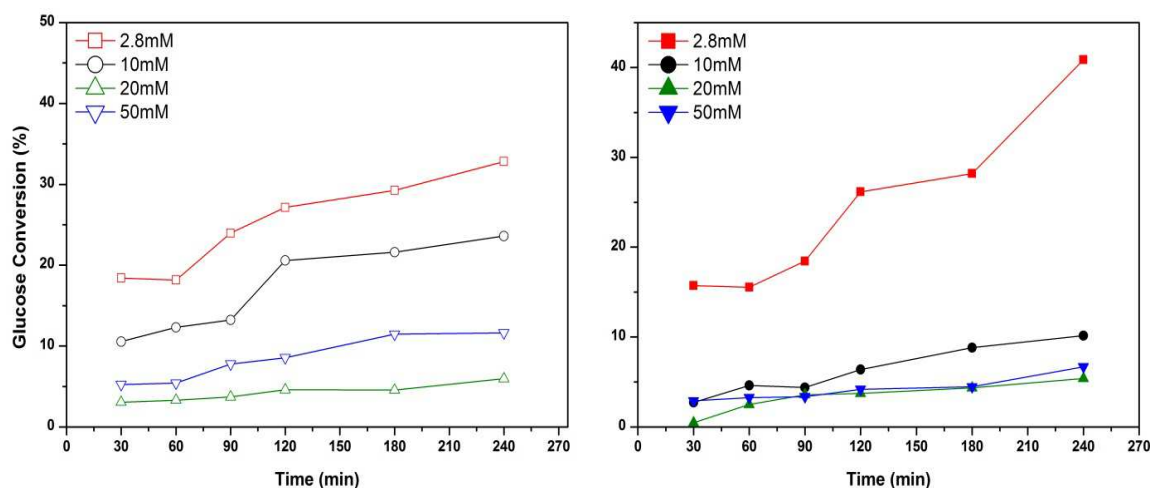


Figure 18: Time-on-line conversion at different catalyst to substrate ratio under UV light (on the left) and visible light (on the right).

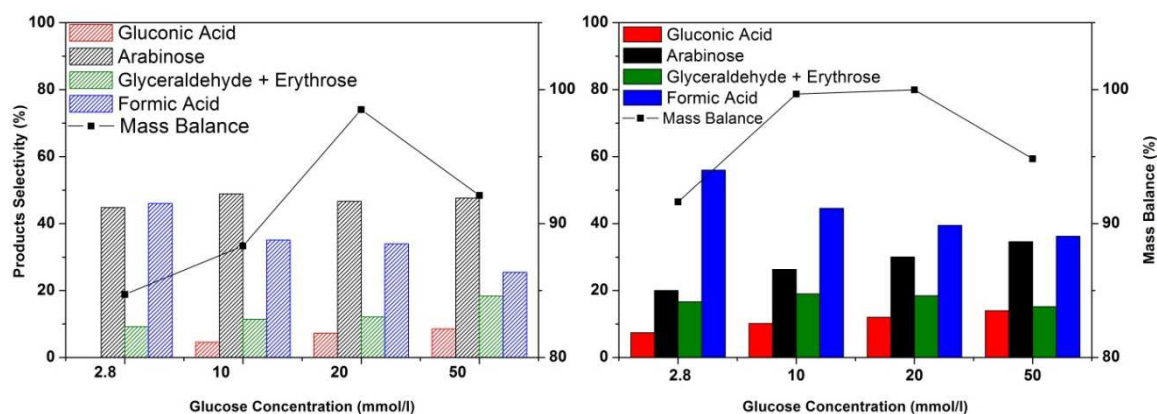


Figure 19: Mass balance and product selectivity at different catalyst to substrate ratio under UV (left) and visible light(right).

Significant differences can be observed in Figure 18 and Figure 19. Selectivity towards arabinose slightly increase under UV irradiation with a similar trends for each concentration of glucose, but gluconic acid selectivities are lower than 10%. Colmenares et al.⁵ suggest a reaction pathway that leads to the production of gluconic acid, glucaric acid and arabitol using UV irradiation. Arabinose was found instead of arabitol leading to the hypothesis of a different mechanism pathway involved instead of the Colmenares one. The mass balance slightly improves increasing substrate concentration in both the reaction systems considered (Table 3). The 20mM glucose concentration was used as a standard solution for all testing, in order to minimize the mineralization reactions to CO₂ and H₂O. The lower mass balance is considered to be due to the formation of CO₂ and H₂ from the total degradation or mineralization pathway which is well documented.^{2,5} Furthermore qualitative offline GC analysis did show the presence of CO₂ and H₂.

The great mineralization of 2.8mM glucose solution seems to be due to the adsorption of glucose in the reactive site and the higher rate of mineralization pathway with the smaller carbohydrates. The adsorption of glucose, at low concentration, seems to be difficult and free reactive sites can be occupied by by-product to give further reaction under visible light and mineralization in case of higher energy as UV light. The trend are the same under visible and UV light, but mineralization is higher under UV. Nevertheless further investigations are required to understand the kinetic order of reaction and the mass transfer involved.

Table 3: Oxidation of glucose results at different catalyst to substrate ratio under UV light.**Products selectivity (%)**

Glucose [mmol/L]	time [h]	Gluconic Acid	Arabinose	Glyceraldehyde + Erythrose	Formic Acid	Mass balance [%]	Conversion [%]
2.8	0.5	14%	36%	15%	35%	96.17%	18.4
2.8	1	0%	47%	10%	44%	92.69%	18.2
2.8	1.5	0%	45%	21%	34%	89.97%	24.0
2.8	2	0%	47%	12%	41%	86.98%	27.2
2.8	3	0%	50%	8%	42%	85.89%	29.3
2.8	4	0%	45%	9%	46%	84.71%	32.8
10	0.5	0%	48%	17%	34%	95.61%	10.5
10	1	0%	50%	11%	39%	95.04%	12.3
10	1.5	6%	44%	10%	41%	96.20%	13.2
10	2	5%	45%	11%	38%	89.39%	20.6
10	3	5%	50%	9%	35%	88.76%	21.6
10	4	5%	49%	11%	35%	88.33%	23.6
20	0.5	0%	45%	24%	31%	99.00%	3.1
20	1	0%	48%	12%	40%	98.86%	3.3
20	1.5	0%	49%	17%	34%	98.91%	3.7
20	2	9%	43%	15%	33%	99.28%	4.6
20	3	7%	45%	8%	40%	99.49%	4.6
20	4	7%	47%	12%	34%	98.51%	6.0
50	0.5	16%	44%	16%	25%	96.62%	5.3
50	1	13%	47%	17%	24%	97.13%	5.4
50	1.5	12%	49%	19%	20%	95.02%	7.8
50	2	11%	48%	17%	24%	94.60%	8.5
50	3	10%	49%	12%	28%	91.88%	11.5
50	4	9%	48%	18%	25%	92.10%	11.6

Table 4 Oxidation of glucose results at different catalyst to substrate ratio under visible light.**Product selectivity (%)**

Glucose [mmol/L]	time [h]	Gluconic Acid	Arabinose	Glyceraldehyde + Erythrose	Formic Acid	Mass balance [%]	Conversion [%]
2.8	0.5	0%	19%	7%	75%	90.94%	15.7
2.8	1	14%	19%	18%	49%	98.72%	15.5
2.8	1.5	9%	23%	18%	50%	100.54%	18.4
2.8	2	10%	22%	19%	50%	96.55%	26.2
2.8	3	8%	21%	19%	53%	99.85%	28.2
2.8	4	7%	20%	17%	56%	91.62%	40.9
10	0.5	0%	26%	22%	52%	100.12%	2.7
10	1	0%	30%	17%	54%	98.71%	4.6
10	1.5	12%	29%	20%	39%	100.67%	4.4
10	2	9%	29%	18%	44%	99.02%	6.4
10	3	9%	25%	20%	46%	99.09%	8.8
10	4	10%	26%	19%	45%	99.67%	10.2
20	0.5	15%	16%	13%	56%	101.57%	0.5
20	1	16%	26%	20%	39%	99.91%	2.5
20	1.5	14%	23%	17%	46%	99.69%	3.6
20	2	15%	23%	14%	48%	100.20%	3.7
20	3	11%	26%	29%	35%	100.88%	4.3
20	4	12%	30%	18%	39%	99.99%	5.4
50	0.5	0%	35%	65%	0%	97.38%	2.9
50	1	0%	45%	55%	0%	97.14%	3.3
50	1.5	0%	61%	39%	0%	97.11%	3.4
50	2	21%	32%	47%	0%	96.94%	4.2
50	3	14%	29%	24%	33%	97.04%	4.5
50	4	14%	35%	15%	36%	94.84%	6.7

3.2. Identification of the pathway and the products of reaction:

The application of photocatalytic processes towards the selective oxidation of glucose has been previously reported by Colmenares *et al.*^{5,75,76} and by Chong *et al.*⁶. These are the first studies in which the first experimental evidences of the selective oxidation of glucose into valuable chemicals (gluconic acid, glucaric acid and arabinose) are reported.

Colmenares *et al.* suggest two parallel schemes of reaction, reported in Figure 31: selective oxidation of glucose, with production of gluconic acid, glucaric acid and arabitol, and total mineralization of reactant into CO₂ and H₂O.

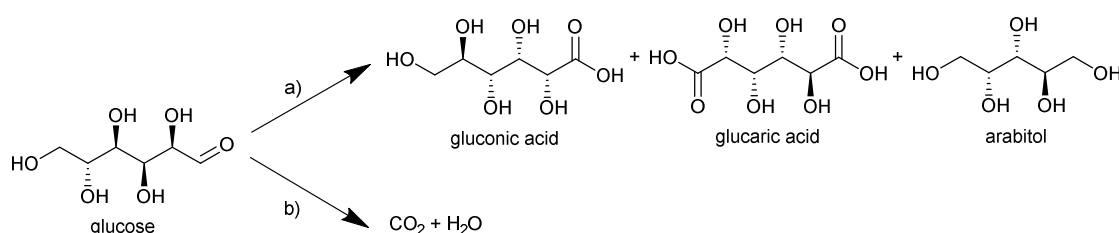


Figure 20: mechanism suggested by Colmenares *et al.*⁵

Chong *et al.*⁶ consider the mechanism of reaction as a sequence of degradations. Glucose is mainly converted into arabinose, with a loss of one carbon of the chain and the formation of formic acid. Arabinose is subsequently degraded into erythrose, with the formation of formic acid. Water is used as mainly main oxidant and the catalyst is made of metal nanoparticles photodeposited on TiO₂.

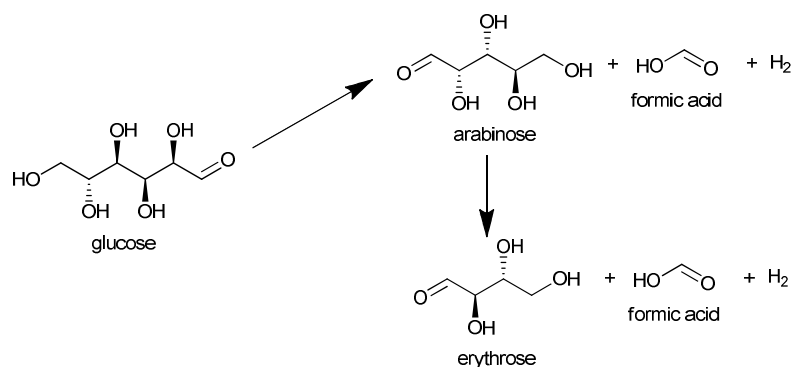


Figure 21: mechanism suggested by Chong *et al.*⁶

Stapley *et al.*⁷⁷ have recently reviewed different mechanisms involved in the decarboxylation of sugar acids for the production of smaller carbohydrates. Ruff degradation is the most interesting reaction mechanism, because it involves a Fenton's like system, composed by Fe(III) and H₂O₂, for the decarboxylation of aldonic acids to produce aldoses with one less carbon. The reaction mechanism is still debated, and multiple reaction pathways are suggested, but they report the experimental evidence that

transition metal ions can catalyse the decarboxylation of organic acids and specifically TiO_2 under UV light. The UV light can generate holes h^+ that can oxidise the organic molecules adsorbed on the surface. The holes, due to their high oxidizing potential, can further oxidize the molecules adsorbed on the surface to CO_2 .

The Ruff degradation occurs via two different reaction pathways, the first producing acid products, the latter producing the aldoses after the decarboxylation of the acid. This reaction pathway corroborates the experimental results obtained, as it was found out that arabinose is the main product of the reaction and gluconic acid is found in smaller concentrations.

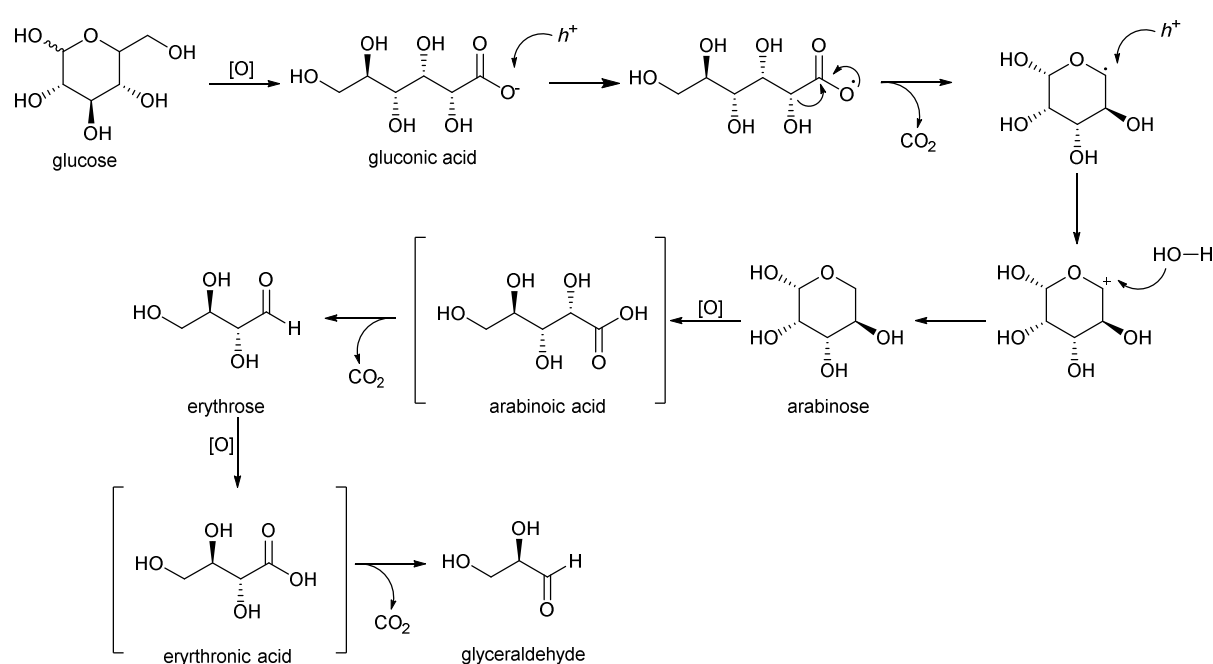


Figure 22: Reaction pathway for the Ruff degradation, following the Kolbe mechanism suggested by Stapley *et al.*⁷⁷ The molecules into brackets are not being isolated.

The reactions considered in this work used TiO_2 -P25 (Degussa), a mixture of anatase and rutile particles with a ratio of 3:1, as a reference material. In fact, this oxide is one of the reference materials in photocatalysis due to its high reactivity.⁷⁸

Moreover, as the produced arabinose (C_5) has a similar structure to the starting glucose, it can undergo the same reaction mechanism thus producing erythrose (C_4) which can further produce glyceraldehyde (C_3). All these products have been identified and their selectivities are reported, but erythrose and glyceraldehyde selectivities have been reported together because they coelute with the HPLC column used, as previously described in paragraph 2.2.3.

Additionally, to investigate the presence of the arabinose instead of the arabitol, as previously suggested by Colmenares *et al.*⁵, HPLC-QTOF analysis have been run and the molecular ions found in the mass spectra rule out definitely the presence of the sugar alcohol from the reaction mixture.

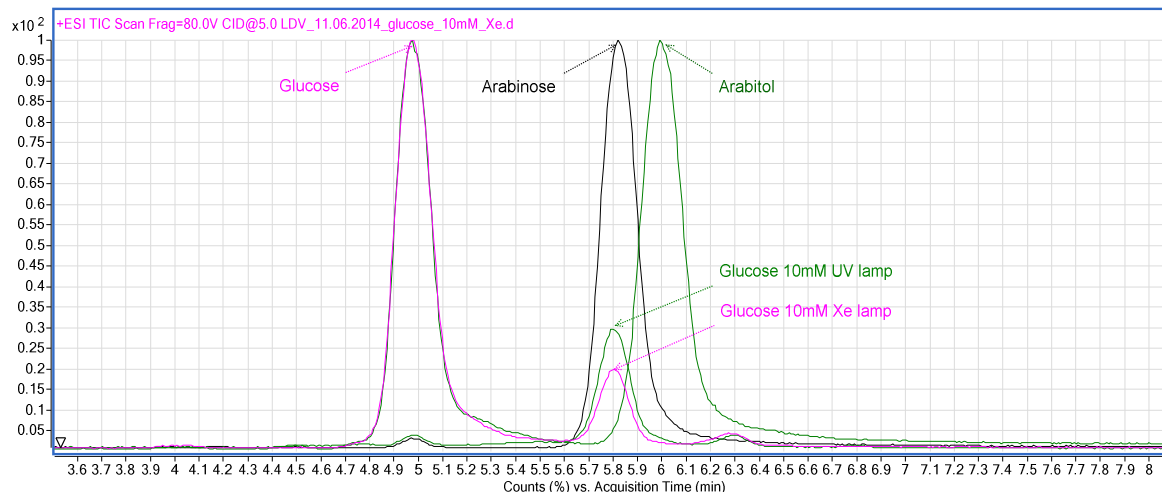


Figure 23: Total Ion Chromatogram for the reaction samples of the 10mM glucose solution with the UV lamp (green) and the Xe lamp (pink) after 4 hours of reaction, compared with arabinose (black) and arabitol (green) standards.

Finally, a gluconic acid and arabinose solutions (20mM) were used under visible light in the same experimental conditions and the products were identified using the same procedure. The chromatograms of these reactions show comparable trends in the products distribution values, as reported in the figures below. (Figure 25 and Figure 26).

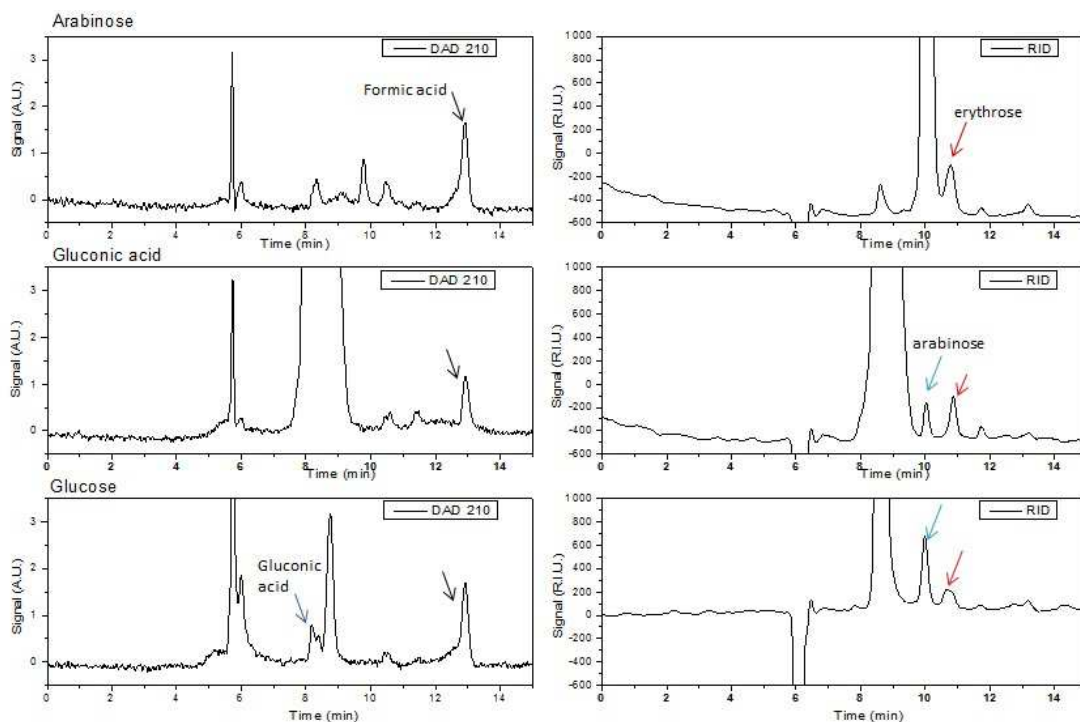


Figure 24: HPLC chromatograms for the reactions with glucose, gluconic acid and arabinose as substrates. RID and DAD at 210nm chromatograms have been reported.

Figure 24 reports HPLC chromatograms of reactions conducted with glucose, gluconic acid and arabinose as substrates.

Formic acid peak can be observed in all DAD 210nm spectra at 12.9 min, and gluconic acid peak can be observed in glucose DAD 210nm spectrum at 8.3min. Presence of arabinose is confirmed by RID spectrum, with peak at 10.0 min. Peak at 10.8 min in RID spectra is coelution of glyceraldehyde and erythrose.

The main products of reactions were identified with HPLC analysis and evaluated with calibration curves previously reported, that confirmed the presence of arabinose as main product, and gluconic acid as co-product. Glyceraldehyde, erythrose and formic acid were identified as by-products of the degradation of the respectively one-more carbon aldoses.

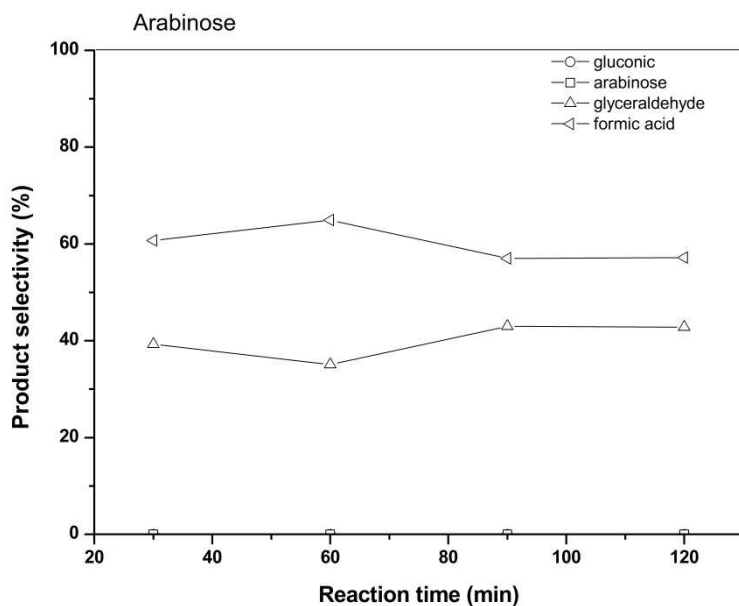


Figure 25: Time-on-line results for the reaction conducted with arabinose as substrate. Selectivity towards the main products are reported.

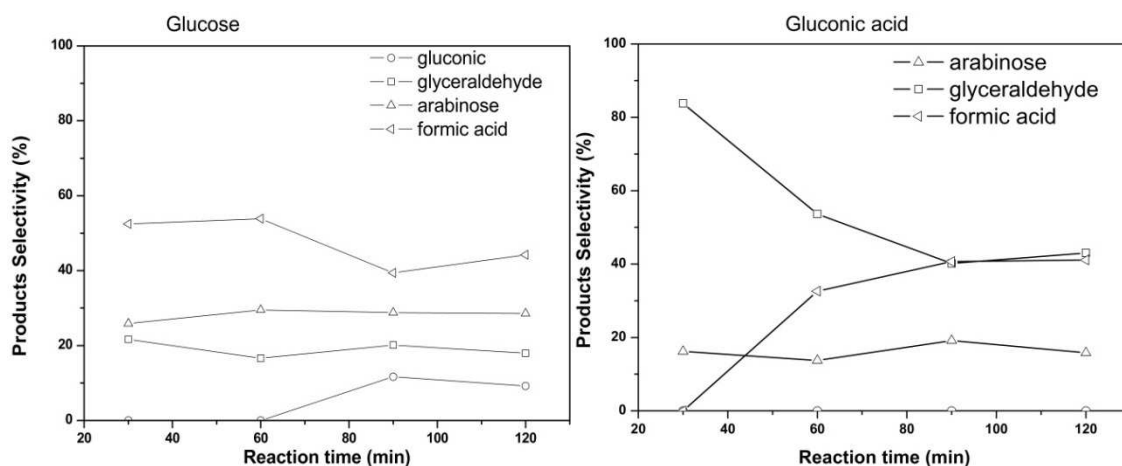


Figure 26: Time-on-line results for the reaction conducted with gluconic acid and glucose as substrates. Selectivity towards the main products are reported.

To look at the stability of the potential intermediates and determine whether arabinose does indeed form from gluconic acid, reactions were conducted with arabinose, gluconic acid, glucose as substrates under visible light. The selectivities are reported in Figure 25 and Figure 26 and show similar trend for every reaction. When glucose was the substrate, arabinose was present already after 30 minutes, then its selectivity went down and presence of gluconic emerged. For gluconic acid as reactant, presence of arabinose was observed and degradation products as glyceraldehyde and erythrose were present as well. When arabinose was utilized as reactant, glyceraldehyde and erythrose were present as degradation products.

Those trends corroborate the hypothesis of Ruff degradation as one of the photochemical pathways. Oxidation and degradation of glucose are competitive reactions, and the latter seems to be the most favourite. The α -scission suggested by Chong seems to be confirmed by the presence of glyceraldehyde, erythrose and formic acid every reaction performed, but the presence of arabinose during the reaction with gluconic acid corroborates the hypothesis of the Ruff's degradation pathway. Those products were used to value selectivities and mass balance of reactions. Selectivities were calculated as a ratio between concentration of the specie and the sum of all products. Mass balance was valuated as a ratio between the total g/L of products and glucose unreacted present at the end of reaction and the mass of glucose present when the reaction started. Missing mass was referred to "other products", such as C₂ species, that cannot be identified precisely, and gases as CO₂ or H₂.

3.3.Role of titania:

3.3.1. Effect of structure:

Titania has different crystalline structures, but only rutile and anatase are photoactive.⁷⁹ The difference between the phases is due to the relative position and coordination of titanium and oxygen atoms in the crystal lattice. Anatase and rutile present a tetragonal structure, but the different position of the atoms in the structure causes different electronic properties in the semiconductor and for this reason the bandgap differs from a phase to another. The values are around 3.4eV for anatase⁸⁰ and 3.0eV for rutile⁴¹ and the excitation falls in the UV region of the spectra.

Several papers reports that the higher activity of anatase than rutile² is due to its higher density of localized states within its bandgap, but there the community is still debating about that. In this work, for example, rutile shows higher activity than anatase and the photo activity of titania P25 seems to be improved when the rutile content is increased. Localized states slow the recombination of charge carriers and improve the production of surface adsorbed hydroxyl radicals. Rutile presents a higher kinetic of electron-hole recombination due to its larger grain size and lower capacity of absorbing species compared to anatase³⁵. Presence of impurities, particle dimension and the surface area are some features of the synthesis that can affect the electron-hole recombination, determining an influence in the catalytic activity of these phases.⁸¹

Ohno *et al.*⁷⁸ demonstrated that the anatase and rutile phases exist separately and they form agglomerates with an average particle size of 25 and 85nm respectively. Additionally, it is reported that the rutile particles in the P25 are considered to have Ti_3^+ ions as during the synthetic process the TiO_2 powders are treated at elevated temperatures. The Ti_3^+ species are considered to be the electron donors. The activity of the different phases of titania was evaluated towards the reaction of oxidation of glucose under UV and VIS irradiation, following the same procedure previously reported.

The activity of rutile and anatase phases was compared with Degussa P25 and later with a physical mixture of rutile and anatase.

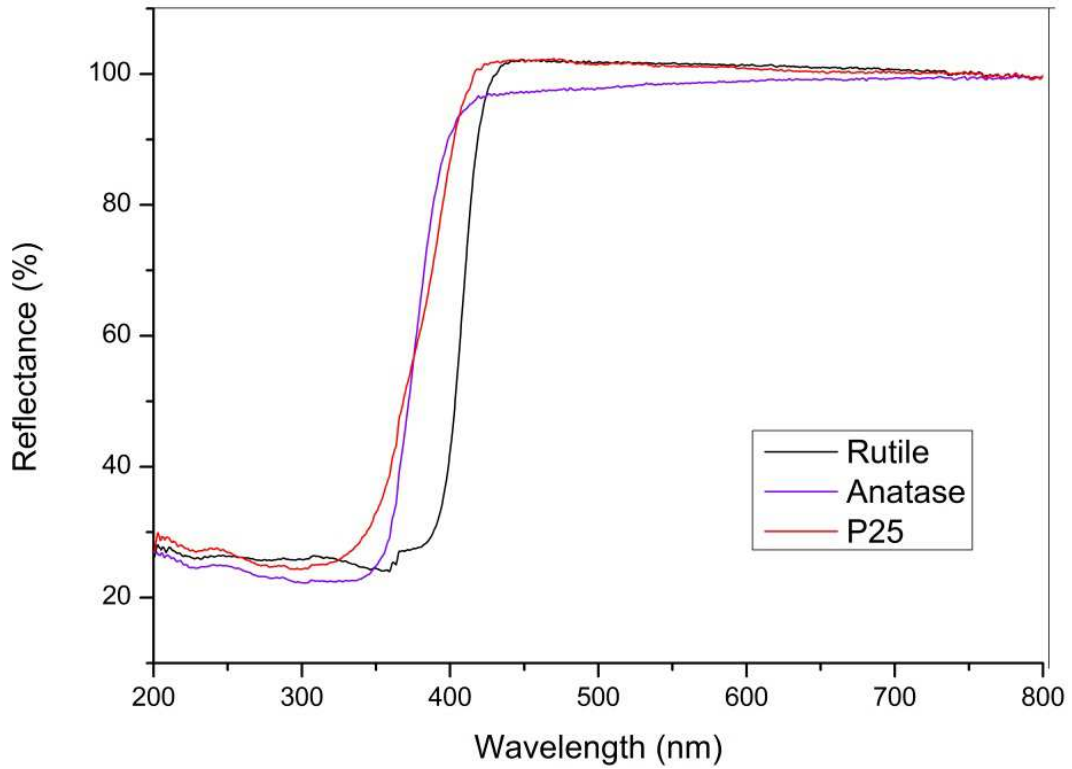


Figure 27: Diffuse reflectance UV/Vis of the different crystalline phases of TiO₂ compared with Degussa P25.

Figure 27 shows the solid UV/VIS spectra of Anatase, Rutile and Degussa P-25. The difference in activity between anatase and rutile can be explained in relation to the bandgap of the two crystalline structures. In fact, the bandgap position for a semiconductor can be determined experimentally from its solid UV-VIS spectrum by extrapolation of the cut-off value from the graph.⁸² Energy bandgap and cut-off wavelength are mathematically related:

$$E = \frac{h \times c}{\lambda} = \frac{4.135 \times 10^{-15} \times 3 \times 10^8}{\lambda}$$

Equation 3: Relation between the energy bandgap (E) and the cut-off wavelength (λ).

Where E is the bandgap energy (eV), h is the Planck constant (eV×s), c is the speed of light (m/s) and λ is the cut-off wavelength in the UV-VIS spectrum (m).⁷ The λ calculated from the above reported bandgaps is respectively 414nm for rutile and 365nm for anatase. This determines that rutile absorbs more energy than anatase because its cut-off value comprehends all the range of the spectrum of UVA emission. On the other hand, anatase only covers the energy given by the emission up to 365nm (emission spectrum in section 2.2.2). Degussa P25 spectrum seems to display a comparative trend with anatase

from 200nm to 350nm and with rutile from 350nm to 800nm. Those trends follow the hypothesis of a synergic effect of these two phases in Degussa P25.

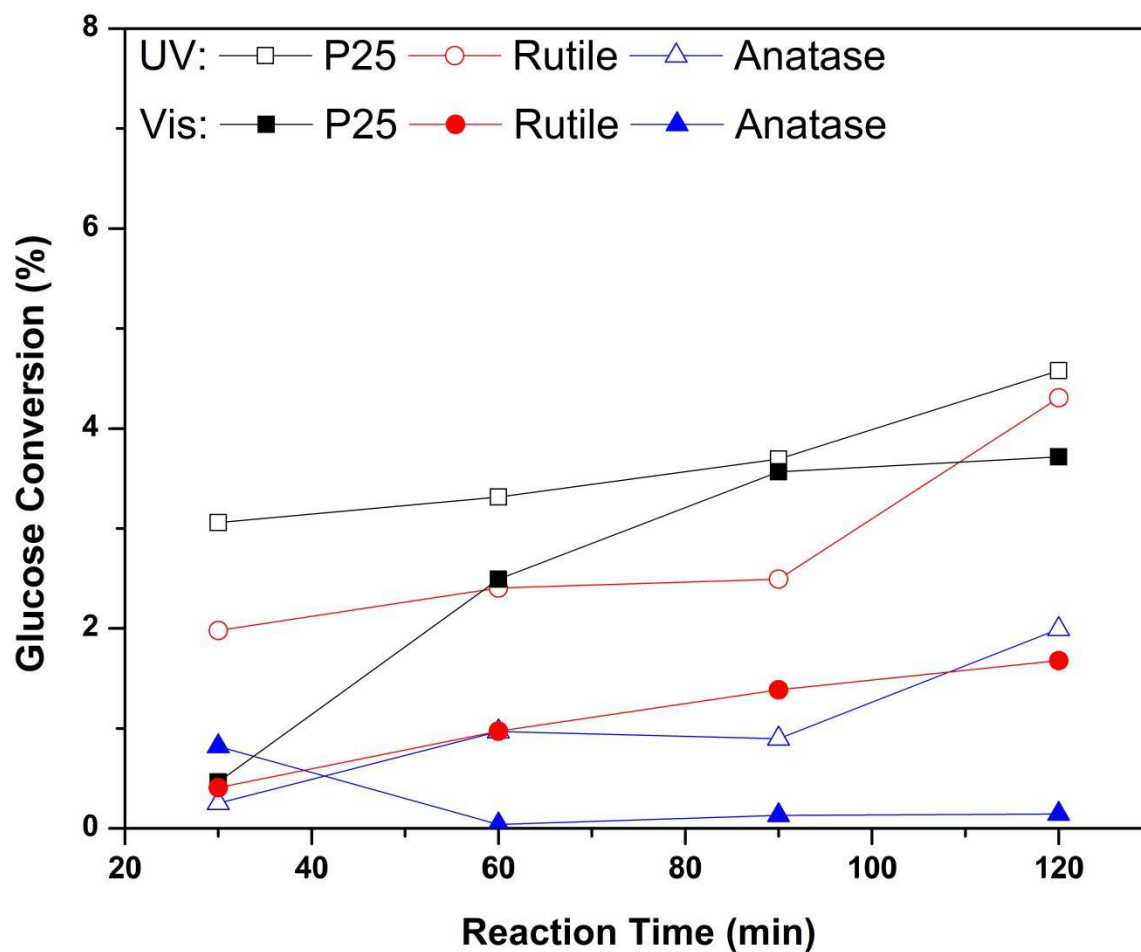


Figure 28: Time on line of the reactions run with the different catalysts under UV and Visible radiation.

In Figure 28 the time on line results of the different TiO₂ crystalline structures (rutile and anatase) are compared against the Degussa P25. The P25 shows higher conversions under UV and visible light, while rutile seems to be a better catalyst than anatase under UV and visible light. Glucose conversion is generally lower than 10% despite the change in the illumination source.

Table 5: Effect of the different TiO₂ crystalline structures on the products selectivity, products concentrations and total mass balance for the reactions run under Visible light [a] and UV light [b].

Catalyst	Products Selectivity [%]				Products Concentration (g/L)						
	Gluconic Acid	Arabinose	GA+Erythrose	Formic Acid	Glucose unreacted	Gluconic acid	Arabinose	GA+erythrose	Formic Acid	Mass balance (%)	Conversion (%)
Rutile ^[a]	0%	39%	41%	20%	3.520	0.0000	0.0284	0.0206	0.0044	99.82	1.7
Anatase	0%	50%	50%	0%	3.652	0.0000	0.0037	0.0025	0.0000	100.03	0.1
P-25	18%	28%	17%	37%	3.499	0.0411	0.0496	0.0206	0.0196	99.88	3.7
Rutile ^[b]	8%	32%	31%	29%	3.497	0.0181	0.0553	0.0365	0.0151	99.12	4.3
Anatase	24%	36%	12%	28%	3.581	0.0296	0.0330	0.0078	0.0080	100.16	2.0
P-25	10%	50%	17%	22%	3.481	0.0216	0.0809	0.0192	0.0111	99.06	4.6

P25 is the only one that shows selectivity towards gluconic acid after 2 hours under visible light (Table 5). Under UV irradiation the gluconic acid selectivity improves slightly but the P25 remains the most selective catalyst towards the acid relative to pure rutile and anatase. It is clear how the coexistence, in P25, of the two different phases of rutile and anatase has synergic effect. For this reason, a physical mixture of the two phases, with a ratio of rutile/anatase of 3:1, was used to simulate the properties of the Degussa P25 under visible and UV light. Results are displayed in Table 6. Surprisingly, the conversion values obtained under visible light of 1.1% and under UV light of 3% are higher than the equivalent values of the pure phases considered. This results confirmed the results previously reported⁷⁸ in which some synergic effects by the contact between the rutile and anatase crystallites was reported to be present without the two phases coexisting on the same solid. Therefore, the high catalytic activity and its importance in photocatalysis justifies the choice of using titania P25 as a support for the synthesized catalysts in this study.

Table 6: Effect of the physical mixture of rutile and anatase in a ratio 3:1 on the products selectivity, products concentrations and total mass balance for the reactions run under visible[a] and UV light [b].

time (h)	Products Selectivity [%]				Product concentrations (g/L)						Conversion (%)
	Gluconic Acid	Arabinose	GA+Erythrose	Formic Acid	Glucose unreacted	Gluconic acid	Arabinose	GA+erythrose	Formic Acid	Mass balance (%)	
30 ^[a]	0%	30%	70%	0%	3.608	0.0000	0.0030	0.0050	0.0000	100.14	0.1
60	0%	38%	62%	0%	3.601	0.0000	0.0091	0.0104	0.0000	100.26	0.3
90	0%	32%	29%	39%	3.593	0.0000	0.0179	0.0112	0.0068	100.51	0.5
120	17%	25%	21%	37%	3.570	0.0204	0.0236	0.0137	0.0106	100.75	1.1
30 ^[b]	0%	33%	28%	39%	3.553	0.0000	0.0223	0.0133	0.0081	99.98	1.2
60	12%	28%	21%	39%	3.551	0.0181	0.0338	0.0179	0.0144	101.06	1.3
90	11%	34%	19%	36%	3.536	0.0181	0.0437	0.0172	0.0144	100.88	1.7
120	10%	29%	14%	46%	3.491	0.0250	0.0538	0.0186	0.0259	100.47	3.0

3.3.2. Effect of calcination temperature:

Effect of calcination temperature in the structure of Degussa P-25 was determined. The aim of this study was the study of the effect in the catalytic activity of Degussa P-25 in order to discriminate every single effect in the study of supported metal nanoparticles as photo-catalyst. To assess the effect of the structure of the Degussa P25, the catalyst was calcined in air at 3 different temperatures 400°C, 500°C and 600°C at 2°C/min for 2 hours. The catalyst was subsequently analyzed with XRD to determine changes in the crystalline structure of the solid. Influence of temperature in crystalline structure and photochemical properties of TiO₂ have already been demonstrated.⁸³

Figure 29 shows the diffraction pattern for untreated TiO₂ P25 and calcined ones and it indicates that the content of the different phases in TiO₂ changes increasing the calcination temperature.

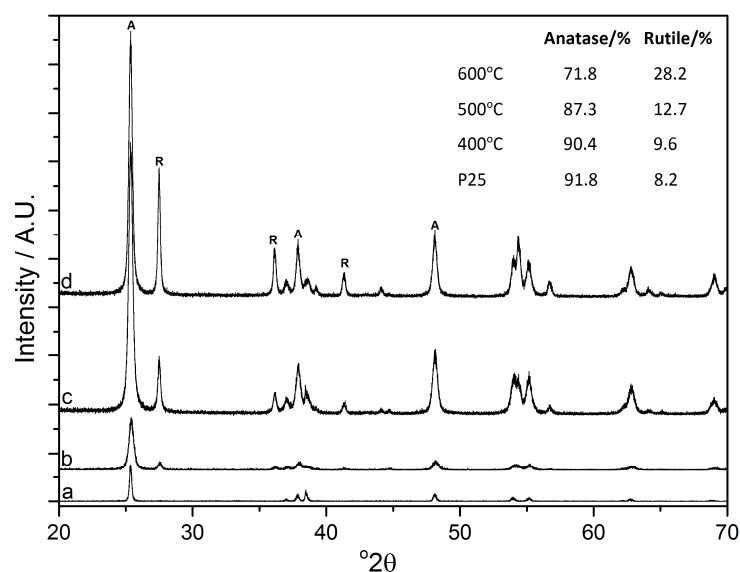


Figure 29: XRD for a) TiO₂ –P25, b) 400°C, c) 500°C, d) 600°C calcined TiO₂.

Solid UV-Vis shows, in Figure 30,a difference in reflectance for 600°C calcined P25. The solid UV/Vis spectra recorded for the different TiO₂ crystalline phase (Figure 27) and the samples calcined at different temperatures (Figure 30) show how, increasing the temperature, the profile of the sample calcined at 600°C is similar to the one recorded for rutile. In fact, at high temperature the Degussa P25 changes its crystalline structure and the initial ratio of 3:1 anatase rutile is not respected anymore. Anatase crystallites starting to change their structure to rutile at 600°C, as observed by Dostanic *et al.*⁸⁴

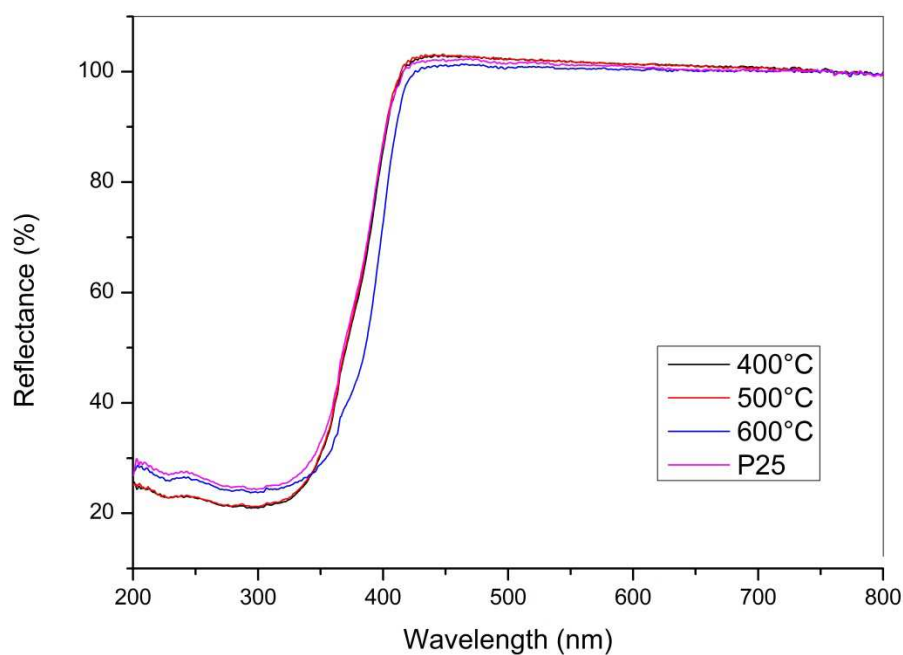


Figure 30: Diffuse UV/Vis reflectance of Degussa P25 samples calcined at different temperatures.

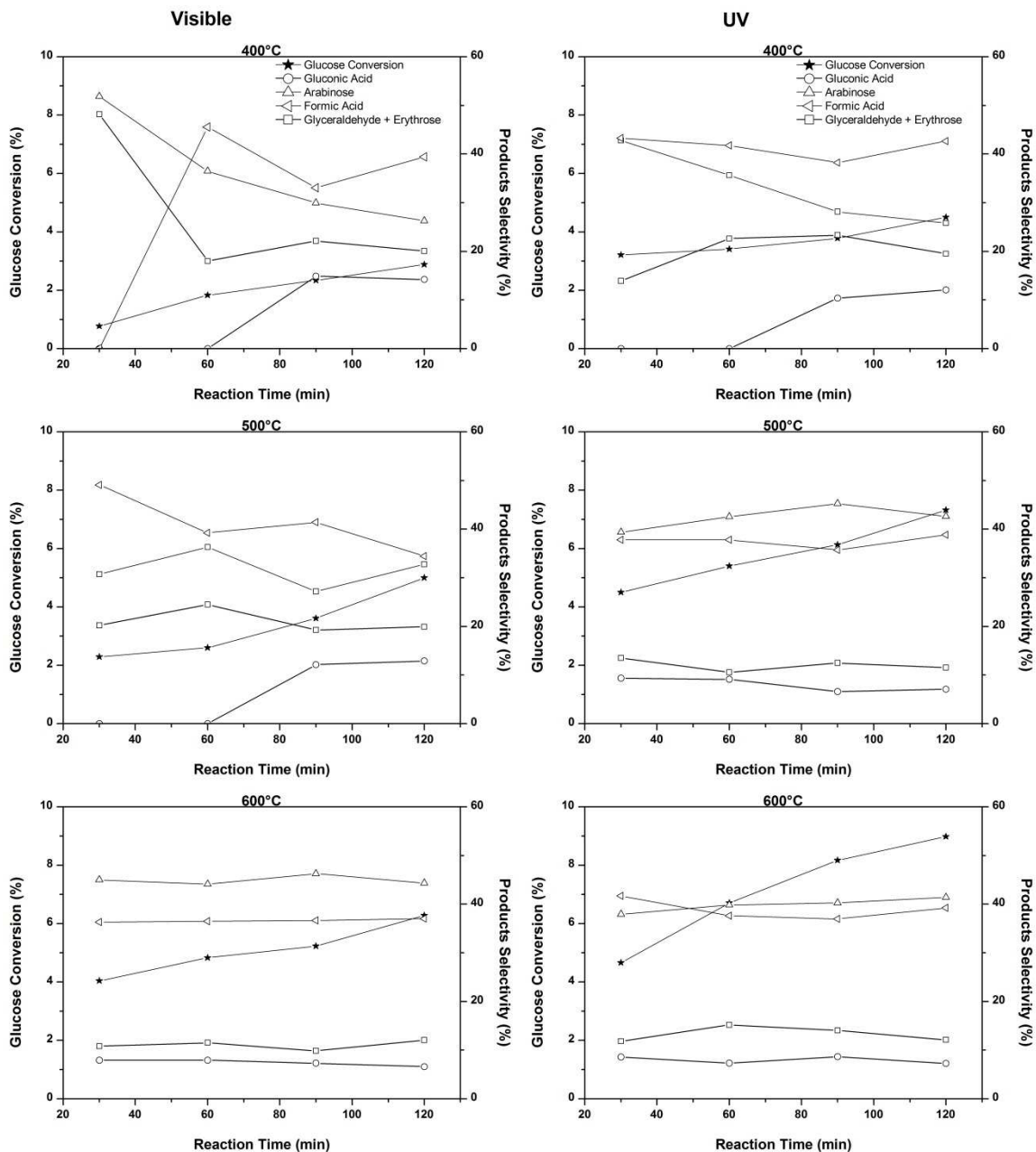


Figure 31: Time on line results of the calcined $\text{TiO}_2\text{-P25}$ at different temperatures. On the left columns the values of the selectivity towards arabinose ($-\Delta-$), gluconic ($-\circ-$), formic acid ($-\triangleleft-$), glyceraldehyde and Erythrose ($-\square-$) and the glucose conversion ($-\star-$) are reported for the visible light (Xenon lamp) and UV light (Luzchem).

Table 7: Effect of the calcination temperature on the P25 on the products selectivity, products concentrations and total mass balance for the reactions run under UV [a] and visible light [b]

Catalyst	Products Selectivity [%]					Products Concentration (g/L)					
	Gluconic Acid	Arabinose	GA+Erythrose	Formic Acid	Glucose Unreacted	Gluconic acid	Arabinose	GA+erythrose	Formic Acid	Mass balance (%)	conversion (%)
P25 ^[a]	9%	43%	15%	33%	3.481	0.0216	0.0809	0.0192	0.0189	99.28	4.6
400°C	7%	43%	11%	39%	3.335	0.0319	0.1471	0.0278	0.0411	99.57	7.3
500°C	7%	44%	12%	37%	3.372	0.0273	0.1410	0.0269	0.0361	100.15	6.3
600°C	7%	41%	12%	39%	3.391	0.0273	0.1197	0.0245	0.0348	96.56	9.0
P25 ^[b]	15%	23%	14%	48%	3.499	0.0411	0.0496	0.0206	0.0310	100.20	3.7
400°C	14%	26%	20%	39%	3.538	0.0319	0.0452	0.0241	0.0208	100.47	2.9
500°C	12%	26%	20%	43%	3.558	0.0250	0.0410	0.0217	0.0208	98.42	4.5
600°C	13%	33%	20%	34%	3.539	0.0250	0.0487	0.0207	0.0157	97.96%	5.0

During the UV testing, a significant difference in glucose conversion was observed. Calcined P25 shows an increasing trend from 400°C to 600°C., but the reaction mass balances decrease with the same trend, from +99% with 400°C and 500°C catalyst to 96% with 600°C catalyst. In other words, a greater degree of mineralization was observed with the P25 calcined at 600°C probably because of it is changing in crystalline phase during the calcination treatment. Arabinose and gluconic acid production were generally the same for each P25 catalyst.

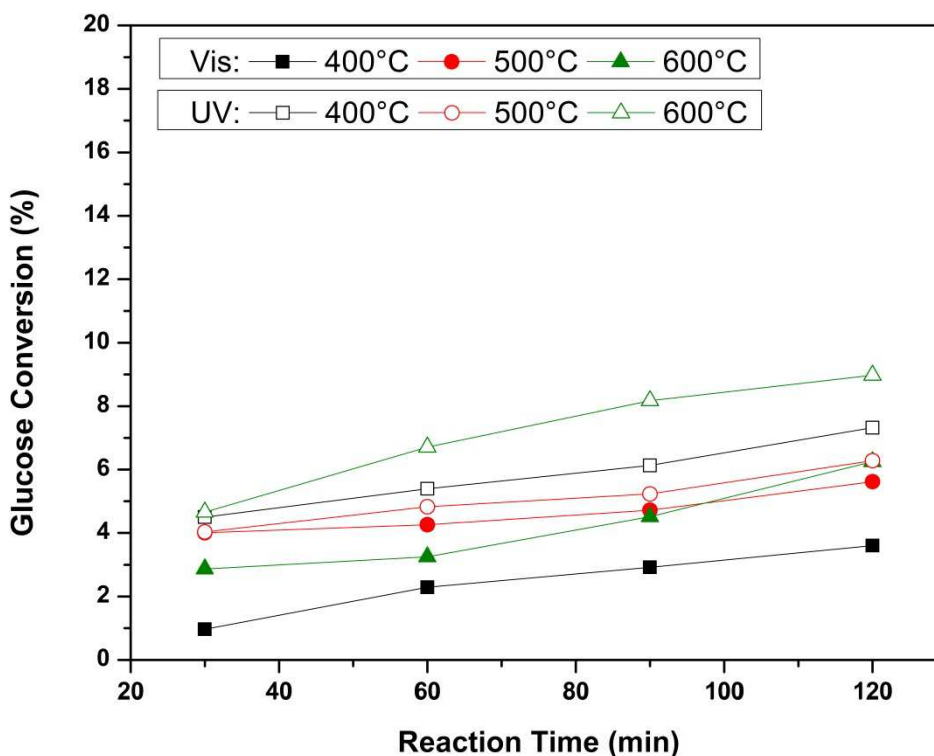


Figure 32: Time-on-line of glucose conversion under UV and visible light.

Figure 32 shows glucose conversion under UV light and visible light. The temperature treatment seems to improve the catalytic activity of Degussa-P25 TiO₂, because there is a general enhancement of glucose conversion with the calcined catalysts. TiO₂ calcined at 600°C shows a significant enhancement of glucose conversion, while the difference between 400°C and 500°C TiO₂ P25 is just 1%.

A slightly decrease in mass balance can be observed for 600°C calcined TiO₂ P25 under UV irradiation, despite a higher conversion than the others. Arabinose production was higher than visible testing, and gluconic acid production as well. A difference in diffusive reflectance between TiO₂ P25 and the one calcined at 600°C, illustrated in Figure 30, is reflected in the differences in terms of selectivity and conversion along the reaction.

Under visible light, conversions are generally lower than the reactions conducted under UV light, but P25 treated at 600°C exhibits an higher conversion than others catalysts. A general trend can be observed between P25 calcined at different temperatures, from the lowest values of conversion of the 400°C one to the highest of the 600°C one, but most interesting is the gluconic acid trend shows in Figure 33.

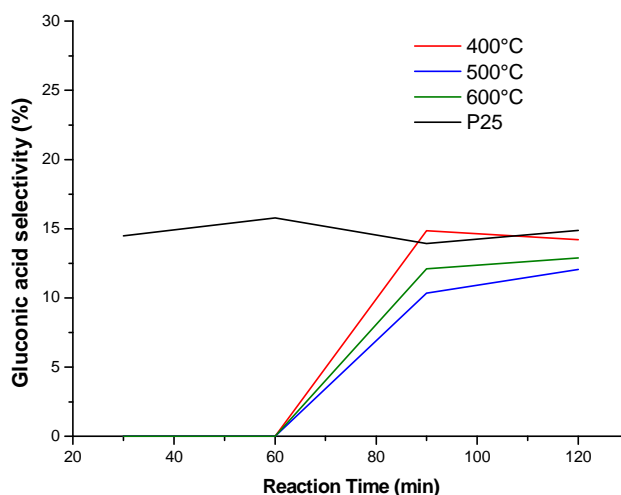


Figure 33: Time-on-line selectivity towards gluconic acid for Degussa P25 and calcined TiO₂ under visible light.

Figure 33 displays Time-on-line of gluconic selectivity. The final results obtained are not so different from each other, with the selectivity towards the acid around 15-18%, but the calcined catalysts start to catalyze the oxidative pathway of the glucose reaction after 60 minutes. In fact, gluconic acid appears after 60 minutes with a final selectivity of 15% for each calcined catalyst, while the production of the acid by TiO₂ P25 starts at the beginning of the reaction time and the final result is the highest.

3.4. Effect of the solvent and irradiation power:

Solvent and irradiation power were investigated, after crystalline structure of titania. Differences between pure water and mixture of acetonitrile/water were observed, and differences between 300W Xenon Lamp and 1000W Xenon Lamp were investigated as well. A 20mM glucose solution in pure water was used. First of all, solvent effect was evaluated using the same 300W Xenon Lamp, with and without a 420nm cut-off filter. Subsequently, 1000W Xenon Lamp was used in the same conditions. A comparison between pure water and mixture of acetonitrile/water was possible, but also an investigation of difference in irradiation power in the same type of solvent.

Degussa P25 was compared with 1% Ag on TiO₂ synthesized with wetness impregnation method.

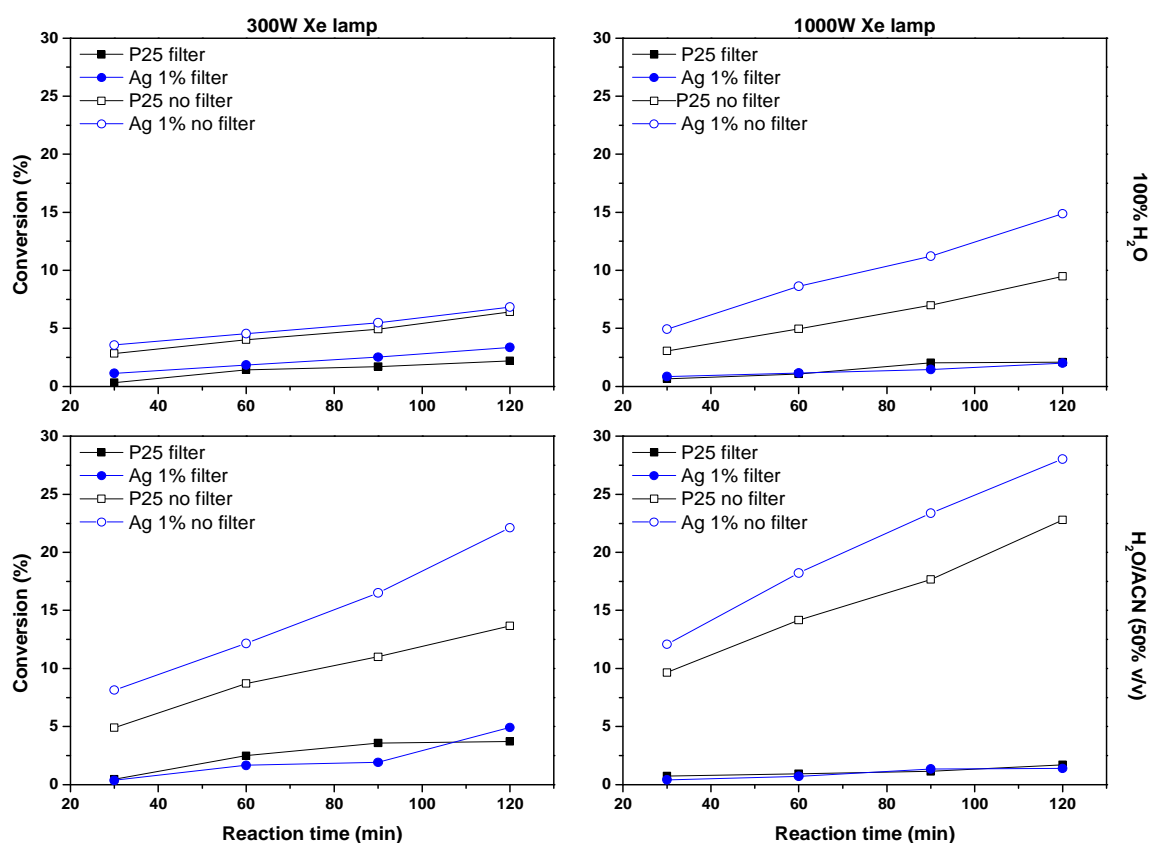


Figure 34: Time on line data of the reactions run with P25 and Ag/TiO₂ (1% w/w) using two different Xe lamp (300W and 1000W) equipped with visible cut off filters ($\lambda=420\text{nm}$). The top two graphs display the values obtained using H₂O as a solvent and the bottom ones using the 50/50 v/v H₂O/ACN mixture. The values without filters are reported using the empty symbols (\square, \circ) and the values obtained with the lamps equipped with the filters are reported with the full symbols (\blacksquare, \bullet).

After having investigated the effect of the crystalline structure, the effect of the presence of the acetonitrile as a co-solvent in the reaction medium was analyzed. In (Figure 34)

the effect of the solvent is evaluated for the two lamps and it can be seen how by incrementing the power of the lamp, there is a general increase in the glucose conversion. As the Xe lamps emits in various regions of the electromagnetic spectrum, as reported in paragraph 2.2.2, with the removal of the visible light filters, the part of the spectrum with a wavelength $\leq 420\text{nm}$ is able to excite also the TiO_2 and the Ag supported onto the catalyst surface with the intraband mechanism. Therefore, higher conversion values were expected for the reactions run with no filters. Mass balances show a enhanced mineralization when the visible light filters were removed. Presence of the part of spectrum with a short wavelengths combined with the presence of Ag nanoparticles, that act as antennas, increase mineralization of the reactant. Those combined effects are highlighted by acetonitrile/water mixture. In fact, mass balances are around 100% when UV filters were used, independent from catalyst, lamp and solvent used, but they go down when the filters were removed. Pure water limits that effect, in fact the mass balance keeps around 97% with 300W lamp, and go down to 93% with Ag catalyst with 1000W lamp.

Acetonitrile/water mixture seems to enhance mineralization process, because the mass balances go down to 95% for P25 and 90% for the supported catalyst with 300W lamp, but they fall to 90% and 87% with 1000W lamp.

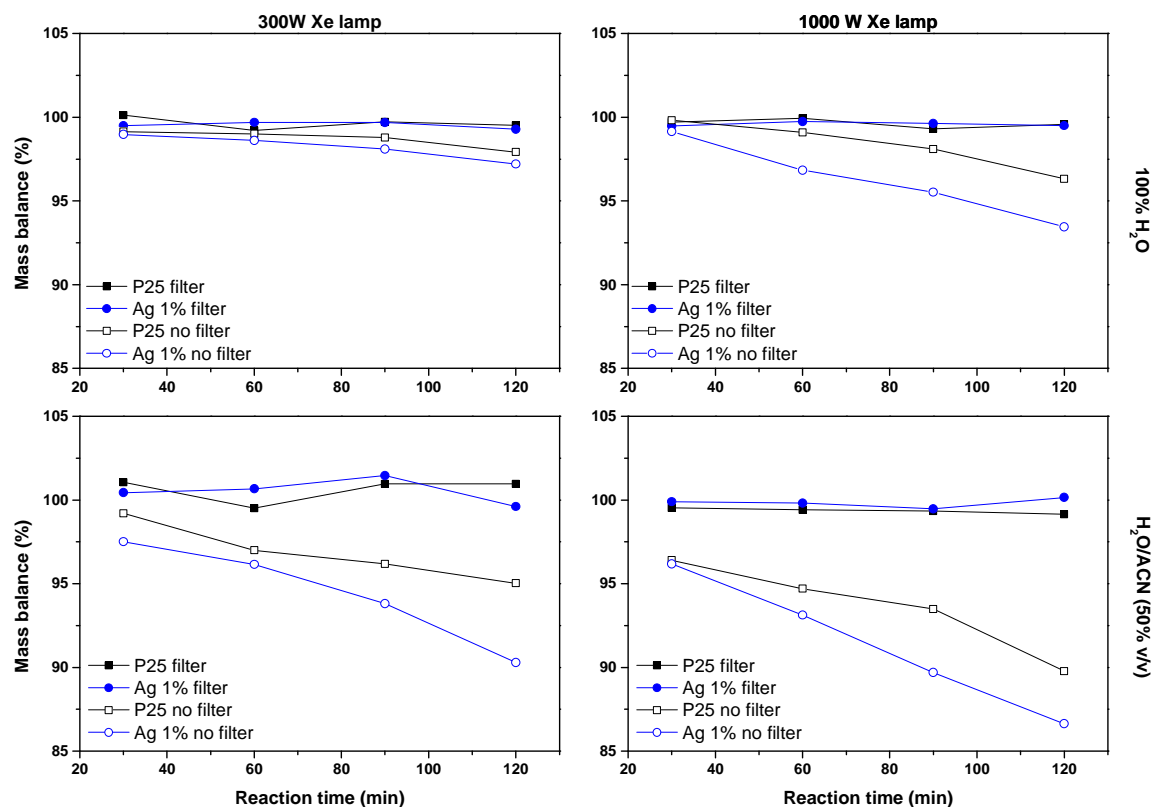


Figure 35: Time on line mass balance of the reactions run with P25 and Ag/TiO₂ (1% w/w) using two different Xe lamp (300W and 1000W) equipped with visible cut off filters ($\lambda=420\text{nm}$). The top two graphs display the values obtained using H₂O as a solvent and the bottom ones using the 50/50 v/v H₂O/ACN mixture. The values without filters are reported using the empty symbols (\square, \circ) and the values obtained with the lamps equipped with the filters are reported with the full symbols (\blacksquare, \bullet).

Irradiation from 1000W lamp with 420nm cut off filters hindered arabinose and gluconic production, independent by solvent used. Conversion was lower than using 300W lamp, and selectivity towards those main products were not high. That kind of irradiation seems to promote glyceraldehyde and erythrose production, so Ruff degradation was enhanced. When visible light filters were removed, a significant improve in conversion and main products selectivity were observed. Conversions increased linearly, and 22-28% of conversion were reached with 1000W lamp and mixture as solvent, when in pure water conversion was lower. Trends of selectivity were pretty much the same when visible filters were removed, independent by solvent used. In fact, Arabinose selectivity was around 63-67% with 1000W lamp, and 52-60% with 300W lamp. Under 1000W irradiation, gluconic selectivity was higher with pure water (8-12%), but in terms of production was the same of using ACN/H₂O mixture.

Under 300W irradiation, conversions and trends were different. Conversions, when visible light filters were used, were slight higher with Acetonitrile/water mixture. When

420nm filters were removed, a significant difference in terms of conversion was observed. In fact, conversion with solvent mixture reach 13.7% with P25 and 22% with 1%Ag/TiO₂, instead of 6-7% when pure water was used. Trends were the same, but despite of higher selectivity towards gluconic, production of that was significant with solvent mixture. Gluconic selectivity followed a common trend, in those cases, and it kept constant during every reaction but with supported catalyst in pure water. There, gluconic produced was kept constant, and its selectivity went down from 34% to 15%. A “plateau-like” step seems to be reached.

Table with product selectivity and concentration, mass balance and conversion of the reactions run with different solvent, lamp power and cut-off filters can be observed in the appendix (Table 10).

The effect of the solvent in the reaction under UV irradiation was investigated as well. Solvent mixture and pure water are used with the same catalysts used above. Conversion shows a significant difference between ACN/H₂O mixture (9%) and pure water (6%) when supported catalyst was used. Selectivity towards formic acid is influenced by water under UV light. It appears after 30minutes and keeps around 10% with Degussa P25, and after 60minutes it appears when Ag catalyst is used. Selectivity's trends of “no-filter” reactions and reactions under UV irradiation are really close. UV impact in this kind of photo reaction seems to be high and, despite of its low content in solar light, its influence can be observed most of all regards arabinose selectivity. The presence of acetonitrile seems to be influent for the reaction pathway, but its role cannot be explained yet. Colmenares *et al.*⁵ suggest that acetonitrile can stabilize the carboxylic acids by solvation, suppressing any further oxidation, and minimizing carboxylic acid adsorption onto the surface and enhancing product selectivity. Further and deeper investigation are required to explain completely its role in the reaction mechanism.

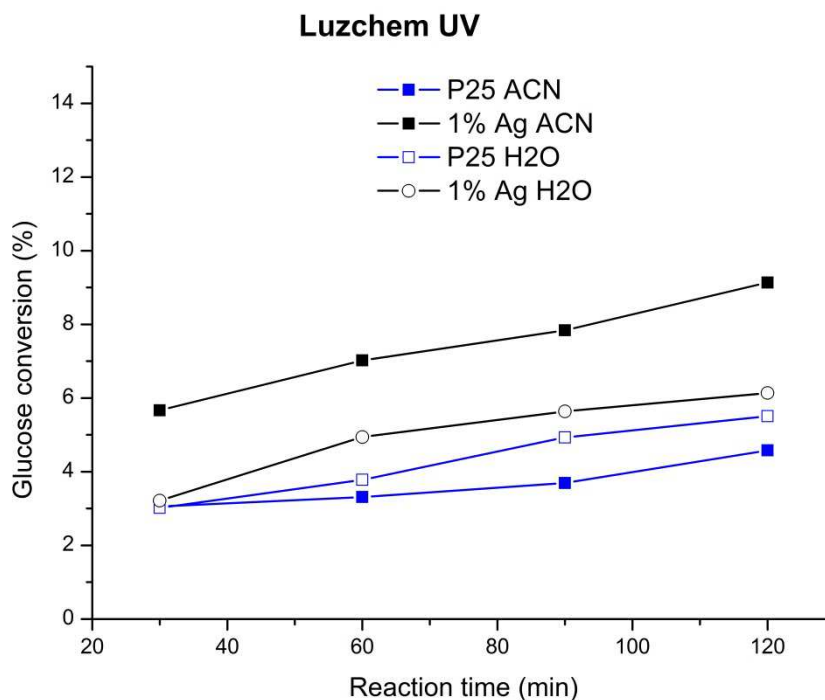


Figure 36: Time on line of glucose conversion under UV light with different solvents and catalysts. Comparison between P25 and Ag catalyst in pure H₂O and H₂O/ACN mixture is illustrated.

Table 8: Effect of the solvent on the products selectivity, products concentrations and total mass balance for the reactions run under UV. H₂O/ACN mixture [a] and pure H₂O [b] are used.

Catalyst	Reaction time (min)	Products Selectivity [%]				Products Concentration (g/L)						Mass balance (%)	Conversion (%)
		Gluconic Acid	Arabinose	GA + Erythrose	Formic Acid	Glucose unreacted	Gluconic	Arabinose	GA+erythrose	Formic Acid			
P25 ^[a]	30	0%	45%	24%	31%	3.536	0.0000	0.0473	0.0179	0.0098	99.00	3.1	
P25	60	0%	48%	12%	40%	3.527	0.0000	0.0553	0.0098	0.0144	98.86	3.3	
P25	90	0%	49%	17%	34%	3.513	0.0000	0.0653	0.0157	0.0142	98.91	3.7	
P25	120	9%	43%	15%	33%	3.481	0.0216	0.0809	0.0192	0.0189	99.28	4.6	
1 Ag/TiO ₂	30	13%	41%	19%	27%	3.382	0.0434	0.1033	0.0333	0.0205	99.93	5.7	
1 Ag/TiO ₂	60	13%	48%	28%	12%	3.334	0.0411	0.1207	0.0486	0.0089	99.09	7.0	
1 Ag/TiO ₂	90	10%	40%	19%	31%	3.304	0.0411	0.1340	0.0448	0.0311	99.16	7.8	
1 Ag/TiO ₂	120	10%	46%	18%	25%	3.258	0.0411	0.1403	0.0387	0.0231	97.65	9.1	
P25 ^[b]	30	18%	51%	32%	0%	3.483	0.0181	0.0400	0.0176	0.0000	99.09	3.0	
P25	60	15%	46%	16%	23%	3.456	0.0227	0.0519	0.0129	0.0081	98.88	3.8	
P25	90	13%	46%	22%	19%	3.415	0.0227	0.0631	0.0206	0.0081	98.26	4.9	
P25	120	12%	50%	20%	18%	3.394	0.0227	0.0728	0.0203	0.0081	97.94	5.5	
1 Ag/TiO ₂	30	30%	45%	25%	0%	3.476	0.0342	0.0401	0.0157	0.0000	99.29	3.2	
1 Ag/TiO ₂	60	22%	48%	31%	0%	3.414	0.0342	0.0576	0.0259	0.0000	98.34	4.9	
1 Ag/TiO ₂	90	19%	41%	21%	18%	3.389	0.0411	0.0679	0.0245	0.0093	98.34	5.6	
1 Ag/TiO ₂	120	18%	45%	20%	17%	3.371	0.0365	0.0716	0.0226	0.0081	97.73	6.1	

3.5. Effect of metal loading:

In the literature^{2,46} is reported that the presence of metal nanoparticles on the surface enhances the light absorption in the visible range for titania and other semiconductors. Supported metal nanoparticles can be prepared via different techniques²³ such as impregnation, deposition, precipitation and immobilization. Last one has great advantages due to the potential high control in morphology and homogeneity of the nanoparticles as compared with simple metal salt impregnation method. The metal nanoparticles act as an electron acceptor when the frequency of excitation source is close to their SPR band. These electrons are then transferred to the titania conduction band and they are responsible for the generation of highly reactive species as hydroxyl and hydroperoxyl radicals.^{2,34,67}

Different effects have been investigated until now for the optimization of the reaction conditions. Enhancing of catalyst through supported nanoparticles on the surface can be observed in the last paragraph. Presence of silver nanoparticles, with influence of calcination temperature, can improve catalytic activity of Degussa P25 especially under 1000W lamp irradiation without 420nm filters with ACN/H₂O mixture as solvent. 1% w/w Ag on TiO₂ is the only one that has been observed so far, and influence of different quantities of metal nanoparticles supported on the surface of Titania has been investigated. Metal nanoparticles on the surface have been evaluated through their weight percentage as previously reported. Different amounts of silver nanoparticles (0.5%, 1%, 2.5%, 5% w/w) have been observed in the same reaction conditions, under visible and UV irradiation.

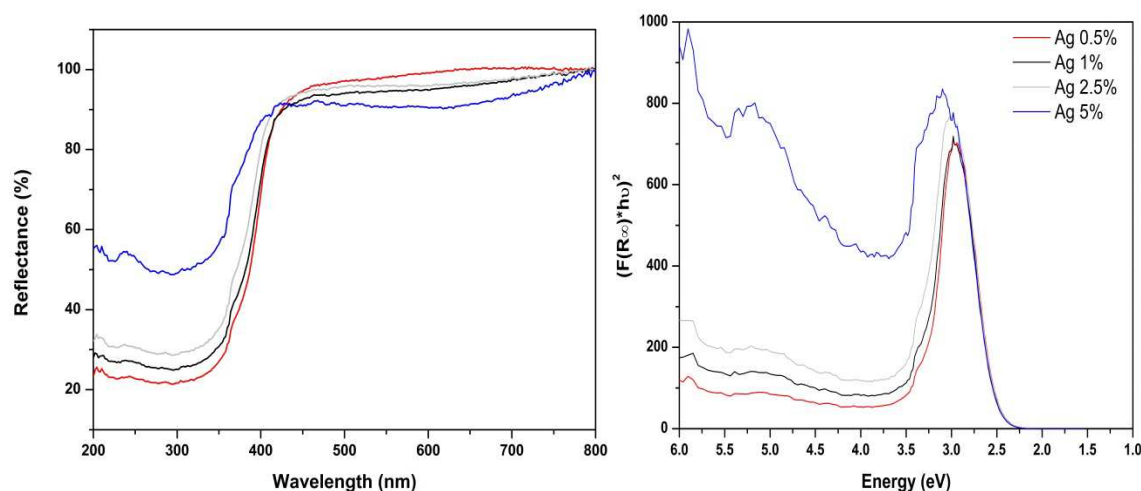


Figure 37: On the left, Diffuse Reflectance spectra of the Ag/TiO₂ with different metal loading. On the right, the peak of the LSPR can be recognised for the catalysts considered.

Diffusive reflectance of those supported catalysts can be seen in Figure 37. From the lowest to the highest amount of Ag, a significant trend can be observed. In fact, peak of LSPR can be evaluated, with a linear increasing trend from 0.5% to 5%, with a direct correlation between the amount of metal and the position of the maximum of the band.

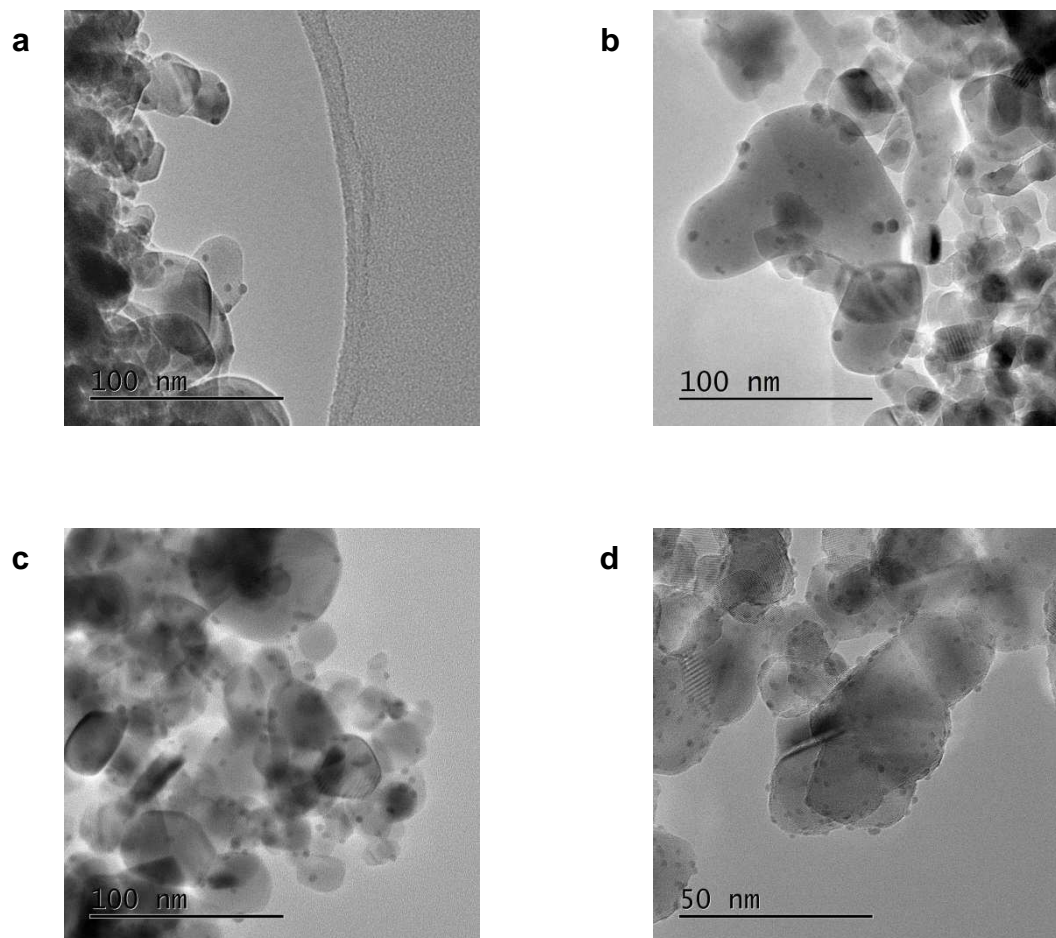


Figure 38: TEM images of a) Ag/TiO₂ 0.5 w/w, b) Ag/TiO₂ 1 w/w, c) Ag/TiO₂ 2.5 w/w and d) Ag/TiO₂ 5 w/w

TEM images of Ag catalysts are reported above. Supported metal nanoparticles can be observed on the surface of titania, and the smallest particles size is obtained with the highest amount of Ag loaded. Size distribution can be evaluated below.

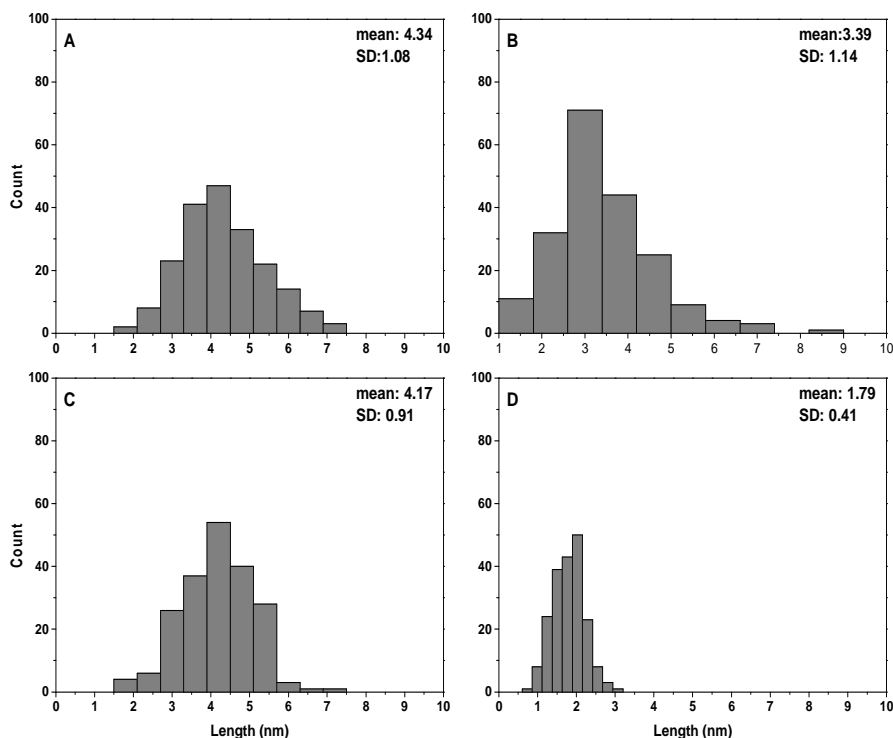


Figure 39: Particle size distribution values for the Ag/TiO₂ catalyst considered. The values are normalized over 200 counts. a) Ag/TiO₂ 0.5 w/w, b) Ag/TiO₂ 1 w/w, c) Ag/TiO₂ 2.5 w/w and d) Ag/TiO₂ 5 w/w.

Different size distribution can be observed in Figure 39. There is not a linear trend of distribution with the increase of silver amount. This is due to the difficult of controlling the nucleation and growth of nanoparticles and to the high mobility of ions during the thermal treatment. This is influenced by the heating ramp that controls thermodynamic and dynamic trends.

Grabowska *et al.*⁶⁷ have been demonstrated that the catalytic activity is not linearly correlated to the metal loading because increasing the quantity of metal leads to an increase in the particle dimension and semiconductor surface coverage. In fact, that study showed that under UV irradiation better performances are reached with high silver loadings on titania P25 (2% w/w), while using visible light the 1% w/w catalyst gave the best results. Latter trend is the same that can be observed below, in Figure 40.

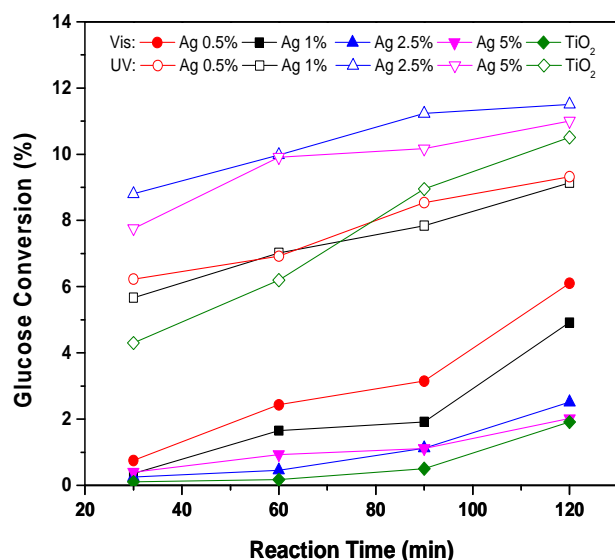


Figure 40: Time on line data of the reactions run with different amount of Ag/TiO₂. The values under UV are reported using the empty symbols and the values obtained under visible light are reported with the full symbols.

In Figure 40, a linear trend under visible irradiation can be observed. That shows a general enhanced of catalytic activity of P25 with metal nanoparticles. Highest conversion has been obtained with the lowest amount of Ag loaded (0.5% w/w), and the lowest conversion has been reached with the highest amount of silver (5% w/w). Under UV irradiation, a not linear trend can be noticed. The highest amounts of silver nanoparticles improve the catalytic activity of titania in terms of glucose conversion, but the lowest amounts reduce that. Catalytic activity of 2.5% Ag/TiO₂ is the highest one, according to Grabowska et al⁶⁷., and a reducing of activity can be correlated to the particles size as reported by Christopher et al.⁶⁹., because mean size of 5% Ag/TiO₂ is really smaller than 2.5% Ag/TiO₂ , and the total amount of metal.

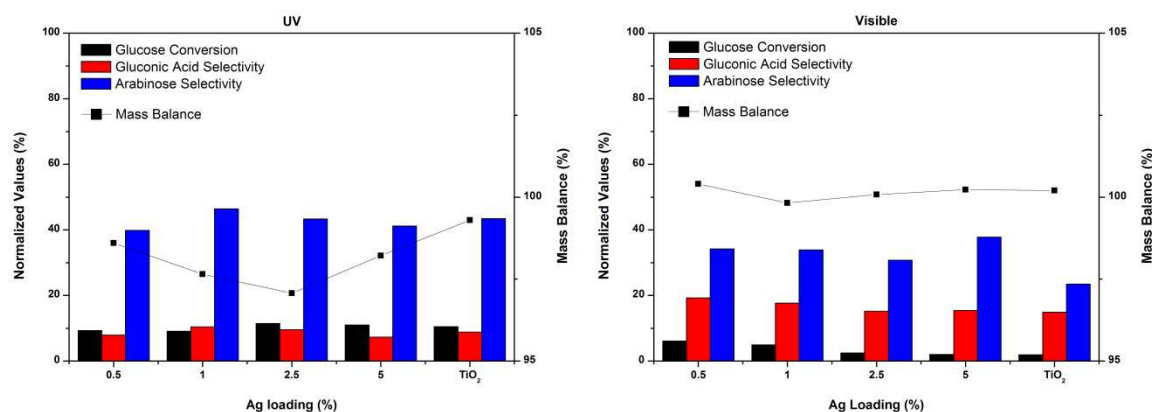


Figure 41: Final selectivity, mass balance and glucose conversion for reactions run with different amount of Ag, under UV (on the left) and visible light (on the right).

In terms of mass balance, the lowest values under UV irradiation is for the higher amount of silver loaded and it can be seen in Figure 41. 2.5% Ag/TiO₂ shows greater mineralization than titania P25 and the catalysts with lower amount of silver. Glucose selectivity slightly increase with higher amount of silver, but in the other hand selectivity towards arabinose decrease increasing the silver amount. Better results have been obtained under Visible irradiation. Silver nanoparticles increase glucose conversion but, in the same time, don't improve mineralization process. Mass balance, in fact, doesn't change with supported catalysts. Greatest conversion of glucose and selectivity towards gluconic acid have been obtained with the lowest amount of silver, as indicated by Grabowska *et al.*⁶⁷

In particular, as reported in Table 9, gluconic acid produced by 0.5 % Ag under visible light is 50% higher than the respectively UV reaction, and it is three times more than reactions conducted with greater amount of silver. While gluconic acid production is favored by visible light, under UV irradiation arabinose production and selectivity reach higher levels than visible ones. Arabinose selectivity doesn't change increasing silver amount, and GA + erythrose and formic acid selectivity increase to the detriment of gluconic acid. Ruff degradation enhancement can be observed under UV light, instead of oxidation of glucose that be improved by silver nanoparticles under visible irradiation.

Table 9: Effect of the Ag loading on the products selectivity, products concentrations and total mass balance for the reactions run with the Xe lamp [a] and the Luzchem [b] photoreactor.

Catalyst	Products Selectivity (%)				Products Concentration (g/L)					Mass balance (%)
	Gluconic Acid	Arabinose	Glyceraldehyde + Erythrose	Formic Acid	Glucose	Gluconic Acid	Arabinose	Glyceraldehyde + Erythrose	Formic Acid	
0.5 Ag/TiO ₂ ^[a]	19%	34%	16%	30%	3.367	0.0733	0.0996	0.0329	0.0271	100.40
1 Ag/TiO ₂	18%	34%	19%	29%	3.475	0.0503	0.0739	0.0294	0.0195	99.82
2.5 Ag/TiO ₂	15%	31%	20%	34%	3.543	0.0250	0.0387	0.0175	0.0131	100.08
5 Ag/TiO ₂	15%	38%	21%	26%	3.561	0.0204	0.0383	0.0148	0.0081	100.23
0.5 Ag/TiO ₂ ^[b]	8%	40%	13%	39%	3.251	0.0411	0.1585	0.0367	0.0475	98.60
1 Ag/TiO ₂	10%	46%	18%	25%	3.258	0.0411	0.1403	0.0387	0.0231	97.65
2.5 Ag/TiO ₂	10%	43%	18%	29%	3.227	0.0503	0.1754	0.0510	0.0361	97.07
5 Ag/TiO ₂	7%	41%	16%	36%	3.191	0.0434	0.1872	0.0497	0.0501	98.21

3.6. Effect of different metal nanoparticles:

Gold and silver catalysts were synthesized following WI method and they were both tested in the same reaction conditions. A comparison between them has been done using 1% of metal loading as sample. Reactions have been performed for 2 hours under visible and UV irradiation, with 1 g/L of catalyst loaded in 14 mL of 20mM glucose solution in ACN/H₂O 50/50 v/v. Samples have been taken every 30 minutes. Reactions have been performed with Degussa-P25 and have been used as blank.

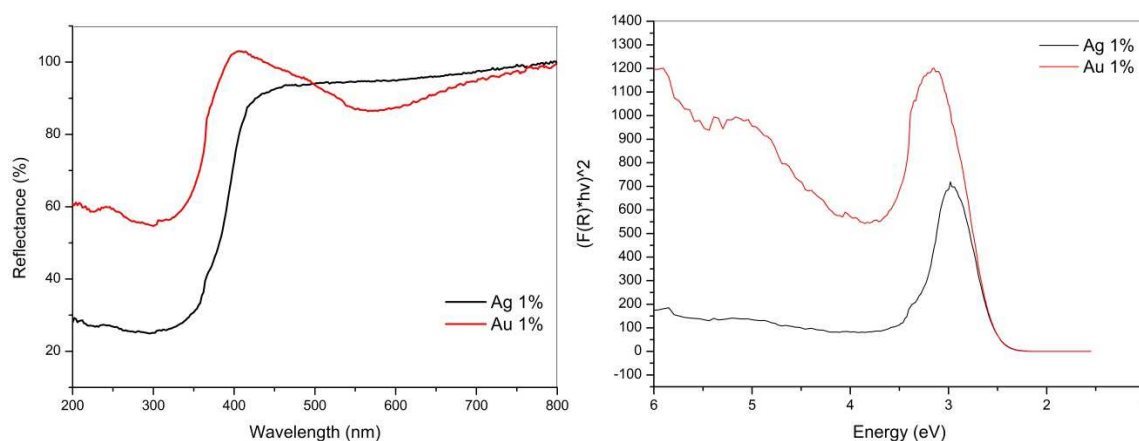


Figure 42: On the left, diffusive reflectance of Au/TiO₂ and Ag/TiO₂. On the right, characteristic LSPR band can be recognized.

In Figure 42, typical LSPR band of gold and silver nanoparticles can be observed. Percentage of metal loaded is the same for both (1% w/w). The position of the maximum of the gold's LSPR band is blue-shifted and the maxima is higher than the silver nanoparticles, so it explained the greater photo-activity of the gold particles than the silver ones under UV light. That is reflected in glucose conversion under UV and visible light in Figure 43.

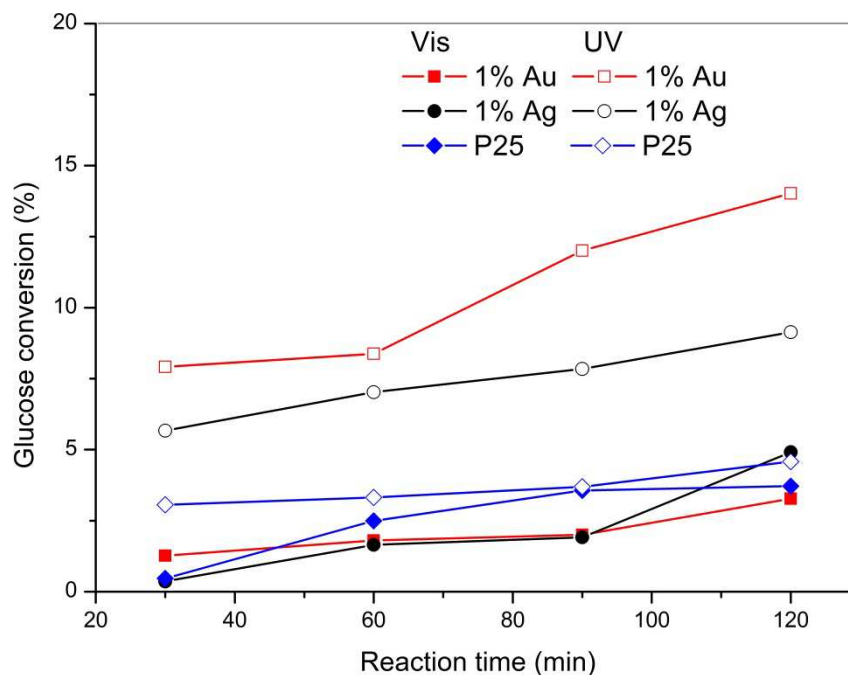


Figure 43: Time-on-line glucose conversion for each catalyst, under UV and visible light.

Conversion of reactions run with gold and silver nanoparticles, under UV and visible light, have been reported in Figure 43. Gold doesn't act as improvement of catalytic activity of titania under visible light. In fact, despite of high conversion reached after only 30 minutes, there is no enhancement of catalytic activity of titania in terms of glucose conversion. Under UV irradiation, an opposite effect can be observed. Catalytic activity of titania has been improved dramatically by metal nanoparticles. Difference in terms of glucose conversion between supported catalysts and pure titania can be observed, and difference between gold and silver nanoparticles can be seen as well.

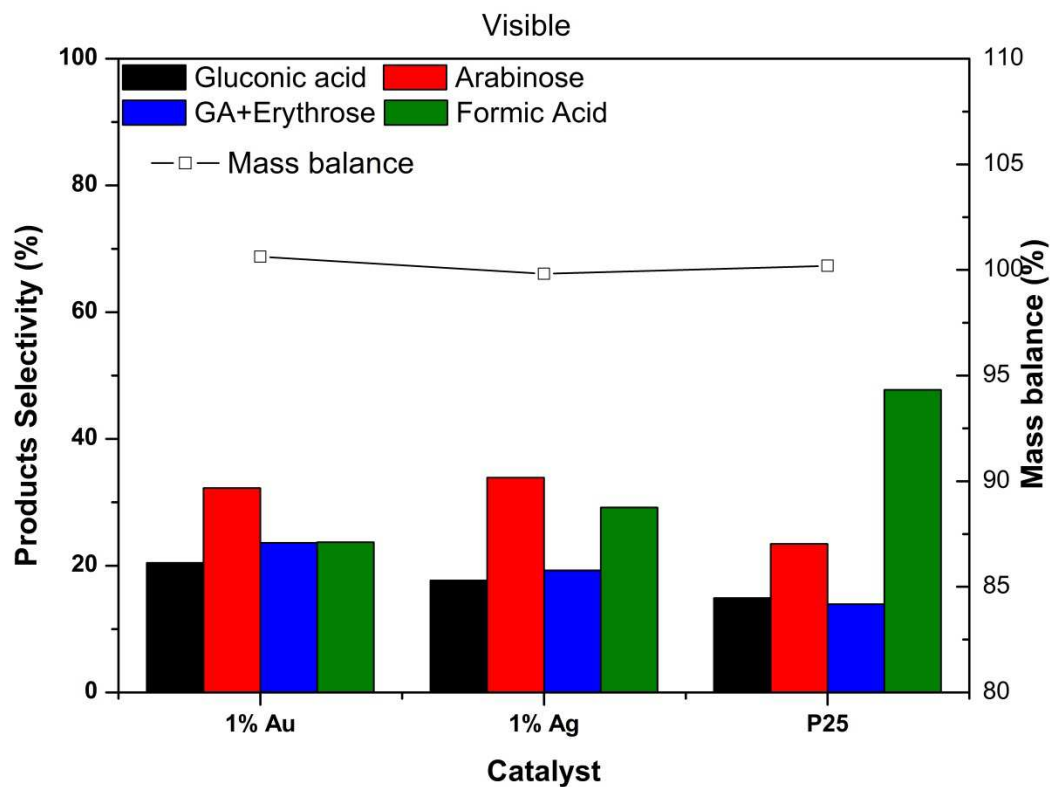


Figure 44: Selectivity and mass balance after 2 hours for each catalysts under visible light.

In terms of selectivity, there is a slight enhancement of selectivity towards gluconic acid by metal nanoparticles that pass from 18% to 20% for supported catalysts. Arabinose also shows an increasing selectivity, passing from 28% to 32% for gold nanoparticles and 38% for silver ones. Decreasing of selectivity towards GA + erythrose and formic acid prove a major capability in the selective oxidation of glucose by supported catalyst, because further degradations of the main products seems to be avoided.

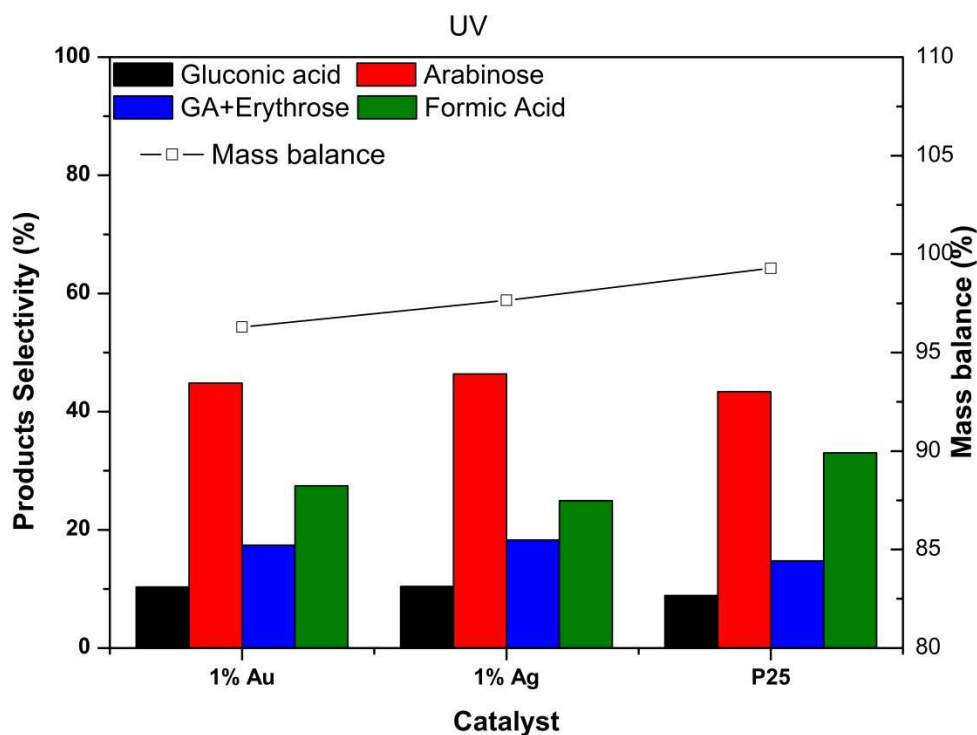


Figure 45: Selectivity and mass balance after 2 hours for each catalysts under UV light.

For UV light tests, selectivity is showed in Figure 45. Supported catalysts don't enhance the selectivity towards gluconic acid, and arabinose suffer a decrease in selectivity. Metal nanoparticles are more active under UV light, due to their LPSR band, and that is reflected on their catalyst behavior. Glucose conversion is higher with supported nanoparticles, but on the other hand, further degradation of the main products are favorites.

3.7. 24h reactions:

Long term reactions have been conducted with the same catalysts used in the last paragraph. The reactions have been run for 24 hours in the same conditions described above, and samples have been taken after 2-4-6-22-24 hours.

Figure 46 shows the results in terms of conversion, mass balance and main products selectivity (arabinose and gluconic acid), under visible and UV light. Trends previously observed have been enhanced in 24 hours reactions.

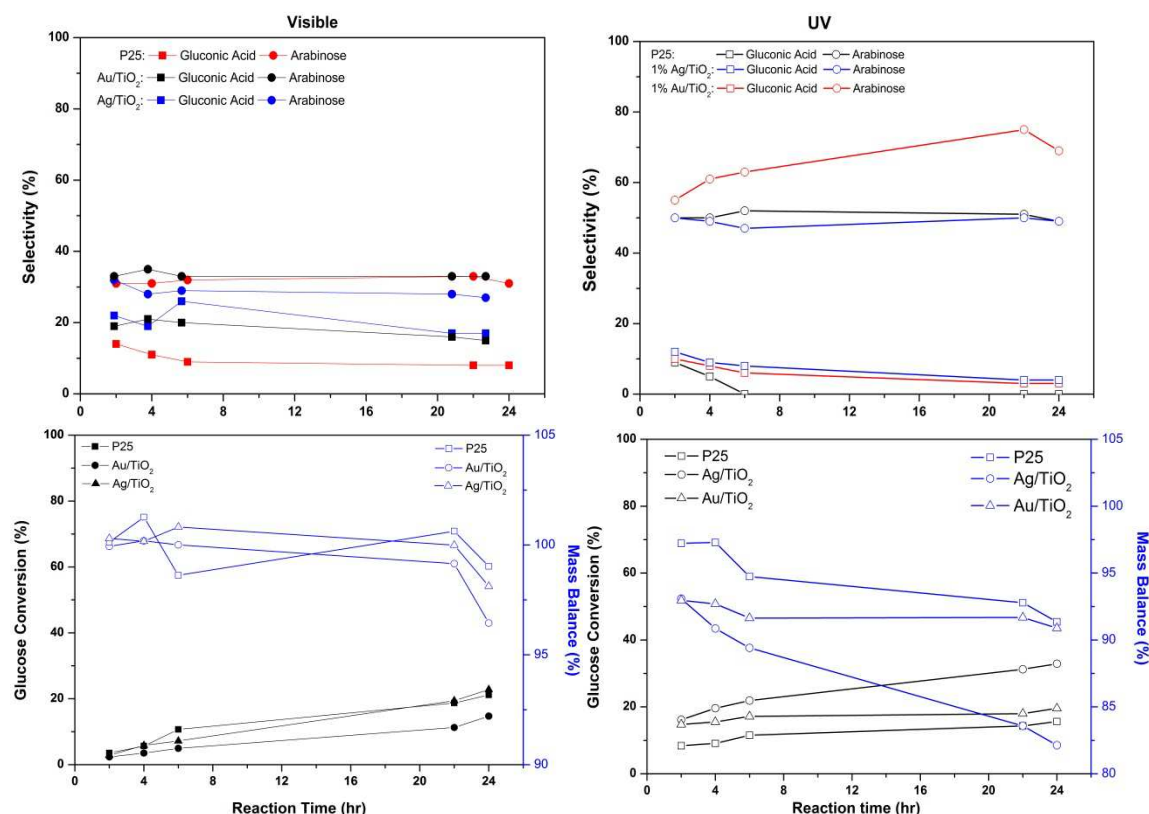


Figure 46: Time-on-line results of long terms reactions under UV and visible light. Selectivity towards main products, mass balance and glucose conversion are reported.

Under UV light, selectivity trends are the same observed until now. In fact, selectivity towards arabinose increase along the reaction, from around 55-60% in the first hours until 60% for P25 and silver nanoparticles and even 70% for the gold catalyst after 22hours, but slight decrease in the last 2 hours due to its further degradation. Selectivity towards gluconic acid is interesting, because while in 2 hours tests no differences could be observed between these three catalysts, now it is possible to observe interesting trends. Degussa P25 shows decreasing selectivity towards the acid production, and after 6 hours no gluconic acid can be observed, while supported catalysts shows low and similar selectivity that decrease from 11-13% to 3-4% after 24 hours. According to

glucose conversion and mass balance, general enhancement by metal nanoparticles can be recognized. Silver nanoparticles improve the selective conversion of glucose because the mass balance reaches 91% and conversion is 20%. Instead, gold nanoparticles improve the mineralization pathway, because mass balance decrease until 82% with 33% of glucose conversion.

Unexpected results have been obtained from the reactions conducted under visible light, in terms of conversion and mass balance. P25 and Ag/TiO₂ display final conversion values close to the values obtained under UV light, but mass balance is constantly up to 95%. In the case of gold catalyst, conversion obtained is lower than the UV test, but the final mass balance is 98%, so a greater amount of glucose has been converted in interesting products. Regarding the selectivity, P25 shows the lowest values towards gluconic acid, despite of arabinose selectivity is not so higher than others.

Therefore, 24 hours reactions have shown how change conversion, mass balance and selectivity in the long run, emphasizing the differences between P25 and supported catalyst, and between silver and gold nanoparticles as well.

3.8. Recyclability tests:

Recyclability tests have been performed with the 1% Ag/TiO₂ catalyst for three runs under UV and visible light. Final results have been illustrated in Figure 47.

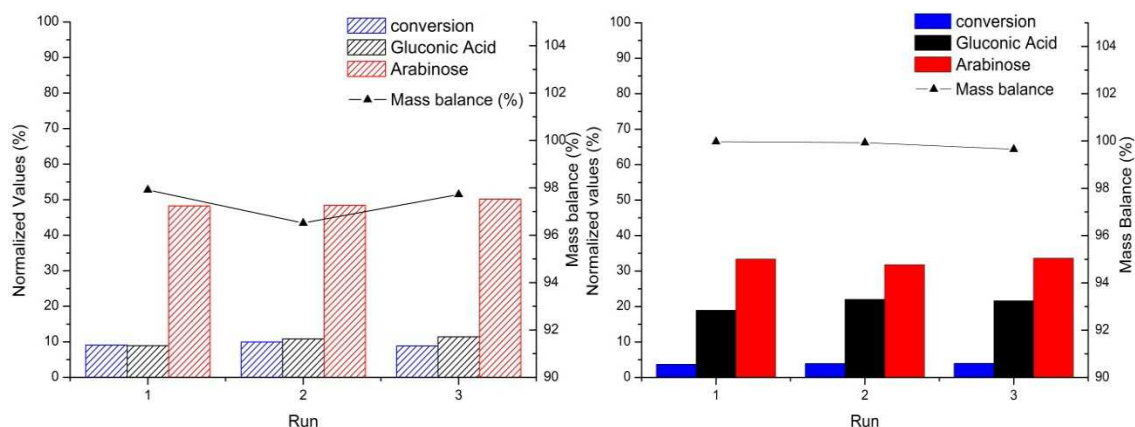


Figure 47: Catalyst recycle runs for the Ag/TiO₂ 1% under UV light (left) and visible light (right). The conversion, mass balance and main product selectivity values reported are taken from the samples after 120mins of reaction.

Under visible light, no differences in terms of glucose conversion and mass balance have been observed, because conversion is around 4% in every run, and mass balance is kept constant to +99%. The same trends have been observed under UV light.

In fact, glucose conversion doesn't suffer significant variation from the first run to the third, and mass balance is kept constant up to 97%. Therefore, catalyst doesn't suffer deactivation or significant changes in morphology if it is reused for three times, independent of the light source.

3.9.Future Work:

The reported data are exploring a new field of photocatalysis, continuing the first works done by Colmenares and Onho. The study reported in this work has tried to explain the mechanism of photo oxidation of glucose, but deeper analysis are required, first of all the quantification of gases produced. Also the effect of solvent in the reaction mechanism have been observed, but the influence of acetonitrile and other mixture in general can be explored in depth.

Gold and silver nanoparticles supported on titania have been used in this study, leading to the observation of effect of different metal amount and different LSPR band. The study can be increased to a wide range of materials, from different support with bandgap as Bi_2WO_6 or Al_2O_3 to different metals, as copper and nickel, trying to increase the yield of the reaction or also the selectivity towards gluconic acid and arabinose. Bimetallic nanoparticles can be investigated as well for this kind of reaction.

Finally, all this studies about the photo oxidation of glucose should be lead, as final step, to the glucaric acid as main product of this oxidation.

The production of glucaric acid from glucose using visible light is one of the main purposes of photocatalysis, because this acid can be used as monomer in the production of bio-polymers.

4. Conclusions:

Titania and metal nanoparticles have been explored as photocatalysts in the selective oxidation of glucose under UV and visible light.

This study continues the first works done by Colmenares *et al.* and Onho *et al.* that have not been completely explained the mechanism of the reaction. The mechanism has been investigated, leading to the hypothesis that the Ruff degradation of glucose have been catalyzed by a Fenton's like system. Gluconic acid and arabinose have been found as main product, instead of arabitol. Further degradation can be catalyzed in presence of high energy as UV irradiation, leading to the production of products as glyceraldehyde and erythrose. Formic acid has been found as well, due to the decarboxylation of gluconic acid and aldoses.

After the investigation of the mechanism, different influences have been evaluated, as structure and phases of Titania and few features of media. The mixed anatase-rutile phase has been found more active and selective under visible light than the individual rutile and anatase phases, with a similar values of Titania P25. These results seem to corroborate the hypothesis of a synergic effect of these phases on Titania P25. Calcination temperature effect has been investigated after that, and changes in morphology during the calcination lead to different results in terms of glucose conversion ,but the same trend in selectivity towards gluconic acid. Also the media has been investigated, and in particular the influence of the solvent and the lamp power. Mineralization pathway can be suppressed through the use of a water/acetonitrile mixture, and power lamp influences the conversion and mass balance only if it is used without the colored cut-off filters.

The addition of both Ag and Au resulted in improved conversions while retaining high selectivity to desired products. The catalyst was also proven to be reusable over a number of repeat reactions showing no loss in activity. The implications of having a low energy, environmentally sound and benign process for valorization of renewable feedstock are profound.

5. Appendix:

Table 10: Effect of solvent and power lamp on the P25 on the products selectivity, products concentrations and total mass balance for the reactions run with and without filters.

Catalyst	Reaction time (min)	Product selectivity (%)				Product concentration (g/L)						Conversion (%)	
		Glucosic Acid	Arabinose	GA+Erythrose	Formic Acid	Glucose Unreacted	Glucosic acid	Arabinose	GA+erythrose	Formic Acid	Mass balance (%)		
TiO ₂ -P25	30	0%	29%	71%	0%	3.612	0.0000	0.0034	0.0060	0.000	99.53	0.7	1000W ACN Filter
TiO ₂ -P25	60	0%	41%	59%	0%	3.604	0.0000	0.0065	0.0065	0.000	99.42	0.9	
TiO ₂ -P25	90	0%	52%	48%	0%	3.597	0.0000	0.0105	0.0068	0.000	99.33	1.1	
TiO ₂ -P25	120	0%	45%	55%	0%	3.577	0.0000	0.0163	0.0140	0.000	99.15	1.7	
1%Ag/TiO ₂	30	0%	28%	72%	0%	3.598	0.0000	0.0040	0.0072	0.000	99.90	0.4	
1%Ag/TiO ₂	60	0%	52%	48%	0%	3.587	0.0000	0.0114	0.0074	0.000	99.81	0.7	
1%Ag/TiO ₂	90	0%	53%	47%	0%	3.564	0.0000	0.0181	0.0110	0.000	99.46	1.3	
1%Ag/TiO ₂	120	24%	39%	37%	0%	3.562	0.0181	0.0227	0.0151	0.000	100.2	1.4	
TiO ₂ -P25	30	10%	54%	15%	20%	3.281	0.0342	0.1471	0.0291	0.017	96.60	9.7	No Filter
TiO ₂ -P25	60	8%	56%	17%	19%	3.118	0.0411	0.2204	0.0459	0.023	94.95	14.2	
TiO ₂ -P25	90	7%	54%	15%	24%	2.990	0.0457	0.2813	0.0534	0.039	93.86	17.7	
TiO ₂ -P25	120	6%	59%	15%	20%	2.804	0.0411	0.3340	0.0592	0.035	90.12	22.8	
1%Ag/TiO ₂	30	12%	49%	21%	17%	3.154	0.0572	0.1749	0.0531	0.018	96.38	12.1	
1%Ag/TiO ₂	60	8%	49%	18%	26%	2.933	0.0526	0.2610	0.0660	0.044	93.54	18.2	
1%Ag/TiO ₂	90	5%	53%	14%	29%	2.749	0.0411	0.3316	0.0594	0.055	90.21	23.4	
1%Ag/TiO ₂	120	5%	58%	14%	22%	2.581	0.0457	0.3842	0.0668	0.045	87.06	28.0	
TiO ₂ -P25	30	15%	16%	13%	56%	3.618	0.0227	0.0197	0.0106	0.021	101.6	0.5	300W ACN Filter
TiO ₂ -P25	60	16%	26%	20%	39%	3.544	0.0250	0.0312	0.0168	0.014	99.91	2.5	
TiO ₂ -P25	90	14%	23%	17%	46%	3.505	0.0319	0.0406	0.0211	0.025	99.69	3.6	
TiO ₂ -P25	120	15%	23%	14%	48%	3.499	0.0411	0.0496	0.0206	0.031	100.2	3.7	
1%Ag/TiO ₂	30	0%	58%	42%	0%	3.641	0.0000	0.0191	0.0099	0.000	100.4	0.4	
1%Ag/TiO ₂	60	13%	24%	19%	44%	3.594	0.0227	0.0327	0.0184	0.018	100.9	1.7	
1%Ag/TiO ₂	90	12%	29%	22%	37%	3.584	0.0296	0.0535	0.0278	0.021	101.7	1.9	
1%Ag/TiO ₂	120	18%	34%	19%	29%	3.475	0.0503	0.0739	0.0294	0.020	99.82	4.9	
TiO ₂ -P25	30	10%	47%	20%	23%	3.437	0.0250	0.0896	0.0262	0.013	99.37	4.9	No Filter
TiO ₂ -P25	60	9%	56%	17%	17%	3.299	0.0296	0.1393	0.0293	0.013	97.16	8.7	
TiO ₂ -P25	90	9%	55%	17%	19%	3.216	0.0388	0.1723	0.0379	0.018	96.39	11.0	
TiO ₂ -P25	120	9%	55%	17%	19%	3.120	0.0457	0.2100	0.0449	0.022	95.27	13.7	
1%Ag/TiO ₂	30	14%	44%	19%	23%	3.332	0.0457	0.1140	0.0348	0.018	97.72	8.1	
1%Ag/TiO ₂	60	10%	46%	23%	21%	3.186	0.0503	0.1749	0.0613	0.025	96.41	12.2	
1%Ag/TiO ₂	90	10%	51%	20%	18%	3.028	0.0595	0.2346	0.0646	0.026	94.09	16.5	
1%Ag/TiO ₂	120	9%	56%	20%	15%	2.825	0.0641	0.2979	0.0726	0.025	90.55	22.1	
TiO ₂ -P25	30	0%	57%	43%	0%	3.613	0.0000	0.0089	0.0046	0.000	99.71	0.7	1000W H₂O Filter
TiO ₂ -P25	60	39%	30%	31%	0%	3.598	0.0181	0.0106	0.0076	0.000	99.94	1.1	
TiO ₂ -P25	90	22%	20%	21%	37%	3.563	0.0204	0.0144	0.0103	0.008	99.44	2.0	

P25												
TiO ₂ -P25	120	21%	23%	29%	27%	3.561	0.0227	0.0190	0.0166	0.007	99.70	2.1
1% Ag/Ti O ₂	30	0%	53%	47%	0%	3.606	0.0000	0.0072	0.0045	0.000	99.48	0.8
1% Ag/Ti O ₂	60	0%	52%	48%	0%	3.595	0.0000	0.0197	0.0128	0.000	99.74	1.1
1% Ag/Ti O ₂	90	0%	32%	29%	38%	3.584	0.0000	0.0220	0.0141	0.008	99.76	1.5
1% Ag/Ti O ₂	120	0%	29%	38%	33%	3.563	0.0000	0.0267	0.0242	0.009	99.63	2.0
TiO ₂ -P25	30	10%	44%	20%	25%	3.468	0.0181	0.0605	0.0193	0.011	99.98	3.1
TiO ₂ -P25	60	10%	55%	14%	22%	3.400	0.0227	0.0979	0.0179	0.012	99.25	5.0
TiO ₂ -P25	90	9%	59%	18%	14%	3.328	0.0250	0.1250	0.0272	0.009	98.23	7.0
TiO ₂ -P25	120	8%	62%	16%	14%	3.238	0.0250	0.1507	0.0270	0.011	96.47	9.5
1% Ag/Ti O ₂	30	14%	48%	23%	15%	3.401	0.0319	0.0828	0.0279	0.008	99.28	4.9
1% Ag/Ti O ₂	60	12%	56%	19%	13%	3.269	0.0342	0.1263	0.0307	0.009	96.97	8.6
1% Ag/Ti O ₂	90	12%	60%	19%	10%	3.177	0.0411	0.1612	0.0355	0.008	95.66	11.2
1% Ag/Ti O ₂	120	11%	60%	18%	10%	3.046	0.0480	0.2017	0.0427	0.011	93.59	14.9
No Filter												
TiO ₂ -P25	30	0%	40%	60%	0%	3.625	0.0000	0.0078	0.0082	0.000	100.1	0.3
TiO ₂ -P25	60	0%	43%	57%	0%	3.585	0.0000	0.0121	0.0111	0.000	99.22	1.4
TiO ₂ -P25	90	25%	33%	42%	0%	3.575	0.0181	0.0181	0.0162	0.000	99.74	1.7
TiO ₂ -P25	120	24%	35%	41%	0%	3.557	0.0204	0.0232	0.0187	0.000	99.51	2.2
1% Ag/Ti O ₂	30	0%	52%	48%	0%	3.551	0.0000	0.0141	0.0090	0.000	99.51	1.1
1% Ag/Ti O ₂	60	17%	28%	22%	33%	3.525	0.0181	0.0221	0.0120	0.008	99.82	1.9
1% Ag/Ti O ₂	90	21%	33%	20%	26%	3.501	0.0273	0.0339	0.0145	0.008	99.81	2.5
1% Ag/Ti O ₂	120	21%	36%	21%	22%	3.471	0.0319	0.0428	0.0170	0.008	99.41	3.4
300W H₂O Filter												
TiO ₂ -P25	30	22%	55%	23%	0%	3.534	0.0204	0.0397	0.0114	0.000	99.14	2.8
TiO ₂ -P25	60	10%	48%	23%	19%	3.491	0.0181	0.0663	0.0218	0.008	99.14	4.0
TiO ₂ -P25	90	13%	52%	19%	16%	3.458	0.0273	0.0831	0.0215	0.008	98.91	4.9
TiO ₂ -P25	120	10%	51%	21%	18%	3.404	0.0250	0.0989	0.0277	0.011	98.06	6.4
1% Ag/Ti O ₂	30	34%	45%	21%	0%	3.463	0.0388	0.0398	0.0130	0.000	98.98	3.6
1% Ag/Ti O ₂	60	20%	41%	22%	17%	3.429	0.0342	0.0554	0.0209	0.007	98.73	4.5
1% Ag/Ti O ₂	90	16%	45%	22%	17%	3.395	0.0319	0.0697	0.0236	0.008	98.23	5.5
1% Ag/Ti O ₂	120	14%	47%	20%	19%	3.346	0.0319	0.0841	0.0243	0.011	97.36	6.8
No Filter												

Acknowledgements:

I would like to thank Tony to permit me to work in his international group. Thank you, Luigi, for the help during this period in the lab and in Liverpool and the patience with me, despite the last events. Many thanks to Tom, because a man with your experience and patience is hard to find.

A great acknowledge goes to Prof. Fabrizio Cavani, for his help and availability from the first to the final day of this project.

Final thanks go to my family and Elena for their support, help and incitement during these last six months, and many thanks to my friends because I past the best period of my life in Bologna.

I would like to write better acknowledgement but my poor English doesn't permit me to write everything I think.

Bibliography:

- (1) Fan, H.; Li, G.; Yang, F.; Yang, L.; Zhang, S. Photodegradation of cellulose under UV light catalysed by TiO₂. *Journal of Chemical Technology & Biotechnology* **2011**, *86*, 1107-1112.
- (2) Primo, A.; Corma, A.; Garcia, H. Titania supported gold nanoparticles as photocatalyst. *Physical Chemistry Chemical Physics* **2011**, *13*, 886-910.
- (3) Enache, D.; Knight, D.; Hutchings, G. Solvent-free Oxidation of Primary Alcohols to Aldehydes using Supported Gold Catalysts. *Catal Lett* **2005**, *103*, 43-52.
- (4) Milone, C.; Ingoglia, R.; Pistone, A.; Neri, G.; Galvagno, S. Activity of Gold Catalysts in the Liquid-Phase Oxidation of O-Hydroxybenzyl Alcohol. *Catal Lett* **2003**, *87*, 201-209.
- (5) Colmenares, J. C.; Magdziarz, A.; Bielejewska, A. High-value chemicals obtained from selective photo-oxidation of glucose in the presence of nanostructured titanium photocatalysts. *Bioresource Technology* **2011**, *102*, 11254-11257.
- (6) Chong, R.; Li, J.; Ma, Y.; Zhang, B.; Han, H.; Li, C. Selective conversion of aqueous glucose to value-added sugar aldose on TiO₂-based photocatalysts. *Journal of Catalysis* **2014**, *314*, 101-108.
- (7) Hoffmann, M. R.; Martin, S. T.; Choi, W.; Bahnemann, D. W. Environmental Applications of Semiconductor Photocatalysis. *Chem. Rev.* **1995**, *95*, 69-96.
- (8) Agbor, V. B.; Cicek, N.; Sparling, R.; Berlin, A.; Levin, D. B. Biomass pretreatment: Fundamentals toward application. *Biotechnology Advances* **2011**, *29*, 675-685.
- (9) Haghghi Mood, S.; Hossein Golfeshan, A.; Tabatabaei, M.; Salehi Jouzani, G.; Najafi, G. H.; Gholami, M.; Ardjmand, M. Lignocellulosic biomass to bioethanol, a comprehensive review with a focus on pretreatment. *Renewable and Sustainable Energy Reviews* **2013**, *27*, 77-93.
- (10) Saeman, J. F. Kinetics of Wood Saccharification - Hydrolysis of Cellulose and Decomposition of Sugars in Dilute Acid at High Temperature. *Industrial & Engineering Chemistry* **1945**, *37*, 43-52.
- (11) Tekin, K.; Karagöz, S.; Bektaş, S. A review of hydrothermal biomass processing. *Renewable and Sustainable Energy Reviews* **2014**, *40*, 673-687.
- (12) Li, M.-F.; Fan, Y.-M.; Xu, F.; Sun, R.-C.; Zhang, X.-L. Cold sodium hydroxide/urea based pretreatment of bamboo for bioethanol production: Characterization of the cellulose rich fraction. *Industrial Crops and Products* **2010**, *32*, 551-559.
- (13) Kusema, B. T.; Murzin, D. Y. Catalytic oxidation of rare sugars over gold catalysts. *Catalysis Science & Technology* **2013**, *3*, 297-307.
- (14) Takagaki, A.; Tagusagawa, C.; Domen, K. Glucose production from saccharides using layered transition metal oxide and exfoliated nanosheets as a water-tolerant solid acid catalyst. *Chemical Communications* **2008**, 5363-5365.
- (15) Menon, V.; Rao, M. Trends in bioconversion of lignocellulose: Biofuels, platform chemicals & biorefinery concept. *Progress in Energy and Combustion Science* **2012**, *38*, 522-550.
- (16) Bin, D.; Wang, H.; Li, J.; Wang, H.; Yin, Z.; Kang, J.; He, B.; Li, Z. Controllable oxidation of glucose to gluconic acid and glucaric acid using an electrocatalytic reactor. *Electrochimica Acta* **2014**, *130*, 170-178.
- (17) Biella, S.; Prati, L.; Rossi, M. Selective Oxidation of D-Glucose on Gold Catalyst. *Journal of Catalysis* **2002**, *206*, 242-247.

- (18) Mirescu, A.; Berndt, H.; Martin, A.; Prusse, U. Long-term stability of a 0.45% Au/TiO₂ catalyst in the selective oxidation of glucose at optimised reaction conditions. *Appl. Catal. A-Gen.* **2007**, *317*, 204-209.
- (19) Holm, M. S.; Shunmugavel, S.; Taarning, E.; Holm, M. S.; Shunmugavel, S.; Taarning, E. Conversion of Sugars to Lactic Acid Derivatives Using Heterogeneous Zeotype Catalysts. *Science* **2010**, *328*, 602-605.
- (20) Song, J.; Fan, H.; Ma, J.; Han, B. Conversion of glucose and cellulose into value-added products in water and ionic liquids. *Green Chemistry* **2013**, *15*, 2619-2635.
- (21) Appendix V - The 12 Principles of Green Chemistry. In *Ionizing Radiation and Polymers*; Drobny, J. G., Ed.; William Andrew Publishing, 2013; pp 267.
- (22) Eustis, S.; El-Sayed, M. A. Why gold nanoparticles are more precious than pretty gold: Noble metal surface plasmon resonance and its enhancement of the radiative and nonradiative properties of nanocrystals of different shapes. *Chemical Society Reviews* **2006**, *35*, 209-217.
- (23) White, R. J.; Luque, R.; Budarin, V. L.; Clark, J. H.; Macquarrie, D. J. Supported metal nanoparticles on porous materials. Methods and applications. *Chemical Society Reviews* **2009**, *38*, 481-494.
- (24) Lopez-Sanchez, J. A.; Dimitratos, N.; Miedziak, P.; Ntainjua, E.; Edwards, J. K.; Morgan, D.; Carley, A. F.; Tiruvalam, R.; Kiely, C. J.; Hutchings, G. J. Au-Pd supported nanocrystals prepared by a sol immobilisation technique as catalysts for selective chemical synthesis. *Physical Chemistry Chemical Physics* **2008**, *10*, 1921-1930.
- (25) Pachón, L. D.; Rothenberg, G. Transition-metal nanoparticles: synthesis, stability and the leaching issue. *Applied Organometallic Chemistry* **2008**, *22*, 288-299.
- (26) Zhu, J.; Wang, T.; Xu, X.; Xiao, P.; Li, J. Pt nanoparticles supported on SBA-15: Synthesis, characterization and applications in heterogeneous catalysis. *Applied Catalysis B: Environmental* **2013**, *130-131*, 197-217.
- (27) Sugano, Y.; Shiraishi, Y.; Tsukamoto, D.; Ichikawa, S.; Tanaka, S.; Hirai, T. Supported Au-Cu Bimetallic Alloy Nanoparticles: An Aerobic Oxidation Catalyst with Regenerable Activity by Visible-Light Irradiation. *Angewandte Chemie International Edition* **2013**, *52*, 5295-5299.
- (28) Santos, V. P.; Carabineiro, S. A. C.; Tavares, P. B.; Pereira, M. F. R.; Órfão, J. J. M.; Figueiredo, J. L. Oxidation of CO, ethanol and toluene over TiO₂ supported noble metal catalysts. *Applied Catalysis B: Environmental* **2010**, *99*, 198-205.
- (29) An, K.; Alayoglu, S.; Ewers, T.; Somorjai, G. A. Colloid chemistry of nanocatalysts: A molecular view. *Journal of Colloid and Interface Science* **2012**, *373*, 1-13.
- (30) Bowker, M.; Nuhu, A.; Soares, J. High activity supported gold catalysts by incipient wetness impregnation. *Catalysis Today* **2007**, *122*, 245-247.
- (31) Yoshihiko Ohama, D. v. G.: *Application of Titanium Dioxide Photocatalysis to Construction Materials: State-of-the-Art Report of the RILEM Technical Committee 194-TDP*
- (32) Gupta, S.; Tripathi, M. An overview of commonly used semiconductor nanoparticles in photocatalysis. *High Energy Chem* **2012**, *46*, 1-9.
- (33) Linic, S.; Christopher, P.; Ingram, D. B. Plasmonic-metal nanostructures for efficient conversion of solar to chemical energy. *Nat Mater* **2011**, *10*, 911-921.
- (34) Kumar, S. G.; Devi, L. G. Review on Modified TiO₂ Photocatalysis under UV/Visible Light: Selected Results and Related Mechanisms on Interfacial Charge Carrier Transfer Dynamics. *The Journal of Physical Chemistry A* **2011**, *115*, 13211-13241.

- (35) Hanaor, D. H.; Sorrell, C. Review of the anatase to rutile phase transformation. *J Mater Sci* **2011**, *46*, 855-874.
- (36) Mott, N. F.; Allgaier, R. S. Localized States in Disordered Lattices. *physica status solidi (b)* **1967**, *21*, 343-356.
- (37) Renz, C. Photo-reactions of the oxides of titanium, cerium, and the earth-acids. *Helvetica Chimica Acta* **1921**, vol. 4, pp. 961-968, .
- (38) Fujishima, A.; Honda, K. Electrochemical Photolysis of Water at a Semiconductor Electrode. *Nature* **1972**, *238*, 37-38.
- (39) Sclafani, A.; Herrmann, J. M. Comparison of the Photoelectronic and Photocatalytic Activities of Various Anatase and Rutile Forms of Titania in Pure Liquid Organic Phases and in Aqueous Solutions. *The Journal of Physical Chemistry* **1996**, *100*, 13655-13661.
- (40) Maschmeyer, T.; Che, M. Catalytic Aspects of Light-Induced Hydrogen Generation in Water with TiO₂ and Other Photocatalysts: A Simple and Practical Way Towards a Normalization? *Angewandte Chemie International Edition* **2010**, *49*, 1536-1539.
- (41) Amtout, A.; Leonelli, R. Optical properties of rutile near its fundamental band gap. *Physical Review B* **1995**, *51*, 6842-6851.
- (42) Linsebigler, A. L.; Lu, G. Q.; Yates, J. T. PHOTOCATALYSIS ON TiO₂ SURFACES - PRINCIPLES, MECHANISMS, AND SELECTED RESULTS. *Chem. Rev.* **1995**, *95*, 735-758.
- (43) Yu, J. C.; Yu, J.; Ho, W.; Zhang, L. Preparation of highly photocatalytic active nano-sized TiO₂ particles via ultrasonic irradiation. *Chemical Communications* **2001**, 1942-1943.
- (44) Paramasivam, I.; Jha, H.; Liu, N.; Schmuki, P. A Review of Photocatalysis using Self-organized TiO₂ Nanotubes and Other Ordered Oxide Nanostructures. *Small* **2012**, *8*, 3073-3103.
- (45) Wen, B.; Ma, J.; Chen, C.; Ma, W.; Zhu, H.; Zhao, J. Supported noble metal nanoparticles as photo/sono-catalysts for synthesis of chemicals and degradation of pollutants. *Sci. China Chem.* **2011**, *54*, 887-897.
- (46) Gong, D.; Ho, W. C. J.; Tang, Y.; Tay, Q.; Lai, Y.; Highfield, J. G.; Chen, Z. Silver decorated titanate/titania nanostructures for efficient solar driven photocatalysis. *Journal of Solid State Chemistry* **2012**, *189*, 117-122.
- (47) Zhu, H.; Chen, X.; Zheng, Z.; Ke, X.; Jaatinen, E.; Zhao, J.; Guo, C.; Xie, T.; Wang, D. Mechanism of supported gold nanoparticles as photocatalysts under ultraviolet and visible light irradiation. *Chemical Communications* **2009**, 7524-7526.
- (48) Xuming, Z.; Yu Lim, C.; Ru-Shi, L.; Din Ping, T. Plasmonic photocatalysis. *Reports on Progress in Physics* **2013**, *76*, 046401.
- (49) Zhou, X.; Liu, G.; Yu, J.; Fan, W. Surface plasmon resonance-mediated photocatalysis by noble metal-based composites under visible light. *Journal of Materials Chemistry* **2012**, *22*, 21337-21354.
- (50) Mie, G. Beiträge zur Optik trüber Medien, speziell kolloidaler Metallösungen. *Annalen der Physik* **1908**, *330*, 377-445.
- (51) Creighton, J. A.; Eadon, D. G. Ultraviolet-visible absorption spectra of the colloidal metallic elements. *Journal of the Chemical Society, Faraday Transactions* **1991**, *87*, 3881-3891.
- (52) Kreibig, U.; Vollmer, M.: Theoretical Considerations. In *Optical Properties of Metal Clusters*; Springer Series in Materials Science; Springer Berlin Heidelberg, 1995; Vol. 25; pp 13-201.

- (53) Link, S.; El-Sayed, M. A. Size and Temperature Dependence of the Plasmon Absorption of Colloidal Gold Nanoparticles. *The Journal of Physical Chemistry B* **1999**, *103*, 4212-4217.
- (54) Kreibig, U.; Genzel, L. Optical absorption of small metallic particles. *Surface Science* **1985**, *156*, Part 2, 678-700.
- (55) Amendola, V.; Meneghetti, M. Size Evaluation of Gold Nanoparticles by UV-vis Spectroscopy. *The Journal of Physical Chemistry C* **2009**, *113*, 4277-4285.
- (56) Narayanan, R.; El-Sayed, M. Some Aspects of Colloidal Nanoparticle Stability, Catalytic Activity, and Recycling Potential. *Top Catal* **2008**, *47*, 15-21.
- (57) Tian, Y.; Tatsuma, T. Mechanisms and Applications of Plasmon-Induced Charge Separation at TiO₂ Films Loaded with Gold Nanoparticles. *Journal of the American Chemical Society* **2005**, *127*, 7632-7637.
- (58) Tsubota, S.; Cunningham, D. A. H.; Bando, Y.; Haruta, M.: Preparation of nanometer gold strongly interacted with TiO₂ and the structure sensitivity in low-temperature oxidation of CO. In *Studies in Surface Science and Catalysis*; G. Poncelet, J. M. B. D. P. A. J., Grange, P., Eds.; Elsevier, 1995; Vol. Volume 91; pp 227-235.
- (59) Haruta, M. Size- and support-dependency in the catalysis of gold. *Catalysis Today* **1997**, *36*, 153-166.
- (60) Corma, A.; Garcia, H. Supported gold nanoparticles as catalysts for organic reactions. *Chemical Society Reviews* **2008**, *37*, 2096-2126.
- (61) Hashmi, A. S.: Gold-Catalyzed Organic Reactions. In *Inventing Reactions*; Gooßen, L. J., Ed.; Topics in Organometallic Chemistry; Springer Berlin Heidelberg, 2013; Vol. 44; pp 143-164.
- (62) Hashmi, A. S. K.; Hutchings, G. J. Gold Catalysis. *Angewandte Chemie International Edition* **2006**, *45*, 7896-7936.
- (63) Hutchings, G. Catalysis: A golden future. *Gold Bull* **1996**, *29*, 123-130.
- (64) Haruta, M.; Yamada, N.; Kobayashi, T.; Iijima, S. Gold catalysts prepared by coprecipitation for low-temperature oxidation of hydrogen and of carbon monoxide. *Journal of Catalysis* **1989**, *115*, 301-309.
- (65) Grirrane, A.; Corma, A.; García, H. Gold-Catalyzed Synthesis of Aromatic Azo Compounds from Anilines and Nitroaromatics. *Science* **2008**, *322*, 1661-1664.
- (66) Aschwanden, L.; Mallat, T.; Maciejewski, M.; Krumeich, F.; Baiker, A. Development of a New Generation of Gold Catalysts for Amine Oxidation. *ChemCatChem* **2010**, *2*, 666-673.
- (67) Grabowska, E.; Zaleska, A.; Sorgues, S.; Kunst, M.; Etcheberry, A.; Colbeau-Justin, C.; Remita, H. Modification of Titanium(IV) Dioxide with Small Silver Nanoparticles: Application in Photocatalysis. *The Journal of Physical Chemistry C* **2013**, *117*, 1955-1962.
- (68) Messaoud, M.; Chadeau, E.; Brunon, C.; Ballet, T.; Rappenne, L.; Roussel, F.; Leonard, D.; Oulahal, N.; Langlet, M. Photocatalytic generation of silver nanoparticles and application to the antibacterial functionalization of textile fabrics. *Journal of Photochemistry and Photobiology A: Chemistry* **2010**, *215*, 147-156.
- (69) Christopher, P.; Ingram, D. B.; Linic, S. Enhancing Photochemical Activity of Semiconductor Nanoparticles with Optically Active Ag Nanostructures: Photochemistry Mediated by Ag Surface Plasmons. *The Journal of Physical Chemistry C* **2010**, *114*, 9173-9177.
- (70) Fu, X.; Long, J.; Wang, X.; Leung, D. Y. C.; Ding, Z.; Wu, L.; Zhang, Z.; Li, Z.; Fu, X. Photocatalytic reforming of biomass: A systematic study of hydrogen

evolution from glucose solution. *International Journal of Hydrogen Energy* **2008**, *33*, 6484-6491.

(71) Lu, X.; Xie, S.; Yang, H.; Tong, Y.; Ji, H. Photoelectrochemical hydrogen production from biomass derivatives and water. *Chemical Society Reviews* **2014**.

(72) Pei, C. C.; Chu, W. The photocatalytic degradation and modeling of 2,4-Dichlorophenoxyacetic acid by bismuth tungstate/peroxide. *Chemical Engineering Journal* **2013**, *223*, 665-669.

(73) Es'haghi, Z.: *Photodiode Array Detection in Clinical Applications; Quantitative Analyte Assay Advantages, Limitations and Disadvantages*, 2011.

(74) Mirescu, A.; Prüße, U. Selective glucose oxidation on gold colloids. *Catalysis Communications* **2006**, *7*, 11-17.

(75) Colmenares, J. C.; Magdziarz, A. Room temperature versatile conversion of biomass-derived compounds by means of supported TiO₂ photocatalysts. *Journal of Molecular Catalysis A: Chemical* **2013**, *366*, 156-162.

(76) Colmenares, J. C.; Magdziarz, A.; Kurzydowski, K.; Grzonka, J.; Chernyayeva, O.; Lisovytskiy, D. Low-temperature ultrasound-promoted synthesis of Cr-TiO₂-supported photocatalysts for valorization of glucose and phenol degradation from liquid phase. *Applied Catalysis B: Environmental* **2013**, *134-135*, 136-144.

(77) Stapley, J. A.; BeMiller, J. N. The Ruff degradation: a review of previously proposed mechanisms with evidence that the reaction proceeds by a Hofer-Moest-type reaction. *Carbohydrate Research* **2007**, *342*, 407-418.

(78) Ohno, T.; Sarukawa, K.; Tokieda, K.; Matsumura, M. Morphology of a TiO₂ Photocatalyst (Degussa, P-25) Consisting of Anatase and Rutile Crystalline Phases. *Journal of Catalysis* **2001**, *203*, 82-86.

(79) Dambournet, D.; Belharouak, I.; Amine, K. Tailored Preparation Methods of TiO₂ Anatase, Rutile, Brookite: Mechanism of Formation and Electrochemical Properties†. *Chemistry of Materials* **2009**, *22*, 1173-1179.

(80) Tang, H.; Lévy, F.; Berger, H.; Schmid, P. E. Urbach tail of anatase $\langle \text{TiO}_2 \rangle$. *Physical Review B* **1995**, *52*, 7771-7774.

(81) Prieto-Mahaney, O.-O.; Murakami, N.; Abe, R.; Ohtani, B. Correlation between Photocatalytic Activities and Structural and Physical Properties of Titanium(IV) Oxide Powders. *Chemistry Letters* **2009**, *38*, 238-239.

(82) Pang, G.; Chen, S.; Kolytyn, Y.; Zaban, A.; Feng, S.; Gedanken, A. Controlling the Particle Size of Calcined SnO₂ Nanocrystals. *Nano Letters* **2001**, *1*, 723-726.

(83) Wu, H.; Ma, J.; Zhang, C.; He, H. Effect of TiO₂ calcination temperature on the photocatalytic oxidation of gaseous NH₃. *Journal of Environmental Sciences* **2014**, *26*, 673-682.

(84) Dostanić, J.; Grbić, B.; Radić, N.; Stojadinović, S.; Vasilić, R.; Vuković, Z. Preparation and photocatalytic properties of TiO₂-P25 film prepared by spray pyrolysis method. *Applied Surface Science* **2013**, *274*, 321-327.